

Thermal diodes, regulators, and switches: Physical mechanisms and potential applications

[Geoff Wehmeyer](#), [Tomohide Yabuki](#), [Christian Monachon](#), [Junqiao Wu](#), and [Chris Dames](#)

Citation: [Applied Physics Reviews](#) **4**, 041304 (2017);

View online: <https://doi.org/10.1063/1.5001072>

View Table of Contents: <http://aip.scitation.org/toc/are/4/4>

Published by the [American Institute of Physics](#)

APPLIED PHYSICS REVIEWS

Thermal diodes, regulators, and switches: Physical mechanisms and potential applications

Geoff Wehmeyer,¹ Tomohide Yabuki,^{1,2} Christian Monachon,^{1,3} Junqiao Wu,^{4,5,a)} and Chris Dames^{1,5,a)}

¹Department of Mechanical Engineering, University of California, Berkeley, Berkeley, California 94720, USA

²Department of Mechanical and Control Engineering, Kyushu Institute of Technology, Kitakyushu, Fukuoka 804-8550, Japan

³Attolight AG, 1015 Lausanne, Switzerland

⁴Department of Materials Science and Engineering, University of California, Berkeley, Berkeley, California 94720, USA

⁵Materials Science Division, Lawrence Berkeley National Laboratory, Berkeley, California 94720, USA

(Received 21 August 2017; accepted 17 October 2017; published online 21 November 2017)

Interest in new thermal diodes, regulators, and switches has been rapidly growing because these components have the potential for rich transport phenomena that cannot be achieved using traditional thermal resistors and capacitors. Each of these thermal components has a signature functionality: Thermal diodes can rectify heat currents, thermal regulators can maintain a desired temperature, and thermal switches can actively control the heat transfer. Here, we review the fundamental physical mechanisms of switchable and nonlinear heat transfer which have been harnessed to make thermal diodes, switches, and regulators. The review focuses on experimental demonstrations, mainly near room temperature, and spans the fields of heat conduction, convection, and radiation. We emphasize the changes in thermal properties across phase transitions and thermal switching using electric and magnetic fields. After surveying fundamental mechanisms, we present various nonlinear and active thermal circuits that are based on analogies with well-known electrical circuits, and analyze potential applications in solid-state refrigeration and waste heat scavenging. *Published by AIP Publishing.*

<https://doi.org/10.1063/1.5001072>

TABLE OF CONTENTS

I. INTRODUCTION	2	B. Convection	13
A. Electrical analogies	2	1. Fluid thermal diodes	13
II. TAXONOMY OF ACTIVE AND NONLINEAR COMPONENTS	2	2. Convection thermal regulators	15
A. Thermal diode	3	3. Gas gap thermal switches	16
B. Thermal regulator	3	4. Controlling fluid heat transfer with electric and magnetic fields	16
C. Thermal switch	4	C. Radiation	17
III. MECHANISMS OF ACTIVE AND NONLINEAR HEAT TRANSFER	5	1. Thermal regulation using emissivity changes across phase transitions	17
A. Conduction	5	2. Radiative thermal diodes	18
1. Changes in k due to phase transitions	5	3. Electrochromic emissivity control	18
2. Conduction thermal diodes	8	4. View factor switching	20
3. Intercalation	8	5. Near field radiation	20
4. Contact thermal switches and regulators	9	IV. POTENTIAL APPLICATIONS AND THERMAL CIRCUITS	20
5. Electrostatic control of electron thermal conductivity	10	A. Solid state refrigeration using thermal diodes	20
6. Controlling phonon k with electric fields	12	B. Waste heat scavenging using switchable and nonlinear thermal devices	22
7. Controlling k with magnetic fields	12	C. Analogous thermal and electrical circuits	23
8. Electrothermal coupling and feedback	13	1. Thermal diode application circuits	24
		2. Thermal switch application circuits	25
		3. Thermal regulator and negative differential resistance circuits	26
		D. Summary and outlook	27

^{a)}Authors to whom correspondence should be addressed: cdames@berkeley.edu and wuj@berkeley.edu

I. INTRODUCTION

Controlling thermal transport is a key challenge of modern technology, energy conversion systems, heating and refrigeration, manufacturing and materials processing, data storage, and electronics thermal management. However, engineers seeking improved thermal control are limited by the traditional toolkit of linear, static, and passive thermal components, such as thermal resistors and thermal capacitors. This paucity of thermal options pales in comparison to the rich selection of highly nonlinear, switchable, and active components in the electrical domain. For example, integrated electrical circuits for information processing rely on nonlinear building blocks such as transistors and diodes, and effectively transmitting electrical power without switches would be a tall order. Since switchable and nonlinear thermal components are not nearly as mature as their electrical counterparts, contemporary thermal research explores many different mechanisms which could provide these new capabilities.

In this article, we review experimental demonstrations of switchable and nonlinear thermal components—thermal diodes, switches, and regulators. Each of these components is defined by a characteristic transfer function connecting the heat flow (Q) to the driving temperature difference (ΔT). Thermal regulators have a nonlinear transfer function, meaning that Q is not linearly proportional to ΔT . The transfer function of a thermal diode depends on the polarity of ΔT : $|Q(\Delta T)| \neq |Q(-\Delta T)|$. This defining asymmetry implies that the diode's transfer function must also be nonlinear, since the ratio $Q/\Delta T$ cannot be a constant everywhere. Finally, the transfer function of a thermal switch can be actively controlled by a non-thermal parameter, such as pressure or voltage. After establishing these definitions in Sec. II, Sec. III surveys the physical mechanisms across the fields of heat conduction, convection, and radiation that lead to thermal rectification, regulation, and switching. With an eye towards potential applications, we focus our attention primarily on mechanisms which can operate near room temperature and atmospheric pressure. In Secs. IV A and IV B, we then examine examples of nonlinear or active thermal circuits which have been developed to improve the efficiency of solid-state refrigeration and energy harvesting cycles. In Sec. IV C, we present nonlinear and active thermal circuits which are analogous to well-known electrical circuits. We summarize the current status and future opportunities for thermal diodes, regulators, and switches in Sec. IV D.

This article complements several other recent reviews. Li *et al.*¹ summarized predominantly computational predictions for nonlinear nanoscale phononic devices. Ben-Abdallah and Biehs² presented theoretical predictions for nonlinear thermal radiation components in the far- and near-field. Roberts and Walker³ summarized rectification mechanisms in bulk solids and theoretical predictions of rectification in nanostructures. DiPirro and Shirron⁴ surveyed thermal switches for cryogenic refrigeration applications, and Shahriari *et al.*⁵ recently discussed boiling and condensation heat transfer switching using electric fields. Compared with these works, this review focuses on experimental demonstrations of thermal diodes,

switches, and regulators across all fields of heat transfer, with an emphasis on the changes in thermal properties across phase transitions and on switching heat transfer using electric and magnetic fields. Though concepts of thermal computing applications have also been proposed,^{1,6} we focus here on possible applications in thermal control and energy conversion.

A. Electrical analogies

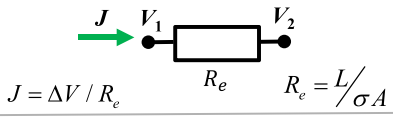
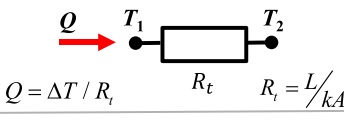
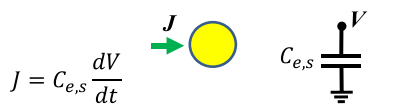
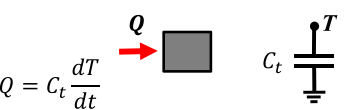

Throughout this review, we will draw upon analogies between thermal and electrical components. This serves the dual goals of understanding thermal systems using intuition from electrical engineering and providing inspiration for adapting useful electrical circuits into the thermal domain. To motivate this approach, Fig. 1 compares the linear response theory of thermal and electrical resistors and capacitors. (There are no thermal elements that are analogous to electromagnetic inductors.⁷) The analogy between current flow in electrostatic resistor networks and heat flow in thermal resistor networks is exact at steady-state, because the governing equation, constitutive relations, and boundary conditions are all identical for electrical and thermal transport.

Analogies involving capacitance, however, must be treated with more caution. There is a strict analogy between the self-capacitance in the electrical domain, which is the voltage change required to increase the charge stored by an isolated conductor, and the thermal capacitance, which is the temperature change required to increase the energy stored by an isolated thermal conductor. However, there is no thermal analogy for the mutual capacitance of the more common parallel-plate capacitor, which characterizes the electrical potential difference between two conductors. Therefore, every capacitor in a thermal circuit must have one terminal grounded, which unfortunately prohibits thermal analogies to certain interesting electrical circuits such as voltage triplers.

Adding nonlinear and switchable thermal components to this traditional toolkit of linear resistors and grounded capacitors leads to qualitatively new thermal capabilities, including tunable thermal control and other examples discussed in Sec. IV such as rectification, heterodyning, and amplification. We now more thoroughly introduce the three primary components discussed in this review: thermal diodes, switches, and regulators.

II. TAXONOMY OF ACTIVE AND NONLINEAR COMPONENTS

Components are characterized by a transfer function (constitutive relation) relating flow rates to their driving potentials. For example, electrical transistors are characterized by their steady-state current-voltage diagrams. In the thermal domain, a convenient representation of the steady-state transfer function is a plot of the heat flow (Q) as a function of the driving temperature difference (ΔT) across the device. Although the absolute magnitude of the applied voltage need not be specified for electrical transfer functions, material properties often do depend on the absolute temperature. Therefore, when presenting the thermal transfer functions, it is most proper to fix the average temperature $T_{avg} = (T_h + T_c)/2$, where T_h is the hot-side temperature and T_c is the cold-side temperature.

	Electrical Conduction	Heat Conduction
Driving Potential	Voltage difference ΔV	Temperature difference ΔT
Flux	Current density j	Heat flux q
Constitutive Relation	$\vec{j} = -\sigma \nabla V$	$\vec{q} = -k \nabla T$
Resistance	 $J = \Delta V / R_e$ $R_e = L / \sigma A$	 $Q = \Delta T / R_t$ $R_t = L / kA$
Capacitance	Self capacitance: Charge required to raise V of an isolated conductor  $J = C_{e,s} \frac{dV}{dt}$	Thermal capacitance: Energy required to raise T of isolated conductor  $Q = C_t \frac{dT}{dt}$
	Mutual capacitance: Interaction between conductors  $J = C_e \frac{d(\Delta V)}{dt}$	No thermal equivalent: All thermal capacitors have one terminal grounded

In this review, we will focus on three fundamental thermal components: thermal diodes, thermal regulators, and thermal switches. Figure 2 shows the symbols, transfer functions, and an illustrative example of a heat conduction mechanism for each component. We now discuss each of these components in detail.

A. Thermal diode

A thermal diode is a two-terminal element that rectifies heat currents. The left column of Fig. 2 shows a typical transfer function of a thermal diode. If the polarity of the temperature difference ΔT is switched at fixed T_{avg} , the magnitude of the heat flow changes. The figure of merit for a thermal diode is the rectification ratio, here defined as

$$\gamma = (|Q_{fwd}| - |Q_{rev}|) / |Q_{rev}|, \quad (1)$$

where the magnitude of the forward heat flow Q_{fwd} is greater than the magnitude of the reverse heat flow Q_{rev} at the same $|\Delta T|$, and it is also understood that T_{avg} is held constant. In general, γ will be a function of ΔT and T_{avg} .

Rectification requires both a spatial asymmetry and a nonlinearity. For example, in an electrical p - n diode, the asymmetry is imposed by the levels of p -type and n -type doping, and the nonlinearity arises from the exponential dependence of the minority carrier concentrations on the voltage difference across the space-charge region.⁸ The second law of thermodynamics poses constraints on rectification which may not be obvious on first glance; for example, the second law implies that an electrical diode cannot rectify the Johnson noise of a load resistor, as long as the resistor and the diode are at the same temperature.⁹ Similar second law restrictions of course also apply for thermal diodes, as we shall see throughout this review.

An example of a thermal diode mechanism is shown in the bottom left panel of Fig. 2 and discussed further below in

Sec. III A 2. This “junction thermal diode” consists of two materials with different temperature-dependent thermal conductivities ($k(T)$) providing the nonlinearity. In the forward mode, when the left material is hot and the right material is cold, both materials have high k and the heat flux is large; in the reverse mode, the materials both have low k and the heat flux is smaller.¹⁰

An example application of thermal diodes is a solid-state refrigeration cycle utilizing the magnetocaloric¹¹ or electrocaloric¹² effect. Thermal diodes allow for strong thermal coupling when heat is pumped out of the refrigerator, while blocking undesirable heat backflow into the refrigerator during other portions of the cycle. Several solid-state cooling cycles using thermal switches to mimic thermal diode behavior have been demonstrated,^{13–16} and in Sec. IV A, we will analyze an electrocaloric refrigeration cycle using thermal diodes. Other applications of thermal diodes are also suggested in Sec. IV C 1.

B. Thermal regulator

A thermal regulator is a two terminal component with a strongly nonlinear $Q - \Delta T$ transfer function at fixed T_{avg} , as shown in the center column of Fig. 2. One common function of a thermal regulator is to maintain a desired critical temperature T_c by switching between a high conductance and a low conductance state. The thermal regulator is analogous to an electrical varistor (portmanteau of “variable resistor”). All thermal diodes are also technically thermal regulators since the transfer function of a diode is nonlinear, but in contrast with a thermal diode, the transfer function of a regulator can be symmetric in ΔT . The essential feature of the diode’s transfer function is the asymmetry, while the essence of a regulator’s transfer function lies in the sharp nonlinear response.

A figure of merit for a thermal regulator is the on/off switching ratio

FIG. 1. Analogies between linear electrical and thermal components. Traditionally, thermal circuits have been limited to the passive linear elements of thermal resistors and capacitors, which are analogous to their electrical counterparts. Many readers will be familiar with the resistance analogies between thermal and electrical transport, which arise from the equivalent constitutive relations (top 4 rows). However, the capacitance analogies (bottom two rows) are more subtle, because thermal capacitance is only analogous to the less-known “self-capacitance” of an isolated electrical conductor, not the more familiar “mutual capacitance” of a typical parallel-plate electrical capacitor. Practically, this means that all thermal capacitors have one terminal grounded. This review focuses on active and nonlinear thermal elements (Fig. 2) which broaden the toolkit of thermal engineers beyond these linear elements.

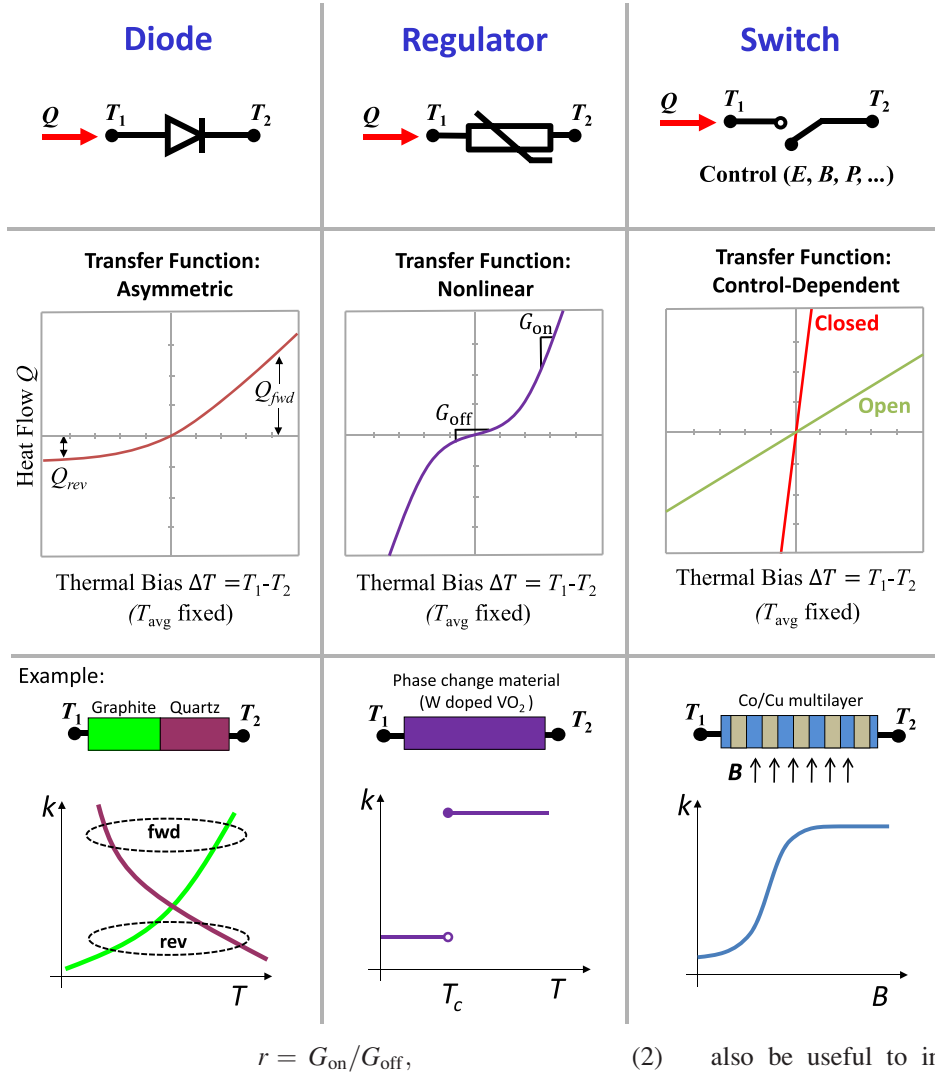


FIG. 2. Nonlinear and switchable thermal components. Thermal devices such as diodes, regulators, and switches are defined by their transfer functions, which relate the heat flow Q to the thermal bias $\Delta T = T_1 - T_2$, in analogy to current-voltage curves in the electrical domain. *Thermal diodes* have asymmetric heat transfer: at a fixed average temperature T_{avg} and $|\Delta T|$, the magnitudes of the forward and reverse heat transfer rates Q differ. *Regulators* have a strongly nonlinear transfer function, which can be symmetric or asymmetric. The transfer function of a *thermal switch* depends on a non-thermal control parameter such as electric field (E), magnetic field (B), or pressure (P). Bottom row: Examples of each type of component, each discussed further below with quantitative data. Conduction junction diodes are presented in Sec. III A 2, the W-doped VO₂ regulator is shown in Fig. 3, and experiments on the giant magnetoresistance Co/Cu multilayer switch are shown in Fig. 7.

where $G = \frac{dQ}{d(\Delta T)}$ is the differential thermal conductance, which is the local slope of the $Q - \Delta T$ transfer function, as shown in the center column of Fig. 2. This figure of merit r represents the ratio of the “on” state, or largest differential conductance G_{on} , to the “off” state, or smallest differential conductance G_{off} .

An example of a thermal regulator shown in Fig. 2 is a phase change material with a sharp change in k at a critical temperature T_c . This regulator example displays a nonlinear but symmetric $Q - \Delta T$ curve with a crossover from a low G to a high G state at $|\Delta T| = |T_c - T_{avg}|$. Quantitative data for two examples of these phase-change thermal regulators are shown below in Figs. 3 and 4. For most thermal regulator applications, phase transition hysteresis would be ideally minimized, such that the temperature is always regulated at the same T_c . Finally, in addition to the substantial change in k at T_c , materials undergoing first-order phase transitions also have a latent heat, which can assist in regulating the temperature at T_c for transient heat loads.

In an example application of regulation, a thermal regulator using bimetallic buckling¹⁷ reduced the power required to maintain the temperature of a chip-scale atomic clock at 70 ± 0.1 °C as the external temperature was varied from -40 to $+50$ °C. Having different G at different temperatures can

also be useful to improve the transient thermal response without sacrificing steady-state performance. A familiar example is a vehicle’s thermostat, which traps heat to quickly raise the engine temperature until the desired temperature T_c is reached. Once the system is at T_c , the wax in the thermostat melts, allowing coolant to flow freely to prevent overheating. In a related application, thermal regulators have been tested on catalytic converters^{18,19} to reduce cold-start emissions by keeping the converter hot enough between drive times, while switching to a high- G state at high temperatures to keep the converter from overheating. Several additional applications of regulators are presented in Sec. IV C 3.

C. Thermal switch

As indicated in the right column of Fig. 2, we define a thermal switch as a two-terminal component with a $Q - \Delta T$ constitutive relation that depends on a non-thermal control parameter, such as an electric field, magnetic field, or applied pressure. Changing this control parameter changes the thermal conductance. The on/off switching ratio r introduced for thermal regulators in Eq. (2) is also a natural figure of merit for a thermal switch, where now G_{on} is the highest differential conductance that can be achieved by tuning the control parameter, and G_{off} is the smallest achievable differential conductance.

An example of a thermal switch is a giant magnetoresistance (GMR) device,²⁰ illustrated in the bottom right of Fig. 2. Since k depends on the magnetic field (B), the heat flux can be tuned by changing B . As shown in Fig. 7, thermal switch ratios of $r = 2$ have been achieved at room temperature using this mechanism in GMR multilayers.²⁰

Spacecraft thermal management²¹ is one motivating example for thermal switches. Radiators which dump the excess heat generated in the spacecraft out to deep space must be sized for the peak heat rejection loads. However, when the spacecraft is generating much less heat, the same radiators may be too effective in rejecting heat, potentially causing the working fluid to freeze. Thermal switches can be used to actively control the heat rejection rates and spacecraft temperature. In Sec. III, we will discuss many different thermal switches, some of which were developed for spacecraft applications using the mechanisms of conduction (Sec. III A 4), convection (Sec. III B 2), and radiation (Sec. III C 4). Developing lighter and faster thermal switches with larger r would reduce costs and improve performance of these spacecraft thermal management systems, and many other potential applications, including the two examples of periodically switched circuits discussed in Sec. IV C 2.

III. MECHANISMS OF ACTIVE AND NONLINEAR HEAT TRANSFER

We now proceed to the heart of this article, which is a review of experimentally demonstrated mechanisms of switchable and nonlinear heat transfer, with a focus on mechanisms which function near room temperature. As a non-exhaustive introduction to Secs. III A–III C, Table I summarizes measured rectification ratios and switching ratios for a variety of physical mechanisms that have been used to make thermal switches, regulators, and diodes.

We organize the following discussion by the dominant mode of heat transfer: conduction, convection, and radiation.

A. Conduction

Heat in solids is primarily carried by electrons in metals and by phonons in semiconductors and insulators. The kinetic

theory model for the thermal conductivity is $k = Cv\Lambda/3$, where C is the volumetric specific heat, v is the group velocity, and Λ is the mean free path. Modifications to the microstructure or environment which change C , v , or Λ can therefore impact k , resulting in thermal diode, regulator, or switch behavior. Here, we discuss changes in k across phase transitions and review recent diode implementations which utilize $k(T)$ nonlinearities. We also review thermal switches and regulators which function by bringing materials into and out of contact, by intercalating ions into layered structures, and by utilizing magnetic and electric fields to control k .

1. Changes in k due to phase transitions

Since steady-state heat transfer depends only on the material's thermal conductivity and not on the specific heat or the latent heat of a phase transition, we focus here on changes in k occurring across phase transitions. For transient thermal regulation, the large latent heats of phase change materials such as waxes, salts, or water can also be useful.

Metal-insulator transitions: Metal-insulator transitions (MITs) dramatically change the electrical conductivity σ . In the best-known example, σ can increase by 5 orders of magnitude when vanadium dioxide crosses a MIT around $T_{MIT} = 340$ K. It is natural to suspect that the thermal conductivity of VO_2 may also show a large change across the MIT, since the standard single-electron Wiedemann-Franz (WF) law (Lorenz number $L = L_0 = 2.44 \times 10^{-8} \text{ W}\Omega/\text{K}^2$) predicts that both electrons and phonons contribute significantly to k in the metallic state, while in the insulating state only the phonon k remains. Indeed, several experiments^{22,23} have measured switch ratios as large as $r = 1.6$ in polycrystalline VO_2 films. However, these experiments measured k in the cross-plane direction and σ in the in-plane direction, so the WF law could not be quantitatively tested.

A recent experiment²⁴ using VO_2 single-crystal nanobeams [Fig. 3(a)] measured k and σ both in the in-plane direction and surprisingly found that the in-plane total k changes by $<5\%$ across the MIT, even with high σ in the metallic state. This small change in the total thermal conductivity across the MIT is consistent with early k measurements of

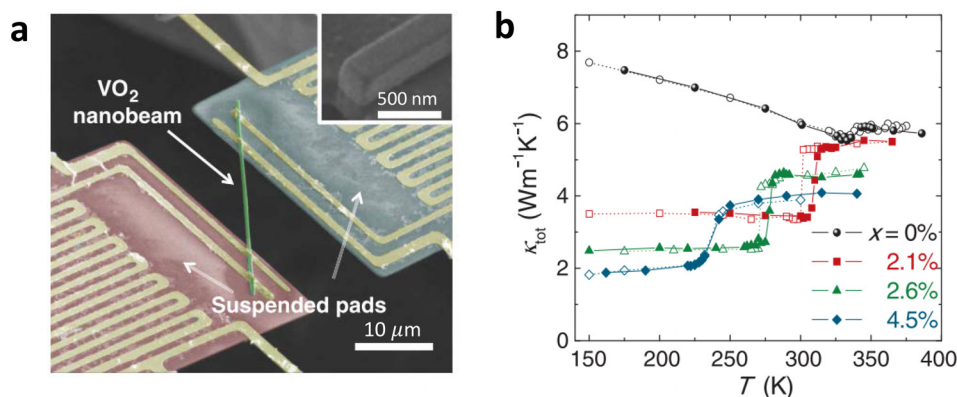


FIG. 3. Doped vanadium dioxide thermal regulator. (a) False color scanning electron microscope (SEM) image of the experimental setup to measure the thermal and electrical conductivity of VO_2 nanobeams doped with W. Inset: SEM image showing VO_2 nanobeam cross-section. (b) Measured total thermal conductivity of VO_2 nanobeams with different W doping fractions. Thermal regulator behavior is observed for the W-doped samples; for example, at 2.1 at. % W, the switching ratio is $r = 1.5$ around a switching temperature $T = 310$ K. Switching ratios of $r = 1.6$ have also been measured in undoped VO_2 thin films.^{22,23} Reprinted with permission from Lee *et al.*, Science **355**, 371 (2016). Copyright 2016 AAAS.

TABLE I. Overview of selected physical mechanisms of experimentally demonstrated nonlinear and switchable heat transfer, emphasizing higher performing and/or novel mechanisms. These examples, and many more, are discussed throughout Sec. III. All mechanisms operate near room temperature and atmospheric pressure unless noted otherwise. These figures of merit depend on the magnitude of the temperature difference and the absolute temperature (see main text).

Mechanism	Material system example	Thermal switches and regulators		Thermal diodes	
		On/off ratio $r = G_{on}/G_{off}$	Rectification $\gamma = \frac{G_{fwd} - G_{rev}}{G_{rev}}$	References	References
Conduction (Sec. III A)					
Metal-insulator transition (Fig. 3)	VO ₂ doped with W	1.5	—	24	
Phase-change memory	(Ge,Sb,Te) alloy	3	—	33 and 34	
Solid-liquid phase transition	H ₂ O	3.5	—	42	
Liquid-solid composites (Fig. 4)	Hexadecane/graphite	3	—	47	
Voltage tuning of ferroelectric k	PbZr _x Ti _{1-x} O ₃	1.1	—	130	
Intercalation control of k	Li _{1-x} CoO ₂	1.5	—	80	
Junction diodes $k(T)$	For example, PNIPAM/PDMS	—	0.1-0.6	64 and 72–74	
Solid-solid contact (>10 kPa contact pressures)	Cu-Cu with grease	>100	90	86 and 111	
Paraffin expansion	Encapsulated waxes	100	—	99	
Liquid bridge switch	Mercury	200	—	86	
Electrostatic gating of k_{el} (Fig. 6)	Graphene (at $T=75$ K)	5	—	126	
Magnetic field tuning of giant magnetoresistance k (Fig. 7)	Cu/Co multilayers	2	—	20	
Liquid crystal alignment	Liquid crystals	1.5	—	159	
Convection (Sec. III B)					
Natural convection diode	H ₂ O	—	7	3	
Heat pipe diode	H ₂ O	—	>100	179	
Jumping droplets (Fig. 8)	H ₂ O, on super-hydrophobic/phillic surfaces	2	150	180 and 201	
Variable conductance heat pipe (Fig. 9)	N ₂ gas and H ₂ O	80	—	189	
Gas gap switch (high vacuum)	H ₂	>500	—	190	
Electrowetting	H ₂ O on dielectric	2.5–15	—	194 and 195	
ElectroadSORption	Surfactants in H ₂ O	10	—	196	
Electrical suppression of Leidenfrost effect	Isopropyl alcohol	20	—	198	
Magnetic nanofluid forced convection	Magnetite	15	—	210	
Magnetorheological fluid chain alignment (Fig. 10)	Fe particles in oil	12	—	212	
Radiation (Sec. III C)					
VO ₂ emissivity across transition (Fig. 11)	VO ₂	2-3	2	256	
Electrochromic (Fig. 12)	WO ₃	2-10	—	257	
Liquid crystal regulators	Liquid crystals	2-5	—	268 and 269	
Louver view factor switching	Metals	6	—	99	
Near field gap size (<200 nm gaps, ultra-high vacuum)	Au-Au surfaces	>100	—	280	

bulk VO₂.^{25,26} Two possible explanations for this behavior have been historically suggested: either the phonon thermal conductivity k_{ph} significantly decreases across the transition to a metallic state as the electron thermal conductivity k_{el} increases in accordance with the WF relation,²⁶ or the change in k_{ph} is small and the typical WF relation ($L = L_0$) is not valid in metallic VO₂.²⁵ Based on calculations of k_{ph} in the metallic state using first-principles phonon dispersions and a fit to experimental measurements of energy-dependent phonon linewidths, Lee *et al.*²⁴ argue that k_{ph} is nearly unaffected by the phase transition, and conclude the correlated electrons in the metallic state of VO₂ carry much less heat than predicted by traditional single-electron theories ($L < L_0$).

Interestingly, however, when the VO₂ nanobeams are doped with only a few percent of W, thermal regulator

behavior is observed.²⁴ As shown in Fig. 3(b), the phase transition temperature of VO₂ is lowered to $T_{MIT} = 310$ K at 2.1 at. % doping of W, and k switches from 3.4 W m⁻¹ K⁻¹ in the insulating phase at low T to 5.2 W m⁻¹ K⁻¹ in the metallic phase at high T , resulting in $r = 1.5$. Lee *et al.*²⁴ interpret the data as indicating that the electrons in the metallic state of VO₂ tend to recover the WF behavior as the W doping increases. Other materials displaying metal-insulator²⁷ or metal-metal²⁸ transitions may also be promising thermal regulators; for example, a ferromagnetic magnetite material²⁹ has shown $r = 1.5$ across a MIT at 200 K.

Phase change memory: Chalcogenides such as Ge₂Sb₂Te₅ (GST), which is used in phase-change memory devices, can be switched between metastable structural states at room temperature.^{30,31} The crystal structure of GST is determined by the

thermal history. Rapidly quenching from a high temperature results in an amorphous state at room temperature, but crystalline structures can be recovered by reheating the material above the crystallization temperature and slowly cooling back to room temperature. Since crystalline materials have larger k than their amorphous counterparts, a thermal switch can be implemented by controlling the crystallinity. Lyeo *et al.*³² showed that the room temperature k of GST can range from 0.2 to 1.5 $\text{W m}^{-1}\text{K}^{-1}$ depending on the thermal history, though reversible switching was not demonstrated. The authors also note that the changes in k achieved using rapid laser crystallization are smaller ($r = 1.2$) than when the global temperature was slowly raised above the crystallization point. Reifenberg *et al.*³³ and Lee *et al.*³⁴ have measured increases in k of a factor of 3 for GST films when the temperature is slowly ramped, but also did not report reversible switching.

Miscellaneous solid-solid transitions: Modest switching ratios have been observed around other solid-solid phase transitions near room temperature. Huesler alloys³⁵ have shown r as large as 1.6 across a magnetostructural phase transition, and $r = 1.8$ has been measured^{36,37} across a structural phase transition near $T = 400$ K in Cu_{2-x}Se . At high pressures (>10 GPa), $r = 3$ has been observed in semiconductor-metal transitions³⁸ due to the enhanced electronic contribution to k . Charge-density wave (CDW) phase transitions can impact both the electron and the phonon

contributions to k . For example, a 25% increase in k of octahedral TaS_2 was observed³⁹ at the CDW transition at 350 K, and similar r has been measured^{40,41} in other CDW systems.

Melting solids: Typically, a liquid will have a lower thermal conductivity than its corresponding solid phase near T_{melt} , so melting a solid decreases k . Several familiar examples in the vicinity of room temperature include H_2O ($r = 3.5$ at $T_{\text{melt}} = 0^\circ\text{C}$),⁴² waxes ($r = 2$, with T_{melt} ranging from 50 to 80°C),⁴³ or liquid metals such as mercury ($r = 4$ at $T_{\text{melt}} = -38^\circ\text{C}$).⁴⁴ In a comprehensive recent study, Kim and Kaviani⁴⁵ analyzed different solid-liquid transitions to find the most promising candidates for achieving high r . They identified an interesting class of materials which are semiconducting in the solid state but metallic in the liquid state (all with $T_{\text{melt}} > 700$ K). Since the electrons in the liquid metal carry the heat effectively, k actually increases in the liquid state. First principles calculations of switching ratios as large as 15 for CdSb at $T_{\text{melt}} = 850$ K were in good agreement with previous measurements⁴⁶ of k and σ .

Composites: Composite materials undergoing liquid-solid transitions can also show thermal regulator behavior. If the liquid matrix freezes into a crystalline structure, the solid composite particles are pushed towards the grain boundaries and into better thermal contact, improving the heat transfer at low temperatures. As shown in Fig. 4, Zheng *et al.*⁴⁷ demonstrated this mechanism using graphite flakes suspended in

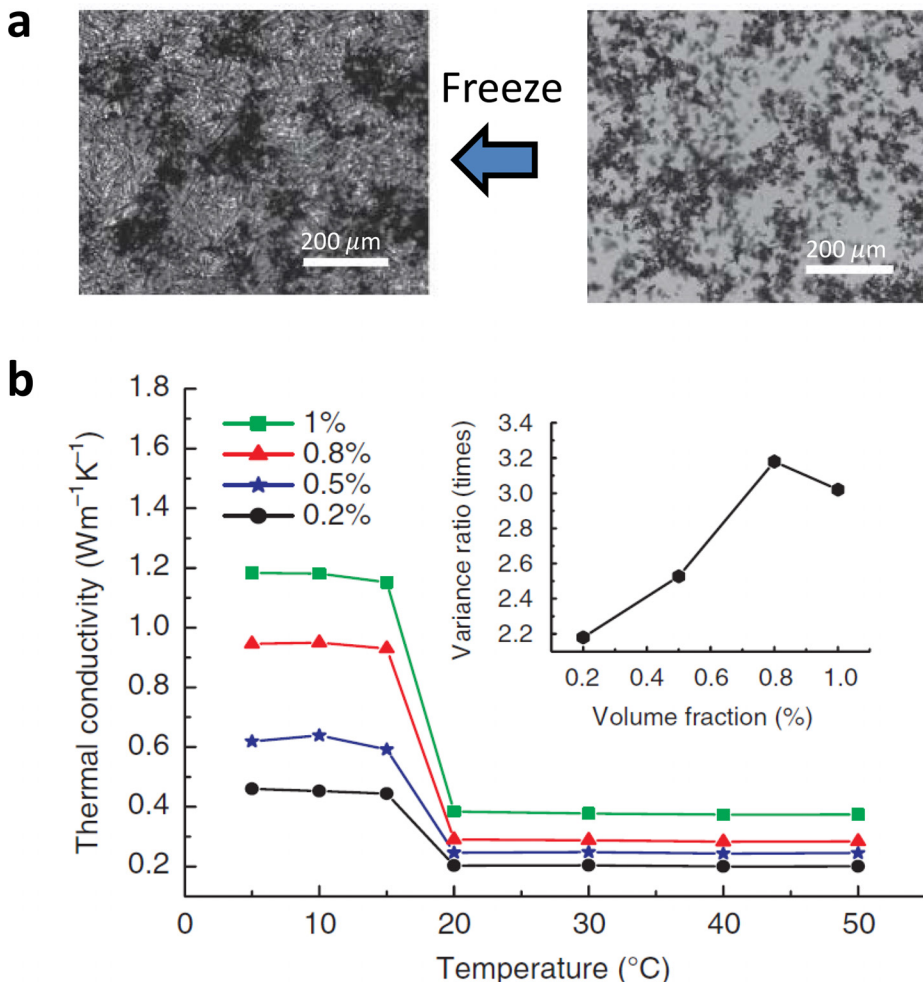


FIG. 4. Liquid-solid composite thermal regulator. (a) Optical images of a frozen (left) and melted (right) graphite-hexadecane composite. When the liquid (lighter color) freezes, the slight volumetric expansion pushes the graphite (darker color) into better contact at the grain boundaries of the hexadecane. (b) The thermal conductivity increases by up to a factor of 3 when the liquid freezes at 20°C , due to the improved graphite percolation pathways. The inset shows that the switching ratios also depend on the volume fraction of graphite. Adapted with permission from Zheng *et al.*, Nat. Commun. 2, 289 (2011). Copyright 2011 Macmillan Publishers Ltd.

hexadecane, and obtained r as large as 3. They also showed that this switching was reversible over 7 thawing/freezing cycles. Schiffres *et al.*⁴⁸ showed that the switching ratio can be tuned by controlling the freezing rate. Additional measurements for a variety of liquids and composite particles^{49–54} also resulted in r in the range of 2–3.

2. Conduction thermal diodes

This section emphasizes new advances in solid-state rectification since the 2011 review of Roberts and Walker.³

Ballistic phonon rectification: The idea of ballistic thermal rectification is to use asymmetric scattering elements, such as internal pyramids or sawtooth shaped surfaces, to preferentially scatter the phonons more strongly in one direction than another. However, such concepts require further careful thinking to ensure the vision remains compatible with the second law of thermodynamics. Maznev *et al.*⁵⁵ showed theoretically that to obtain a ballistic phonon thermal diode, a nonlinearity must be present in the system in addition to an asymmetric scattering structure. In accordance with this theory, Chen *et al.*⁵⁶ and Kage *et al.*⁵⁷ measured no measurable phonon rectification in asymmetrically etched silicon structures which lacked a significant nonlinearity. Although Schmotz *et al.*⁵⁸ inferred thermal rectification from measurements in an asymmetrically etched silicon membrane, Maznev *et al.*⁵⁵ showed that the experimental design lacked the proper symmetry reversals to conclusively claim rectification.

Rectification measurement technique: Chiu *et al.*⁵⁹ recently demonstrated a new experimental technique to test for nonlinearities. Since nonlinear systems generate higher order harmonics, time-periodic heating of a thermal diode should cause higher harmonics in the temperature response. These higher harmonics can be easily measured using a lock-in amplifier, although electrical nonlinearities also need to be considered. Using this technique, Chiu *et al.*⁵⁹ observed no rectification above the measurement threshold of 0.5% for either pristine nanowires or asymmetrically loaded mass-loaded BN nanotubes with diameter $d = 100$ nm. This null result contradicts the previously reported 7% rectification reported for asymmetrically mass-loaded BN nanotubes with $d \approx 30$ nm.⁶⁰ Chiu *et al.*⁵⁹ attribute this difference to the improved experimental design of the higher-harmonics technique compared with the previous steady-state measurement, but also note that the different nanotube diameters might also play a role.

Junction diodes: A simple mechanism for a solid-state thermal diode arises in composite bars made of two materials with different temperature-dependent thermal conductivities $k(T)$. If the thermal conductivities of materials 1 and 2 scale like $k_1 \propto T^{n_1}$ and $k_2 \propto T^{n_2}$, then for small temperature differences after optimizing geometry,¹⁰ the rectification is

$$\gamma = (n_1 - n_2)(T_h - T_c)/4T_{\text{avg}}. \quad (3)$$

Many demonstrations^{61,62} of this “junction diode” rectification mechanism were performed at low temperatures, where

$(T_h - T_c)/T_{\text{avg}}$ is large and k depends strongly on temperature. Above room temperature, Takeuchi *et al.*⁶³ achieved $\gamma = 0.1$, and Nakayama and Takeuchi⁶⁴ measured $\gamma = 0.6$ with $\Delta T = 240$ K. Recently, Wang *et al.*⁶⁵ used a focused ion beam to create nanopores in one region of suspended graphene, causing the irradiated and pristine sections to have different $k(T)$ trends near room temperature. Unexpectedly, the reported measurement of $\gamma = 0.26$ for $\Delta T = 35$ K exceeds the maximum rectification predicted by Eq. (3) by a factor of 3, warranting closer examination.

New junction diode theory: Interestingly, although measurements of $\gamma = 0.2$ were initially reported for a single material with an asymmetric shape,⁶⁶ further theoretical investigations by Wang *et al.*⁶⁷ showed that, in fact, rectification should not occur in asymmetric single materials with position-independent $k(T)$. Similarly, Go and Sen⁶⁸ showed that rectification is forbidden for steady state one-dimensional heat flow if the thermal conductivity can be separated as $k(T, x) = X(x)\Theta(T)$, where $X(x)$ is a function which depends only on position and $\Theta(T)$ is a function which depends only on temperature. In the junction diode mechanism, the composite bar’s thermal conductivity depends on (x, T) in a nonseparable manner, and rectification is observed. In another recent theoretical advance, Herrera, Luo and Go⁶⁹ numerically examined transient thermal transport in junction diodes, and predicted that the transient rectification ratios can be even larger than the steady-state values.

Phase transition junction diodes: Junction thermal diodes utilizing the temperature dependence of k across phase transitions have also been recently investigated. Both Zhang and Lou⁷⁰ and Cottrill and Strano⁷¹ constructed analytical models to describe rectification in junction diodes where one material undergoes a phase change. These models can be used to optimize γ by selecting the dimensions and the temperature range of the diode. Experimental demonstrations of such phase-transition-exploiting junction diodes include a diode constructed of a Nitinol shape memory alloy and graphite which displayed⁷² $\gamma = 0.5$ for $\Delta T = 160$ K, a diode made of gadolinium and silicon showed⁷³ $\gamma = 0.6$ for $\Delta T = 30$ K, and a diode constructed from a phase-change polymer PNIMAP and PDMS resulted in⁷⁴ $\gamma = 0.5$ for $\Delta T = 20$ K. Kobayashi *et al.*⁷⁵ measured $\gamma = 0.1$ with small temperature differences of 2 K across an oxide structural phase transition. Wang *et al.*⁷⁶ developed a foam-paraffin composite to utilize the solid-liquid phase transition of paraffin while maintaining mechanical stability. They measured $\gamma = 0.35$ with $\Delta T = 30$ K for this paraffin composite and PMMA junction diode. Excitingly, Wang *et al.*⁷⁶ also used these junction thermal diodes to build a thermal diode bridge which rectified an oscillating temperature profile (see Sec. IV B for a related rectification application). Finally, asymmetric VO₂ nanobeams displayed⁷⁷ $\gamma = 0.3$ for $\Delta T = 1$ K, which was attributed to the existence of metal-insulator domains along the length of the nanobeam.

3. Intercalation

Intercalating atoms between the atomic planes of layered materials changes the bonding strength and microstructure. *Ex situ* measurements indicate that permanent intercalation affects the thermal conductivity,^{78,79} and recent *in situ*

experiments^{80,81} have gone even further to show that electrochemistry can be used to reversibly switch k . Delithiating the battery cathode material LiCoO_2 decreased k by up to 40%,⁸⁰ and the changes were reversible upon re-lithiation. The switching timescales were on the order of 1 hour, limited by the ion diffusion time. It was also recently shown that intercalating Li ions between black phosphorous layers⁸¹ decreases the thermal conductivity in all three of the distinct crystallographic directions. For example, in the cross-plane direction, reversible switching ratios of $r = 1.6$ were demonstrated over 100 cycles.

4. Contact thermal switches and regulators

An efficient form of thermal switching, with some of the highest demonstrated switching ratios, relies on the simple mechanism of bringing materials in and out of contact. Achieving the largest r requires reducing the parasitic heat pathways in the off state due to convection or radiation, and minimizing the thermal contact resistance at the conducting interface in the on state by using polished surfaces, a thermal interface material, and moderate to high contact pressures (at least 10 kPa recommended to obtain $r = 100$).^{82,83} For example, McKay and Wang⁸⁴ used a bistable latching solenoid to make and break thermal contact in their thermal switch circuit discussed in Sec. IV B, and Wang *et al.*¹⁵ fabricated a silicon-based contact switch integrated with a linear actuator to achieve a measured $r = 27$ (see also Sec. IV A). Westwood⁸⁵ constructed a switch with an estimated $r = 2000$ using a silicone interface and 10 kPa contact pressures to increase the on-state conductance G_{on} between two metals in contact, and also reduced G_{off} by inserting a low- k aerogel between the metals in the off state.

Utilizing liquids to make thermal contact at the interface can overcome the need for high contact pressures in solid-solid interfaces. A liquid metal droplet switch⁸⁶ showed $r > 200$ due to the high liquid metal k . This switch achieved 100 Hz switching frequencies, and was used in a MEMS piezoelectric heat engine demonstration.⁸⁷ Thermal switches using dielectric fluid droplets^{88–90} have also been implemented to obtain high G_{on} , though G_{off} was not reported.

Electrostatic actuation: Another technique to improve thermal contact uses electrostatic forces to snap plates together. These electrostatic switches have been used to control the heat flux reaching spacecraft radiators,^{91–93} but typically require large snap-in and snap-out voltages to overcome stiction. Supino and Talghader⁹⁴ achieved $r = 2$ using an electrostatic MEMS thermal switch with an applied voltage of 26 V. Interestingly, since the electrostatic actuation time was much shorter than the characteristic thermal time constants in this application, pulse-width electrostatic modulation was used to achieve continuous sweeping of the effective thermal conductance G_{eff} . Kim *et al.*⁹⁵ built a MEMS electrostatic thermal switch which used an applied voltage of 100 V to snap suspended gold beams into contact with a hot source, decreasing the thermal resistance to the heat sink. The switching ratio was $r = 5–6$, and the switching was shown to be repeatable over > 200 cycles.

Nanoscale contact switching: The thermal conductivity of boron nanoribbon bundles⁹⁶ has been reversibly switched

by 20% by wetting the nanoribbons using different liquids, which changes the bonding strength between nanoribbons. Thermal switching ratios of 5 were achieved by “telescoping” multi-wall carbon nanotubes.⁹⁷ By cutting the outer nanotube walls and pulling on the nanotube, the outer walls slide past the rigid inner walls, reducing the pathways for heat transfer.

Thermal expansion regulators: A common example of a thermal regulator utilizing temperature-dependent mechanical contact is the thermal expansion valves in HVAC systems. These valves use the thermal expansion of a gas or liquid to control the cross-sectional area and resistance to fluid flow, passively maintaining the temperature at an optimal setpoint. Similarly, the expansion of paraffin waxes in the liquid state has been used to create regulators⁹⁸ with $r = 60$ for applications such as thermal control of a Mars rover. Chapter 10 in the Gilmore textbook⁹⁹ includes several designs of paraffin regulators that achieved $r = 100$ at room temperature. Copic and Hart¹⁰⁰ combined paraffin and carbon nanotubes forest to obtain large-stroke thermal switching actuators with a small footprint. Thermal expansion of metal droplets upon melting¹⁰¹ has been used to create thermal regulators with estimated $r = 25$. As an example of solid-state thermal expansion regulators, a bimetallic disc scavenged from a commercial thermostat has been used as a thermal regulator¹⁷ with $r = 1.2$ in air and $r = 1.8$ in vacuum. Thermal diodes utilizing the effects of asymmetric bimaterial thermal expansion have also been developed, with measured $\gamma = 0.07$ in solid composites¹⁰² and $\gamma = 1$ for a mercury-air interface.¹⁰³

Very large r can be obtained if small gaps between objects are pressed closed due to thermal expansion. To achieve good thermal contact between objects for high G_{on} , small gap sizes and high coefficient of thermal expansion (CTE) materials are desirable; however, manufacturing costs and cycling performance are concerns associated with small gap sizes, and high- k and machinable metals typically do not have large CTE. Innovative geometries and composite systems have been developed to address these problems. Guo *et al.*¹⁰⁴ reported that the thermal expansion of a flexible rod bringing metal pieces into contact at room temperature yield switching ratios $r = 400$, and Marland *et al.*¹⁰⁵ reported $r > 1000$ at $T = 230$ K using high CTE polymers to open and close a $100 \mu\text{m}$ gap between metal pieces.

At the nanoscale, Choe *et al.*¹⁰⁶ recently demonstrated a thin film VO_2 nanogap thermal regulator with $r = 2–2.5$. The VO_2 film expands when the temperature is increased above the metal-insulator transition temperature T_{MIT} , pressing together two polysilicon layers which are separated by a nanogap. The nanogap was created by etching a 20 nm sacrificial layer deposited between the poly-silicon. The switching was reversible over 100 cycles, and the fastest switching speeds were estimated to be ~ 1 ms.

Rather than using thermal expansion as the mechanism for making/breaking thermal contact, Bulgren *et al.*¹⁰⁷ used the temperature dependent magnetization of permanent magnets to reversibly actuate a thermally conducting disc. At low T , the strong magnetic force keeps the disc thermally coupled to the magnet, but at high T , the magnetization decreases and springs pull the disc out of contact. Further investigation of r for this mechanism would be of interest.

Shape memory alloys: SMAs are promising thermal regulators due to the large mechanical deformation induced when the SMA is heated above the solid-solid phase transition. Benafan *et al.*¹⁰⁸ used SMA springs to create a thermosiphon-based regulator with $r=4$, and SMA springs have also been used to regulate fluid flowrate and control the convective heat transfer.¹⁰⁹ SMAs have been combined with bimetallic strips in a thermal diode demonstration.¹¹⁰ Tso and Chao¹¹¹ designed and fabricated a SMA spring-based thermal diode with $\gamma > 90$, showing that very large switching and rectification can be achieved near room temperature using SMAs.

5. Electrostatic control of electron thermal conductivity

Electrons transport both charge and heat. The well-known Wiedemann-Franz (WF) relation, which is strictly applicable for elastic scattering in metals, relates the electronic conductivity (σ) and the electronic contribution to

thermal conductivity (k_{el}) as $k_{el} = \sigma TL$, where L is the Lorenz number. For many metals, L is within 10% of the free electron (or Sommerfeld) value¹¹² $L_0 = 2.44 \times 10^{-8} \text{ W}\Omega\text{K}^{-2}$.

Gating thermal conductivity: It would be quite appealing to re-appropriate electronic transistor technologies such as MOSFETs to control heat currents via electrostatic gating, as illustrated in Figs. 5(a) and 5(b). However, it turns out that the phononic contribution to the thermal conductivity k_{ph} often swamps the electronic contribution k_{el} in the regime where the electronic concentration n can be readily gated. Figure 5(c) displays this fundamental tradeoff for bulk materials.

For small n typical of moderately doped semiconductors, gating can effectively change k_{el} by controlling the local carrier concentration, but the total conductivity $k_{tot} = k_{el} + k_{ph}$ is negligibly affected, because $k_{ph} \gg k_{el}$. A typical estimate of the minimum possible k_{ph} for a fully dense amorphous material at room temperature ranges from $k_{ph,min} \approx 0.3\text{--}3 \text{ W m}^{-1}\text{K}^{-1}$; for a specific material, $k_{ph,min}$

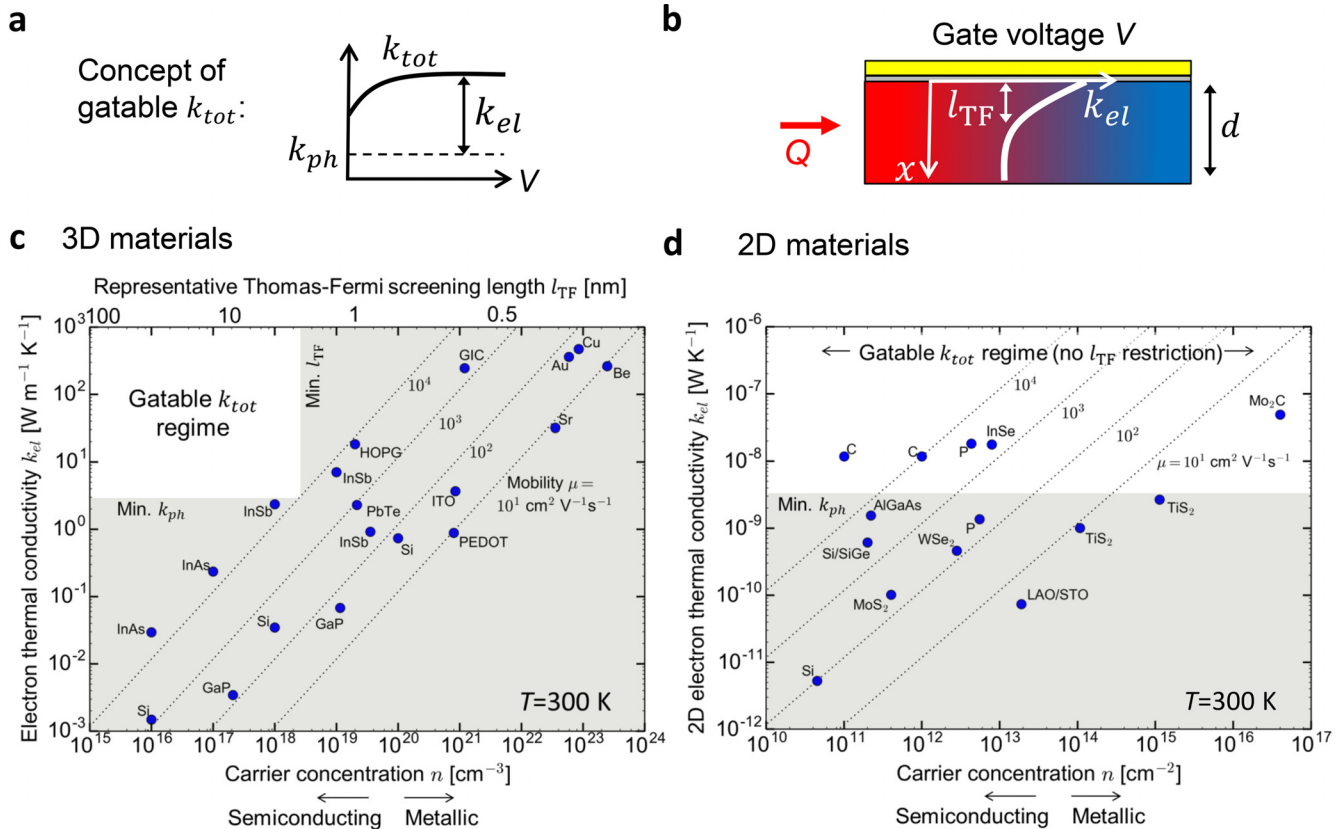


FIG. 5. A roadmap for electrostatic gating of the total thermal conductivity. (a) Since electrons carry both charge and heat, it is tempting to try to re-appropriate electronic transistors to modulate the heat flow by gating the electron contribution k_{el} . However, the phonon conductivity k_{ph} often dominates the total thermal conductivity k_{tot} in materials which can be electrically gated, overwhelming the variable k_{el} . (b) Schematic of gating k_{el} in a sample of thickness d . Since the characteristic Thomas-Fermi screening length l_{TF} sets the lengthscale over which k_{el} can be electrically modified from the far-field value, l_{TF} needs to be comparable with d to appreciably impact the total heat flow Q . (c) Here, we investigate the opportunity for gatable k_{tot} . Measured electronic conductivities σ for various 3D materials^{307–316} are converted to k_{el} using the Wiedemann-Franz law and plotted as a function of the carrier concentration n . (Several materials are represented with multiple points, which correspond to different doping levels). Intrinsic and lightly doped semiconductors ($n \leq 10^{17} \text{ cm}^{-3}$; bottom-left of plot) are readily gated since their l_{TF} (estimated on the upper axis using silicon's dielectric constant) are relatively large ($>10 \text{ nm}$); unfortunately, k_{el} is still far too small compared with even an optimistic lower-bound estimate of the phonon conductivity $k_{ph,min} \sim 0.3 \text{ W m}^{-1}\text{K}^{-1}$. On the other hand, metals (top-right of plot) have large $k_{el} \gg k_{ph}$, but metals screen electric fields so efficiently that the applied voltages cannot appreciably change k_{el} . These conflicting restrictions (shaded areas) prevent k_{tot} from being tuned, though materials with high mobilities μ (diagonal dotted lines) offer the best tradeoff between high k_{el} and low n . (d) A similar analysis for 2D materials and 2D electron gases. These appear more promising for tunable k_{tot} due to their high μ and the weak screening of out-of-plane electric fields. Again, experimental measurements^{116,118,119,317–325} of σ are converted to k_{el} and plotted as a function of n . We use the natural 2D units for k_{el} and n to convert to more familiar 3D units, simply divide by the sample thickness. Though 3D metals are not effectively gated, it is possible that n and k_{tot} could be gated with large electric fields in recently fabricated metallic 2D materials such as Mo_2C .¹¹⁸

can be more accurately estimated using the model of Cahill, Watson, and Pohl.¹¹³ For many single- or poly-crystalline materials, k_{ph} can be up to several orders of magnitude larger than $k_{ph,min}$; the purpose of using the optimistic (low) value $k_{ph} \approx k_{ph,min}$ here is to illustrate that if k_{el} is already much smaller than $k_{ph,min}$, gating k_{tot} in the real material would be quite challenging.

For large n found in heavily doped semiconductors or metals, k_{el} is a significant (or even dominant) portion of k_{tot} ; however, the challenge now is that it is difficult to gate large n . The depth of the gated channel, where n and thus k_{el} are substantially altered from their far-field bulk values, can be estimated by the characteristic Thomas-Fermi screening length (l_{TF}).¹¹⁴ Representative values of l_{TF} at 300 K are given along the top axis of Fig. 5(c) assuming a free electron dispersion relation and using the dielectric constant (ϵ) of silicon. For semiconductors ($n < 10^{20} \text{ cm}^{-3}$) at room temperature, l_{TF} reduces to the simpler Debye screening length $l_d = \sqrt{\frac{\epsilon k_b T}{e^2 n}}$, where ϵ is the dielectric constant, k_b is the Boltzmann constant, and e is the electron charge. Note crucially that l_d is proportional to $1/\sqrt{n}$, indicating that free carriers are very effective in screening electric fields. Due to this screening restriction, the maximum n for which significant gating effects on k_{tot} can occur in a channel at least $\sim 2 \text{ nm}$ thick is on the order of $n \sim 10^{18} \text{ cm}^{-3}$.

Considering these competing effects, the potential sweet spot for seeking gatable k_{tot} in 3D materials at 300 K lies in the regime of low k_{ph} , moderate n , and large mobility μ , as indicated by the un-shaded regime in the upper-left of Fig. 5(c). It will be necessary to achieve σ at the very least larger than 1400 S/cm ($\rho < 0.7 \text{ m}\Omega \text{ cm}$) to obtain $k_{el} > 1 \text{ W m}^{-1} \text{ K}^{-1}$ (comparable to $k_{ph,min}$), yet with n no more than $\sim 10^{18} \text{ cm}^{-3}$ to maintain a channel of at least $\sim 2 \text{ nm}$ thickness. Interestingly, the requirements of high σ and low k_{ph} at intermediate n are also shared by thermoelectric materials,¹¹⁵ so some thermoelectric systems may be promising avenues for electrostatic gating of k .

Recent developments in fabricating two-dimensional (2D) materials with high σ may open new opportunities for gating k_{el} , as illustrated in Fig. 5(d). 2D semimetals or semiconductors such as graphene and black phosphorene have enticingly large mobilities, but also typically have large k_{ph} . A different approach is to gate 2D metals, which compensate for their small μ with large n to achieve k_{el} comparable to the minimum k_{ph} . 2D systems also have a unique advantage because their carriers are confined to the 2D plane, which means they cannot efficiently screen electric fields applied in the out-of-plane direction. Thus, the carrier concentration even in metals can be controlled by electrostatic gating without strong screening effects.¹¹⁶ Recently, high- σ 2D metals and semimetals such as Ti_2Se ,¹¹⁶ encapsulated NbSe_2 ,¹¹⁷ and Mo_2C ¹¹⁸ have been fabricated, and metallic 2D electron gases have been observed at oxide interfaces.¹¹⁹ The conclusion of this analysis [Fig. 5(d)] is that k_{tot} switching may be possible in 2D materials, though large electric fields would be required to make significant changes to n for 2D metals. Another critical requirement will be to keep any parasitic

shunt heat transfer pathways through encapsulating layers and substrates to an absolute minimum.

Wiedemann-Franz breakdown: Another avenue for gating k_{tot} can be found in the regimes where the WF relation breaks down. If the electrons carry much more heat than predicted by the WF law ($L \gg L_0$), k_{el} could be larger than k_{ph} , even in the low σ materials which are easily gated. One significant breakdown of the WF law occurs when the carriers are strongly interacting and the classic Fermi liquid (single-electron) picture no longer accurately describes the transport.^{120,121} Though many of the deviations from the WF law occur at low temperatures,^{122,123} Wakeham *et al.*¹²⁴ used measurements of the thermal Hall effect to infer a large $L/L_0 > 10$ at room temperature in $\text{Li}_{0.9}\text{Mo}_6\text{O}_{17}$. However, Cohn *et al.*¹²⁵ conducted additional transport measurements for this material and proposed an alternative bipolar transport model with $L \approx L_0$.

Non-Fermi liquid behavior has been recently observed in graphene at liquid nitrogen temperatures.¹²⁶ When the electron-electron scattering is strong, the carriers come to their own local equilibrium and $L \gg L_0$.¹²¹ Figure 6, reproduced from Crossno *et al.*,¹²⁶ shows that k_{el} of h-BN encased graphene (measured using a novel Johnson noise thermometry technique¹²⁷) can be switched by a factor of 5 using electrostatic gating at 75 K. In this strongly interacting regime near zero gate voltage (Dirac point), k_{el} is much larger than predicted by the WF relation ($L/L_0 \sim 22$), while at larger gate voltages, the transport is well-described by the Fermi liquid picture and the WF law holds. In addition, at higher temperatures, the increased electron-phonon scattering rate breaks the strongly interacting regime near zero gate voltage,

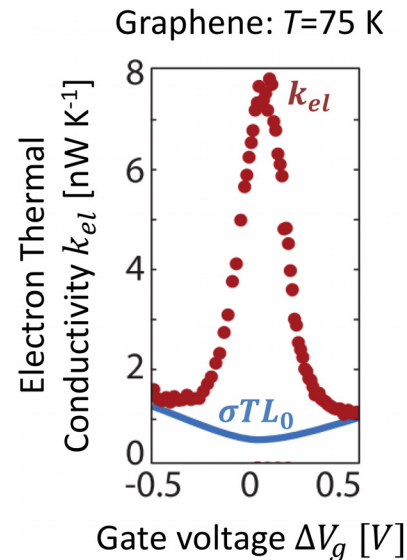


FIG. 6. Gating electronic thermal conductivity in graphene. The electronic thermal conductivity k_{el} in hBN-encapsulated graphene can be switched by a factor of 4 at $T = 75 \text{ K}$ using electrostatic gating. The strong carrier interactions in graphene cause k_{el} to be much larger than the Wiedemann-Franz (WF) law $k_{el} = \sigma T L_0$ near the charge-neutral (Dirac) point at zero gate voltage. The WF law becomes accurate for larger gate voltages and for $T > 100 \text{ K}$ (not shown). The phonon contribution to k_{tot} was not measured but may be significant at these temperatures, so from these results it is not yet clear whether the total thermal conductivity is also significantly gatable. Reproduced with permission from Crossno *et al.*, *Science* **351**, 1058 (2016). Copyright 2016 AAAS.

decreasing k_{el} and reducing the efficiency of thermal switching. A previous study¹²⁸ using resistance thermometry also showed that k_{el} of suspended graphene can be gated from $2\text{--}4\text{ Wm}^{-1}\text{K}^{-1}$ at 100 K. It must be noted that these exciting studies^{126,128} only measured k_{el} , so future work measuring k_{tot} as a function of gate voltage and temperature would be very useful to understand the fundamental limits for thermal switching using graphene.

6. Controlling phonon k with electric fields

Although phonon transport in most materials is unaffected by electric fields (E), materials such as ferroelectrics, which display a spontaneous electric polarization below the Curie temperature, offer promise for tunable k_{ph} using E fields.

Domain walls: The ferroelectric domain wall density is thought to impact phonon transport.¹²⁹ In the absence of a poling E field, large samples have domains with different polarizations. By applying an E field, the domain wall density decreases as the dipoles align with the field. Room temperature k switching by reconfiguring domain walls was recently demonstrated¹³⁰ in $\text{Pb}(\text{Zr,Ti})\text{O}_3$, resulting in an $\sim 8\%$ change in k with 475 kV/cm E fields and sub-second switching times. The proposed mechanism envisions that the domain walls scatter phonons in a manner analogous to grain boundary scattering, so controlling the domain wall density with an E field can switch k_{ph} .

Ferroelectric transitions: Ferroelectric phase transitions involve atomic displacements. This atomic re-arrangement near the phase transition can be influenced by E fields, as indicated by heat capacity measurements, $C(E)$.¹³¹ Though field-dependent k measurements at high temperatures are sparse, E fields of 4.2 kV/cm were used to increase k_{ph} by 20% in the ferroelectric material triglycine sulfate¹³² near the phase transition at 48°C . $k(T)$ ¹³³ and $C(T)$ ¹³¹ measurements indicate that BaTiO_3 may be another promising candidate for achieving $k_{ph}(E)$.

Ferroelectric strain coupling with metals: If E fields induce strain in a dielectric substrate, and that induced strain affects the electrical conductivity of a metallic thin film, then k_{el} of the metallic film could be tuned. Though the thermal conductivity was not measured, 20% σ modulation in metallic FeRh alloy films on ferroelectric substrates has been observed¹³⁴ using 1 kV/cm electric fields near the FeRh magnetic phase transition at 375 K. Using the WF relation, this σ modulation would correspond to a thermal conductivity change of $\Delta k_{el} \sim 5\text{ Wm}^{-1}\text{K}^{-1}$.

7. Controlling k with magnetic fields

Thermomagnetic phenomena arise from the transport of heat by charged particles in a magnetic field (B). The WF relation still holds in the presence of B fields,¹³⁵ so the $k_{el}(B)$ tensor can in principle be determined from the dependence of the σ tensor and the thermoelectric tensors on the magnetic field B . Given the numerous tensorial quantities in play, care must be taken to account for the various thermoelectric and thermomagnetic phenomena when reconstructing the k tensor from electrical measurements.

Magnetoresistance: Though classical longitudinal and transverse magnetoresistance models for bulk materials¹³⁵ predict that the B field increases the electrical resistivity and decreases k_{el} , the magnitude of this effect is negligible ($<1\%$) for most metals at room temperature. For ferromagnetic metals, the anisotropic magnetoresistance effect utilized in magnetic read heads can change k by several percent.¹³⁶ Interestingly, larger classical magnetoresistance effects have been observed in semimetals such as bismuth which have atypical Fermi surfaces. Early B -dependent measurements of bismuth¹³⁷ and bismuth-antimonide alloys¹³⁸ measured k switching ratios around $r = 1.2$ near room temperature. More recent measurements of room temperature σ have shown electrical switching ratios up to 2.5 at 4 T in bismuth thin films¹³⁹ and 2.5 at 9 T in single crystals of high- σ NbP.¹⁴⁰ (Here, and throughout this review, we report the free-space magnetic field $B = \mu_0 H$, where μ_0 is the vacuum magnetic permeability.) Further investigation of the maximum achievable k switching ratios in these semimetals could be quite interesting.

Giant magnetoresistance (GMR) occurs when nanoscale metallic ferromagnets are separated by thin nonmagnetic metallic domains.¹⁴¹ The resistivity in both the cross-plane and in-plane directions depends on the relative magnetizations of the ferromagnetic domains; if the magnetic moments are anti-parallel, then the resistivity is high, while aligning the moments with an external field decreases the resistivity. In these metallic systems, the electrons dominate the heat transfer, and magnetic switching of k has been demonstrated both at cryogenic^{142–145} and room temperatures.^{20,146,147} Figure 7(a) shows an experimental setup used by Kimling *et al.*²⁰ to measure the cross-plane k of a Co/Cu multilayer. Figure 7(b) shows that k switching ratios of $r = 2$ can be achieved with 0.2 T fields at room temperature. The in-plane k of GMR multilayers also depends on the B field,^{146,147} with measured $r = 1.2$.

Though other forms of magnetoresistance have displayed large σ switching, for the purposes of k switching, it is essential to consider whether electrons or phonons carry the heat. For example, tunnel magnetoresistance (TMR)¹⁴⁸ occurs when metallic ferromagnets are separated by nonmagnetic insulating domains. Unlike in the GMR metal-metal systems, the thermal transport at these TMR junctions is likely dominated by phonons, since applying the interfacial form of the WF relation¹⁴⁹ to measured contact resistance values in Fe/MgO/Fe interfaces¹⁴⁸ yields electronic thermal boundary conductances at least three orders of magnitude smaller than typical phonon boundary conductances.¹⁵⁰ Likewise, the colossal magnetoresistance (CMR)^{151–154} effect associated with the paramagnetic-ferromagnetic phase transition in some oxides can produce electronic switching ratios as large as 10^3 near the phase transition. However, k_{ph} is often much larger than the WF prediction for k_{el} in these materials due to the small n . Interestingly, Visser *et al.*¹⁵⁵ reported a k switching ratio around $r = 1.3$ in CMR systems with low σ , indicating that the phonon transport may also be impacted by the B field near the phase transition. Euler *et al.*¹⁵⁶ also measured $r = 1.2$ near the CMR phase transition and attributed the switching to a combination of electron and phonon contributions.

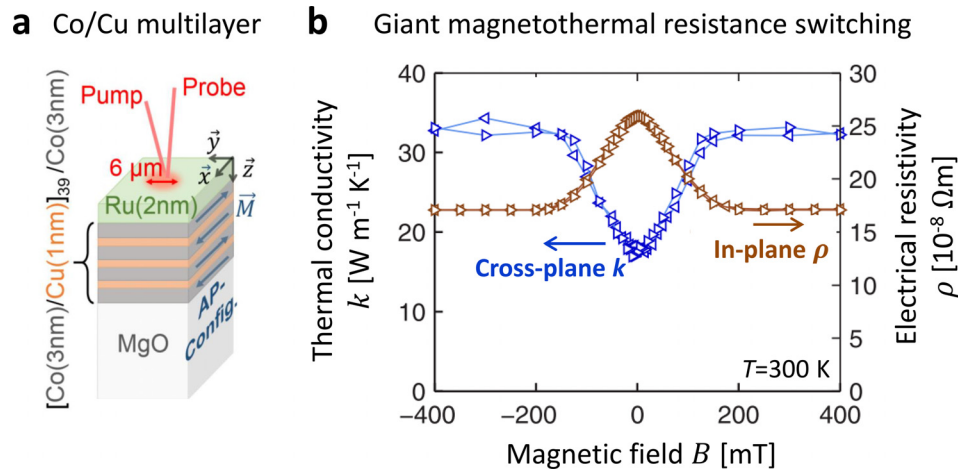


FIG. 7. Magnetic control of thermal conductivity in giant magnetoresistance (GMR) Co/Cu multilayers. (a) Schematic of cross-plane thermal conductivity measurement of Co/Cu multilayers. The transport properties depend on whether the magnetization (\vec{M}) of the alternating Co layers is parallel (P) or anti-parallel (AP). (b) Applying an external magnetic field (B) aligns the layer magnetizations, which reduces the electron scattering rates and increases the cross-plane k by a factor of 2. The direction of the triangles (left or right) indicates the direction of the B field sweep. Reprinted with permission from Kimling *et al.* Phys. Rev. B **91**, 144405 (2015). Copyright 2015 American Physical Society.

B field microstructure alignment: Magnetic forces can change the microstructure of some materials, which is another route to obtain $k_{ph}(B)$. One example is the magnetic alignment of liquid crystals,¹⁵⁷ which are assemblies of molecules with a preferred alignment in their low-temperature nematic phase. Since heat is more efficiently carried along the backbone of the molecule than between molecules, aligning the molecules increases k in the aligned direction and reduces k in the perpendicular directions.¹⁵⁸ Shin *et al.*¹⁵⁹ achieved $r = 1.5$ by heating the liquid crystal to a high temperature disordered state, applying a B field to align the molecules, and then cooling to the high-viscosity aligned state to freeze in the orientation before removing the field. Sahraoui *et al.*¹⁶⁰ measured similar r using E fields to align polymer-dispersed liquid crystals. In this measurement, the liquid crystal recovered its isotropic orientation once the E field was removed. Thermal devices such as concentrators¹⁶¹ and diodes¹⁶² have been proposed using the dependence of k on liquid crystal alignment.

Other low-dimensional materials with anisotropic magnetic susceptibilities such as nanotubes,¹⁶³ graphene oxide,¹⁶⁴ and graphene¹⁶⁵ can also be oriented in aqueous suspensions using B fields. Sun *et al.*¹⁶⁶ showed that the thermal conductivity of suspended graphite flakes with attached magnetic nanoparticles can be switched by a factor of 3 in 0.05 T fields, though mild hysteresis was observed over 10 cycles.

8. Electrothermal coupling and feedback

Joule heating is a nonlinear coupling between the electrical and thermal domains. If σ depends on temperature (or other external parameters), the heat dissipated via Joule heating can be controlled, even though the thermal properties themselves (e.g., k) are not varying. This electrothermal coupling was recently utilized¹⁶⁷ to passively prevent battery thermal runaway. If the battery overheats, thermal expansion breaks a percolation pathway, which increases the electrical resistance and reduces the Joule heating. Transition-edge

bolometers¹⁶⁸ use electrothermal feedback to quickly reset the bolometer at the desired temperature after the electrical resistance is perturbed by the absorption of light. The electrothermal coupling near the phase transition in a VO₂ nanobeam was also exploited¹⁶⁹ to create a thermal Schmitt trigger, where a small increase in the input temperature results in a large increase in output temperature, due to the VO₂ metal-insulator transition and the electrothermal feedback.

B. Convection

The key engineering parameter in convection is the average heat transfer coefficient $h \equiv Q/(A\Delta T)$, where A is the surface area. h depends on the geometry, fluid properties, flow velocity and state (laminar or turbulent), and whether the fluid is driven by an external pressure gradient or induced by buoyancy (forced vs. free convection), any of which represents a potential mechanism to control the heat transfer.

Switchable and nonlinear convection have been widely investigated for many years. Clearly, highly efficient thermal switching is regularly achieved using valves or pumps to control the fluid flowrates, and therefore h . From a fundamental perspective, nonlinear convective heat transfer has also been extensively studied because the coupling between the hydrodynamic and thermal domains leads to rich physics. Indeed, Lorenz's nonlinear model for natural convection led to the discovery of chaotic behavior in deterministic systems.¹⁷⁰

Our coverage of switchable and nonlinear heat convection here focuses on recent experimental demonstrations of thermal rectification, thermal switching with thin gas gaps, and heat flux control with electric and magnetic fields. In addition, we illustrate several examples of mature thermal diode and regulator technologies utilizing liquid-vapor phase change in heat pipes.

1. Fluid thermal diodes

Natural convection: Consider a fluid which is confined between two horizontal plates that are separated by a

distance L . Since this configuration has no free surfaces (i.e., no liquid-vapor interfaces), surface tension phenomena such as the Marangoni effect do not come into play. Most fluids have positive thermal expansion coefficients (β), so fluids in a gravitational field (g) which are heated from below will expand and rise. This bulk fluid motion results in efficient heat transfer from the hot bottom plate to the cold top plate. However, when this same fluid is heated from above while the bottom plate is cold, the fluid is stable against natural convection and the heat is transferred only by conduction, a broken symmetry which results in rectification. The rectification ratio increases with increasing Rayleigh numbers Ra_L , a dimensionless group defined as $Ra_L = g\beta\Delta TL^3/\alpha\nu$, where L is the confining fluid gap distance, α is the thermal diffusivity, and ν is the kinematic viscosity. Using an experimental correlation¹⁷¹ valid over the range $3 \times 10^5 < Ra_L < 7 \times 10^9$, and neglecting a weak dependence on the Prandtl number $Pr = \nu/\alpha$, the predicted rectification is $\gamma \approx 0.07Ra_L^{1/3}$. For liquid water at room temperature with $\Delta T = 50$ K and $L = 1$ cm, this correlation gives $\gamma \approx 7$. In this Ra_L regime, γ increases linearly with L , so very large rectification ($\gamma > 100$) is accessible for large gaps ($L > 15$ cm) and temperature differences ($\Delta T = 50$ K).

From the Ra_L definition, we see that increasing the material property figure of merit $\beta/\alpha\nu$ will increase γ . Interestingly, although gases have larger β , liquids have much smaller α and ν , and correspondingly much larger γ can be achieved using liquids (such as water or ethylene glycol) than using gases.³ However, this natural convection mechanism may be restricted to use in only specialized applications, since γ depends critically on the orientation with respect to gravity, and relatively large temperature differences are required to obtain high forward-mode h (for example, $\Delta T = 50$ K is required to obtain $h = 500 \text{ Wm}^{-2}\text{K}^{-1}$ for water).

Heat pipes: Larger γ with higher forward-mode conductances at smaller ΔT can be achieved using the liquid-vapor phase change in heat pipe thermal diodes. Heat pipe diodes are a relatively mature technology, and they have been developed for diverse applications ranging from temperature control of spacecraft sensors and electrical devices,¹⁷² thermal energy storage,¹⁷³ nighttime radiative cooling,¹⁷⁴ and temperature control of buildings for reduced energy consumption.¹⁷⁵

In a large-scale infrastructure application, gravity-driven heat pipe thermal diodes known as thermosiphons were installed on the Trans-Alaska Pipeline System¹⁷⁶ and the Qinghai-Tibet Railway¹⁷⁷ to prevent permafrost melting. Many different heat pipe thermal diode designs with asymmetric shapes have been demonstrated (including the liquid trap diode, the liquid blockage diode, and the gas blockage diode), and these designs have been discussed in textbooks.^{175,178}

One example that provides a sense of heat pipe thermal diode performance is the liquid trap diode developed by Groll *et al.*¹⁷⁹ This diode has an asymmetric shape, with a liquid trap appended on one end of a traditional heat pipe. In the forward mode, the end of the heat pipe with the liquid trap is heated, the liquid in the liquid trap evaporates, and the thermal diode functions as a typical heat pipe. When the other end of the heat pipe is heated, however, the liquid condenses in the liquid trap and cannot return to the hot section. Evaporation ceases, and heat is carried only by conduction. This liquid-trap diode has a large forward-mode conductance ($G_{fwd} = 13.8 \text{ W/K}$, in agreement with an estimated evaporation heat transfer coefficient $h = 7000 \text{ Wm}^{-2}\text{K}^{-1}$) and shows large rectification ($\gamma = 310$) with a small temperature difference ($\Delta T = 10$ K). However, like other heat pipe thermal diodes, the liquid-trap diode only works for certain gravitational orientations, since the liquid trap floods the main heat pipe if tilted.

Jumping droplets: The jumping droplet thermal diode^{180,181} illustrated in Fig. 8 is a phase change convective thermal diode which does not depend on the gravitational orientation. The jumping droplet mechanism occurs when multiple small droplets coalesce into a large droplet and use the energy gained from reducing the surface area to jump off a superhydrophobic surface.¹⁸²

Figure 8(a) shows a schematic of the jumping droplet thermal diode. In the forward mode, the vapor evaporated from the hot superhydrophilic surface condenses on the cold superhydrophobic surface. The liquid is efficiently returned to the hot side by droplet jumping from the cold side. In the reverse mode, droplet jumping does not occur on the cold superhydrophilic surface, and fluid circulation in the diode ceases. As a result, the heat is mainly transferred by conduction through the spacer, and the diode has a low G_{rev} . As shown in Fig. 8(b), Boreyko, Zhao, and Chen¹⁸¹ constructed

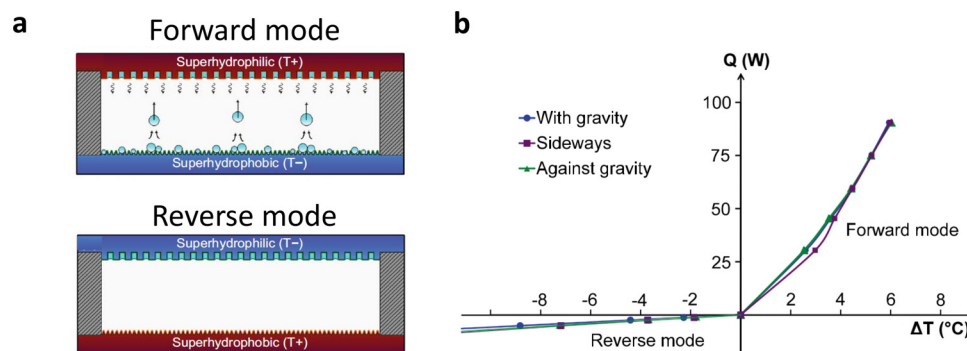


FIG. 8. Jumping droplet thermal diode. (a) In the forward mode, coalescing water droplets jump off the cold superhydrophobic surface to be later evaporated at the hot superhydrophilic surface, leading to high conductance. In the reverse mode, droplets remain on the cold superhydrophilic surface, and the heat flux is much smaller. The gap between the plates is 1.6 mm. (b) Experimental results showing a rectification ratio of $\gamma = 23$ with a fixed cold side temperature $T_c = 25^\circ\text{C}$ and pressure $P = 10$ kPa. The rectification does not depend on the orientation with respect to gravity. From Appl. Phys. Lett. **99**, 234105 (2011). Copyright 2011 AIP Publishing LLC.

a jumping droplet thermal diode with $\gamma = 23$, and showed that there was no dependence on gravitational orientation. Increasing the vapor temperature increased the rectification, with measured values as large as $\gamma = 150$. Zhou *et al.*¹⁸³ demonstrated a similar jumping droplet thermal diode with $\gamma = 5$. They reported partial surface degradation after use, which will be an important consideration in applications.

Tsukamoto *et al.*¹⁸⁴ also utilized superhydrophobic and hydrophilic surfaces in a thermal diode. However, instead of using the jumping droplet mechanism to return the condensed water to the hot hydrophilic surface in the forward mode, their MEMS device uses surface tension forces to propel the droplets back to the hot surface by wicking through microchannels. This device achieved $\gamma = 2$ with very small temperature differences ($\Delta T = 1^\circ\text{C}$).

2. Convection thermal regulators

Liquid-vapor phase change: The strong nonlinearities of h during liquid-vapor phase change can be used for thermal regulation. Here, we give only a few illustrative examples of nonlinearities in pool boiling¹⁷¹ and refer the reader to the phase change heat transfer literature for more details.^{185,186}

Boiling heat transfer coefficients can increase by more than a factor of 100 with only small (10°C) increases in superheat above the saturation temperature T_{sat} . The temperature dependence of the heat flux q'' also evolves through the phase change. In the crossover from laminar natural convection to nucleate boiling, for example, the temperature scaling of q'' changes from $(\Delta T)^{5/4}$ to $(\Delta T)^3$. This strong $h(T)$ dependence could be used to regulate the temperature $5\text{--}10^\circ\text{C}$ above T_{sat} where the onset of nucleate boiling occurs. Finally, and most dramatically, fluid dryout at the critical heat flux (q''_{CHF}) can even lead to negative differential thermal resistance (NDR), in which q'' decreases as the controlled ΔT increases until the heat flux reaches a minimum value q''_{min} at the Leidenfrost point. In Sec. IV C 3, we discuss a circuit which could utilize this NDR in a thermal amplifier. If the heat flux q'' is controlled instead of the temperature, the boiling curve displays hysteresis (where ΔT at a given q'' value depends on the thermal history) and instability (where large jumps in ΔT result from small changes in q'' near q''_{CHF} or q''_{min}).

Variable conductance heat pipe (VCHP): The VCHP^{99,175,187} is a widely studied thermal regulator. Figure 9(a) shows a gas-blockage VCHP, which has a low G at low temperature and a high G at high temperature. The working fluid vapor travelling from the evaporator towards the condenser sweeps the non-condensable gas (NCG) along with the vapor, until the NCG is concentrated at the condenser end of the heat pipe. The vapor then condenses and is refluxed towards the evaporator using a wick. For a low evaporator temperature (T_{evap}), there is relatively little working fluid vapor, so the NCG blankets the cold condensation section at temperature T_{cond} and the effective heat transfer area on the cold side is small. At higher temperatures, the working fluid's vapor pressure increases and the vapor compresses the NCG, increasing the effective area for condensation, and correspondingly G . The switching temperature can

be varied by controlling the amount of the NCG. In addition, if an external temperature control unit is set around the gas reservoir to control the NCG volume and pressure, the VCHP can act as an active thermal switch.¹⁸⁸ The gas blockage VCHP has been used for temperature control in spacecraft¹⁸⁸ and vehicle¹⁸⁹ components.

Figure 9(b) compares experimental data from Leriche *et al.*¹⁸⁹ for an ordinary heat pipe and a VCHP. When the temperature rise $\Delta T = T_{evap} - T_{cond}$ reaches 50°C (corresponding to $T_{evap} = 80^\circ\text{C}$) the VCHP switches to a high conductance state, with switch ratios around 200. This sharp change in the $Q - \Delta T$ curve means that the VCHP can regulate the temperature effectively. However, this VCHP did not work for all gravitational inclinations, which was thought to be due to the gravitational forces limiting the rate at which the condenser liquid was wicked back to the evaporator.¹⁸⁹

a Variable conductance heat pipe (VCHP)

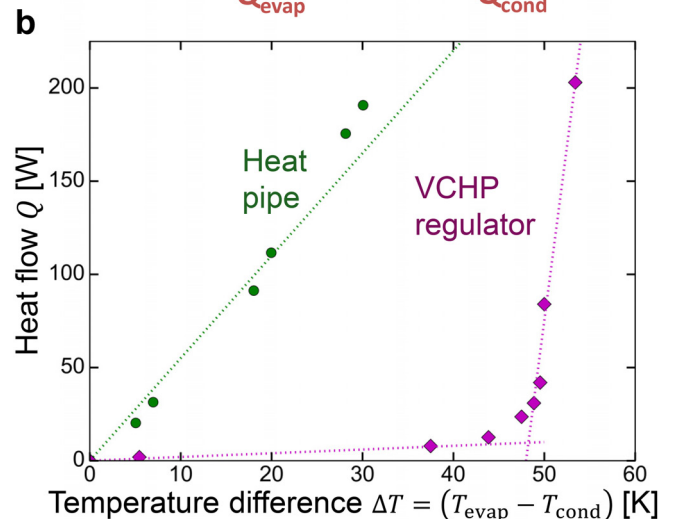
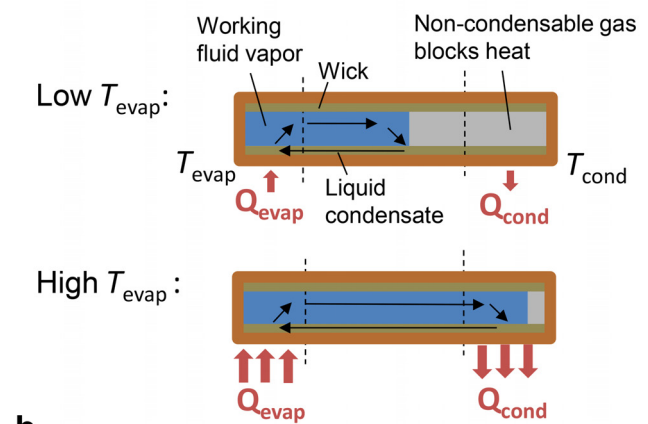


FIG. 9. Variable conductance heat pipe (VCHP) thermal regulator. (a) At low evaporator section temperatures T_{evap} , a non-condensable gas (NCG) is swept to the end of the heat pipe by the evaporating working fluid. The NCG blocks the vapor from reaching the condenser region at T_{cond} where heat is removed, leading to a small heat flow Q . The condensed fluid is wicked from the condenser back to the evaporator. As T_{evap} increases (at fixed T_{cond}), the working fluid vapor pressure increases and further compresses the NCG, allowing for large Q due to the increase in condensation surface area. (b) Experimental data for a heat pipe and comparable VCHP thermal regulator, both using water as the working fluid and with $T_{cond} = 30^\circ\text{C}$. The VCHP also includes a charge of N_2 as the NCG. Dotted lines are guides to the eye. This VCHP shows a regulator switching ratio $r \approx 200$ around $\Delta T = 50\text{ K}$, which corresponds to regulation of $T_{evap} \approx 80^\circ\text{C}$. Data from Ref. 189.

3. Gas gap thermal switches

A gas gap thermal switch tunes the heat transfer by changing the pressure P of an encapsulated gas. Gas gap switches operate in the boundary scattering (Knudsen flow) regime, where the gas molecule mean free path Λ is set by the confining gap width d rather than by the intrinsic molecule-molecule collisions. In this boundary scattering regime, $k \propto P$ at fixed temperature, since the volumetric heat capacity of the gas scales linearly with the gas density. Gas gap switches do not work at higher pressures or for larger gaps because in the bulk regime where molecule-molecule scattering dominates, $\Lambda \propto P^{-1}$ and k becomes independent of P . Therefore, the gas gap switch requires pressures $P_{\text{crit}} < (760 \text{ Torr})(\Lambda_{\text{RP}}/d)$, where Λ_{RP} is the intrinsic mean free path in the gas at room pressure. Since impractically small gaps of $d < 100 \text{ nm}$ would be required for air at STP to be in the boundary scattering regime, gas gap switches operate at lower pressures. Gas gap switches with measured room temperature $r > 500$ have been fabricated¹⁹⁰ using helium under high vacuum ($5 \times 10^{-7} \text{ Torr}$) and $= 250 \mu\text{m}$.

More recently,¹⁹ room-temperature switching ratios of $r = 10$ have been measured with $d = 20 \text{ mm}$ using hydrogen gas. Here, a thermal regulator was created by pulling a high vacuum and controlling the hydrogen pressure via the temperature-dependent hydrogen adsorption onto an adjacent metal hydride. In another recent example, freeze-casted polymer foams¹⁹¹ with small pore sizes of $d = 20 \mu\text{m}$ showed $r > 10$ using helium at 0.5 Torr and room temperature. From an applications perspective, cryocoolers using gas gap switches may cool down faster than traditional insulation systems,¹⁹² since the large gas k in the bulk regime at high T allows heat to be quickly removed from the cryocooler, until the boundary scattering regime is reached at low T to provide steady-state insulation.

4. Controlling fluid heat transfer with electric and magnetic fields

This section supplements the recent review by Shahriari *et al.*,⁵ which summarized the use of electric fields to control boiling and condensation heat transfer rates.

Electrowetting: The contact angle (wettability) between a droplet and a dielectric substrate can be changed with an electric field.¹⁹³ Cha *et al.*¹⁹⁴ developed an electrowetting thermal switch with two parallel plates and a liquid droplet on the dielectric bottom plate. The droplet height depends on the contact angle, so a DC voltage can switch between droplet contact and noncontact with the upper plate using the electrowetting effect, showing $r = 2.4$ for water droplets. McLanahan *et al.*¹⁹⁵ made a thermal switch using electrowetting to control the lateral droplet motion. In the on state, heat is transferred by convection and conduction through a glycerin droplet bridging two plates, while in the off state, the droplet is shuttled aside using an electric field, and heat is transferred only through the air gap. Switching ratios of $r = 4$ at ambient pressure and $r = 15$ at 80 Pa were obtained.

Boiling control with E fields: Cho, Mizerak, and Wang¹⁹⁶ showed that E fields can be used to enhance nucleate boiling by attracting charged surfactants to the electrodes. The

adsorbed surfactants make the surface more hydrophobic, so the E field enhances the bubble nucleation rate and increases the boiling h . Similarly, if the E field repels the surfactants, the nucleation rate decreases as the surfactants desorb, and the boiling h decreases. Switch ratios as large as $r = 10$ were measured using relatively small voltages (0.1 to 2 V) in boiling of de-ionized water with sodium dodecyl sulfate surfactants at superheats of $\Delta T = 8 \text{ K}$. Images of the bubble nucleation showed that the switching times were $< 1 \text{ s}$, and the h measurements showed good repeatability.

Larger E fields can also be used to suppress the Leidenfrost effect, in which liquid droplets are levitated by a thin vapor film over the superheated substrate. If a voltage is applied between the substrate and the liquid, then an electrostatic force pulls the liquid droplet into contact with the substrate.¹⁹⁷ Using measurements of the droplet vaporization lifetime, Shahriari, Wurz, and Bahadur¹⁹⁸ estimated that the film boiling heat transfer rate of isopropyl alcohol superheated by 120°C could be increased by a factor of 20 with an applied voltage of 1 kV to break the Leidenfrost state. Shahriari, Hermes, and Bahadur¹⁹⁹ also showed that the film-boiling heat flux from a hot metal sphere quenched in isopropanol can be increased by a factor of 5 using a DC bias of 2 kV.

E field effect on jumping droplets: The jumping droplet mechanism utilized in the thermal diodes discussed in Sec. III B 1 has also been used in thermal switches. After the droplets jump off a superhydrophobic surface, the droplet motion can be controlled with electric fields because the droplets have a remnant surface charge.²⁰⁰ Miljkovic *et al.*²⁰¹ showed that applying electric fields of 75 V/cm can enhance h in water condensation by a factor of 2. The E field prevents the droplets from returning to the surface after they have jumped off, which makes more room for new droplets to condense, and results in larger condensation rates. In one application of a jumping droplet thermal switch, Oh *et al.*²⁰² used 200–300 V/cm E fields to direct jumping droplets towards electronics hotspots, increasing the heat removal rate by 20% compared with the no-field measurements.

Ferrofluids: Magnetic fields affect heat transfer in ferrofluids,²⁰³ which are fluids containing suspensions of nanoscale magnetic particles such as magnetite. It is energetically favorable for the magnetic moments of the particles to align with the B field, but the average magnetization (M) decreases at higher T due to the increased thermal fluctuations. This $M(T)$ dependence induces natural convection when magnetic fields are applied, leading to measured switch ratios of $r = 2$.^{204,205} Magnetic enhancements of forced convection also have been reported,²⁰⁶ and B -field induced particle agglomeration is another possible mechanism for increased heat transfer.^{203,207–209} Applying non-uniform B fields to ferrofluids causes forced convection resulting from the magnetic body force, leading to $r = 16$ switching.²¹⁰ In one recent application, Puga *et al.*²¹¹ developed a ferrofluid thermal switch with $r = 2.6$, investigated the frequency response from 0.1 to 30 Hz and demonstrated that the switch could be used to cool an LED (see also Sec. IV C 2).

Magnetorheological fluids: As compared with the ferrofluids, magnetorheological fluids (MRFs) have larger

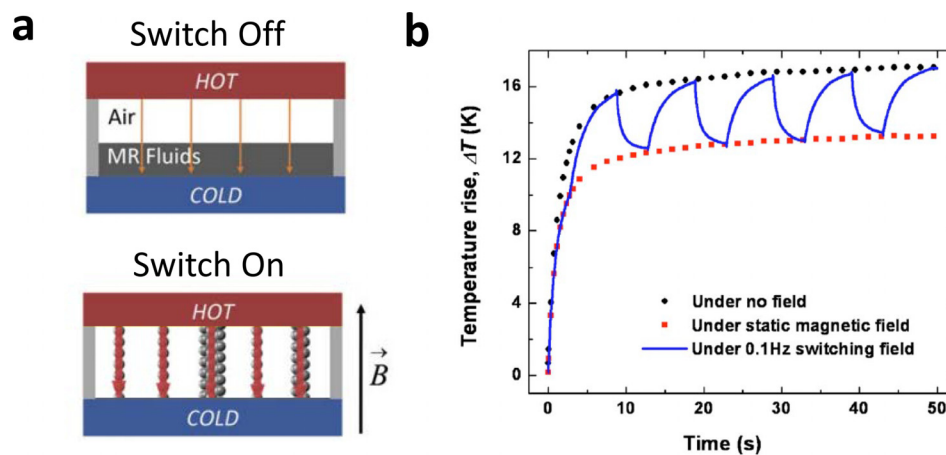


FIG. 10. Thermal switching in magnetorheological fluids (MRF). (a) Concept of the MRF thermal switch. In the off state, an insulating layer of air impedes heat transfer. Applying a magnetic field (B) causes the MRF to form parallel chains that provide effective heat transfer pathways through the 1 mm gap between the hot and cold plates. (b) The temperature rise above ambient (measured on the hot side of the switch) as a function of time is shown for constant heating at the top side of the switch with no magnetic field, in a DC field of 0.1 T, and in a square wave AC field of amplitude 0.1 T switched at 0.1 Hz. These data correspond to a switching ratio $r = 1.3$ for the full device, while additional thermal conductivity measurements (not shown) without the parasitic series thermal resistance of the cold-side heat sink indicate that the intrinsic switching ratio of this MRF switch can be as large as 12. From J. Appl. Phys. **107**, 09B505 (2010). Copyright 2010 AIP Publishing LLC.

magnetic particles which do not remain suspended in solution. Cha *et al.*²¹² made a thermal switch using MRFs of 1–3 μm carbonyl iron particles dispersed in silicone oil. As illustrated in Fig. 10(a), the MRF partially fills the chamber, but in a B field, the MRF aligns in columns which bridge the gap with high- k heat conduction pathways²¹³ between hot and cold plates. Figure 10(b) shows how the thermal conductance of the MRF can be switched between the on and off states using a 0.1 Hz magnetic field. The MRF k switching ratio was measured to be as large as 12, but the switching ratios shown in Fig. 10(b) was reduced to $r = 1.3$ due to the additional series resistance of heat dissipation from the cold side of the switch to the ambient air.

Single-component fluids: The framework of magnetoconvection^{214,215} describes heat transfer in electrically conducting fluids in the presence of external fields. Switching ratios of $r = 2$ have been observed in natural convection^{216–218} or forced convection²¹⁹ of liquid metals with B fields up to 0.5 T. Controlling the heat transferred from a surface to an ionized gas or an electrolyte using B fields would be appealing for applications such as orbital re-entry or hypersonic flows,^{215,220} but prohibitively large B fields are required to achieve significant heat transfer modulation. Electric fields have been shown to enhance convection in gases by up to a factor of 5 using the “corona wind” effect,^{221,222} where large electric fields ionize the gas and the Coulomb force repels the charged electrons. Electrophoretic effects of electric fields on free charges in gases and liquids also increase the heat transfer rates, though the enhancement depends on a number of experimental variables.^{221,223} Finally, natural convection augmentations as large as a factor of 3 have been reported in low- σ fluids,^{223,224} and it is also known that E or B fields can influence natural convection in ordered liquid crystals.^{225,226}

C. Radiation

Thermal radiation is a broadband phenomenon, with most of the heat at room temperature carried by photons in

the near infrared wavelengths. The spectral hemispherical emissivity (ϵ_λ) describes how well a surface emits over all angles, compared with a blackbody emitting at the same wavelength. The total emissivity ϵ_{tot} is obtained by integrating over all wavelengths, weighted by the Planck spectrum at a given T .

In this section, we discuss how ϵ_{tot} (and closely associated properties such as the absorptivity, reflectivity, or transmissivity) depends on T , particularly near phase transitions. We review photon diode mechanisms and emissivity switching with electric fields. The heat transferred between objects depends on the geometrical view factors, which can be controlled using louvers. Finally, we discuss recent experiments showing that thermal radiation in the near field is highly dependent on the distance between objects.

1. Thermal regulation using emissivity changes across phase transitions

To construct radiative thermal regulators, materials with highly temperature dependent optical properties are required. Many materials have weakly temperature dependent $\epsilon_{tot}(T)$, which can originate either from fundamentally T -dependent ϵ_λ (e.g., the Hagen-Rubens relation predicts that $\epsilon_\lambda(T)$ scales as $T^{1/2}$ for metals²²⁷), or from the T -dependent Planck distribution weighting (e.g., $\epsilon_{tot}(T)$ of Al_2O_3 decreases²²⁸ roughly as $T^{-1/2}$ due to the increased Planck weighting of the smaller ϵ_λ for $\lambda < 2 \mu\text{m}$ at high T). However, to achieve high switching ratios, more dramatic changes in ϵ_{tot} are needed.

Metal-insulator transitions: The broadband emissivity of vanadium dioxide^{229,230} changes across the metal-insulator transition (MIT) at 68 $^\circ\text{C}$, indicating that VO_2 can be used as a thermal radiative regulator. The low-temperature insulating state has a larger emissivity than the high-temperature metallic state, with recently reported^{231–233} ϵ_{tot} switching ratios of $r \approx 2$ –3 across the MIT. These large changes in ϵ_{tot} have been utilized in temperature-tunable

infrared absorbers using VO₂ thin films,^{234–236} and VO₂ has also been investigated as a coating to modulate the solar transmittance through windows for building climate control.²³⁷ Ito *et al.*²³⁸ recently demonstrated that the near-field radiative transport (see also Sec. III C 5) across a 370 nm gap between VO₂ and fused quartz also decreases as the VO₂ temperature increases above T_{MIT} . Other materials displaying metal-insulator transitions can also be thermal regulators; for example, ϵ_{tot} of doped manganese oxides^{239,240} increases by a factor of 3 as the temperature is increased from -50 to $+50$ °C. In Sec. III C 2, we will discuss an implementation of a thermal diode using the VO₂ MIT.

Interestingly, since ϵ_{tot} dramatically decreases across the phase transition, the total power radiated from VO₂ is non-monotonic, displaying negative differential thermal resistance (NDR). This non-monotonic dependence of emitted power on temperature difference has been utilized to demonstrate thermal camouflaging,²⁴¹ where VO₂ films at different temperatures emit the same radiative power.

Phase-change memory: In the visible wavelengths, the different reflectivities of amorphous and crystalline phase-change materials such as GST are utilized in data storage applications. However, amorphous and crystalline GST also have quite different properties in the near infrared wavelengths relevant for thermal radiation.²⁴² For example, ϵ_λ of GST films on a metal substrate were switched²⁴³ by a factor of 10 over the wavelength range of 8–14 μm , and similar switching was also observed in the transmissivity over 1.4–2 μm in a gold grating filled with germanium telluride.²⁴⁴

As a side note, the term “thermochromic” is sometimes used to indicate T -dependent optical properties in the visible (rather than infrared) wavelengths. Although there are many thermochromic polymers and liquid crystals that are used for temperature sensing,^{245,246} the broadband infrared properties relevant for thermal emission are typically much less affected by temperature.²⁴⁷ Likewise, though metamaterials displaying temperature-dependent resonance or narrowband absorption phenomena have also been developed,^{248,249} broadband phenomena are required to switch ϵ_{tot} and affect the heat transfer.

2. Radiative thermal diodes

Fundamentals of photon rectification: The Lorentz reciprocity relations²⁵⁰ state that in any optical system which is linear and obeys time-reversal symmetry (TRS), the total transmitted power is invariant under TRS, even though individual modes may have asymmetric transmission. The second law of thermodynamics provides additional constraints on radiative diodes, stating that no rectification can be observed in linear systems, even in the presence of magnetic fields²⁵¹ which break TRS. To achieve rectification, both a nonlinearity (such as temperature dependent ϵ_{tot}) and an asymmetry are required.⁵⁵ The necessity for both nonlinearity and asymmetry was illustrated experimentally by some control measurements on a ballistic photon diode,⁵⁶ which observed no rectification when an asymmetric pyramidal scatterer was placed between blackbody reservoirs. That study also highlights the importance of paying close attention to experimental symmetries when exploring

rectification, since the other experiments⁵⁶ were subsequently found to have a fundamental symmetry flaw^{252–254} which invalidated their attempts to demonstrate rectification.

Interestingly, $\epsilon_{tot}(T)$ and an asymmetry are necessary, but not sufficient, conditions for rectification. For example, consider two diffuse parallel plates (1 and 2), each of which have arbitrary spectral emissivity, $\epsilon_{\lambda,1} \neq \epsilon_{\lambda,2}$. Though the spectral emissivities do not depend on T , the Planck weighting still gives each plate (i) a different temperature-dependent $\epsilon_{tot,i}(T) = \int_0^\infty \epsilon_{\lambda,i} E_b(\lambda, T) d\lambda / \sigma T^4$, where $E_b(\lambda, T)$ is the Planck blackbody emissive power. Perhaps unexpectedly, however, it can be shown²⁵⁵ that no rectification occurs in this scenario, even with the asymmetry and nonlinearity of the two plates with different $\epsilon_{tot,i}(T)$. Furthermore, Chen *et al.*⁵⁶ showed that rectification is, in fact, strictly forbidden between any two surfaces with temperature-independent but otherwise arbitrary ϵ_λ , as long as any scattering phenomena in the volume between the two surfaces are *elastic*. However, if photons are scattered *inelastically* between the two plates, rectification can occur, even if ϵ_λ does not depend on T . For example, if a thin, opaque, diffuse, black plate is placed between plates 1 and 2 to inelastically absorb and re-emit photons, rectification now becomes possible.³

Demonstration of a radiative diode: As shown in Fig. 11(a), Ito *et al.*²⁵⁶ fabricated a radiative diode consisting of a VO₂ film on a silicon wafer, exchanging radiation with quartz. This diode utilizes the highly nonlinear emissivity of VO₂ around the MIT, as discussed in Sec. III C 1. Figures 11(b) and 11(c) show that this demonstration achieved rectification ratios around 2 with $\Delta T = 70$ K. In addition, doping the VO₂ with W decreased the MIT temperature T_{MIT} by 25 K while maintaining γ . The rectification ratio is independent of ΔT once the hot side temperature is increased above T_{MIT} . From a diode design perspective, it was desirable to use a high- ϵ second material such as quartz, since the total resistance to radiation in the reverse mode should be dominated by the low ϵ of the metallic VO₂. In addition to rectification, this demonstration also displays negative differential thermal resistance, since the decrease in ϵ across the MIT reduces the heat flux, even though ΔT is increasing.

3. Electrochromic emissivity control

Electrochromic materials have optical properties which depend on the electric field. To influence the radiative emission, broadband changes in ϵ_λ over the infrared wavelengths are required. Since solar energy lies mostly in the visible wavelengths, changing the absorptivity or transmissivity in the visible range can also modify the heat transfer if the material is receiving solar irradiation.

Electrochromic chemical reactions: Commercial electrochromic systems use reduction/oxidation (redox) processes to modify the optical properties of electrochromic solids or liquids.^{257,258} If a solid-state electrochromic material such as WO₃ is used, a voltage at the electrode drives lithium cations from an electrolyte into the WO₃. The resulting redox reactions in the WO₃ cause large changes in the broadband optical properties. Figure 12(a) shows transmittance measurements²⁵⁹ from an electrochromic glass

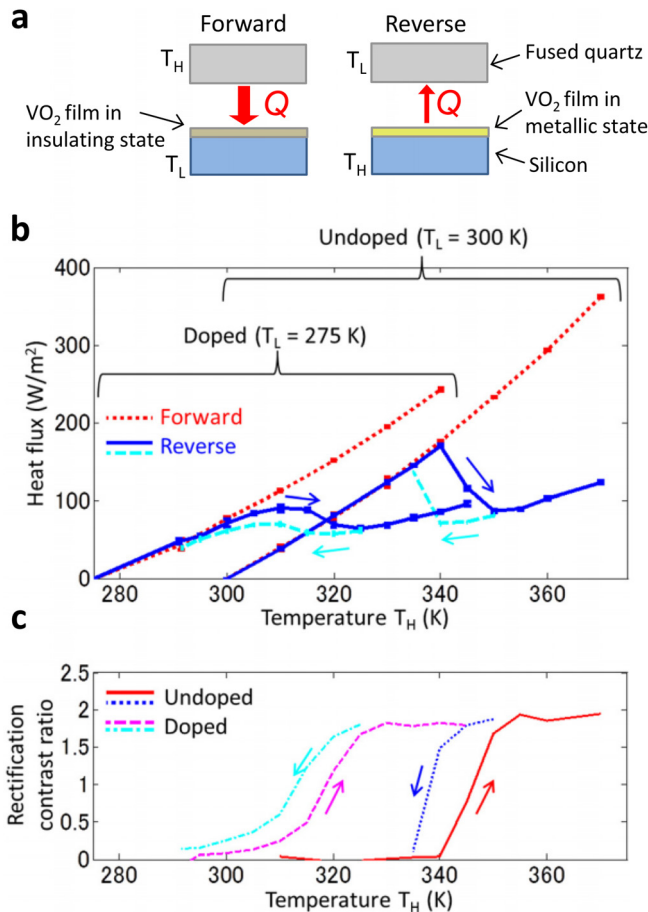


FIG. 11. Vanadium dioxide radiative diode. (a) The low-temperature insulating phase of VO_2 has a high emissivity, while the high-temperature metallic phase has a low emissivity. This temperature dependence leads to rectification in the radiative heat transfer between a VO_2 film and a quartz plate. The gap size here is 1 mm. (b) Both undoped VO_2 and W-doped VO_2 display rectification as the hot side temperature T_H is increased above the critical phase transition temperature ($T_c = 340$ and 315 K, respectively). Negative differential thermal resistance is also observed in the middle section of the reverse biased curves, where the magnitude of the heat flux decreases with increasing temperature difference ($T_H - T_L$). (c) Rectification ratios γ as large as 2 are obtained for this system, with a slightly sharper transition observed for the undoped VO_2 . From Appl. Phys. Lett. **105**, 253503 (2014). Copyright 2014 AIP Publishing LLC.

manufactured by the company Gesimat. This device uses complimentary WO_3 and Prussian Blue (ferrite ferrocyanide) electrochromic films separated by a polymer electrolyte. Changing the polarity of the applied DC voltage (0.5–2 V) switches the integrated transmittance over the incident solar irradiation by a factor of 9. The switching timescales in this demonstration were around 10 min.

Similar reflectance switching ratios have been measured using polymers in the near infrared,²⁶⁰ and redox processes can also modify the reflectivity in the far infrared.²⁶¹ Figure 12(b) shows reflectivity measurements of conducting polymers by Topart and Hourquebie²⁶² with $r = 2.5$ between 5 and 20 μm . Switch ratios of $r = 2$ across the wavelength band of 2–40 μm have also been reported in an all-solid state electrochromic system.²⁶³

Liquid crystals: Ordered liquid crystals display birefringence, leading to optical phase shifts that depend on the liquid crystal orientation.²⁶⁴ With the assistance of polarizing

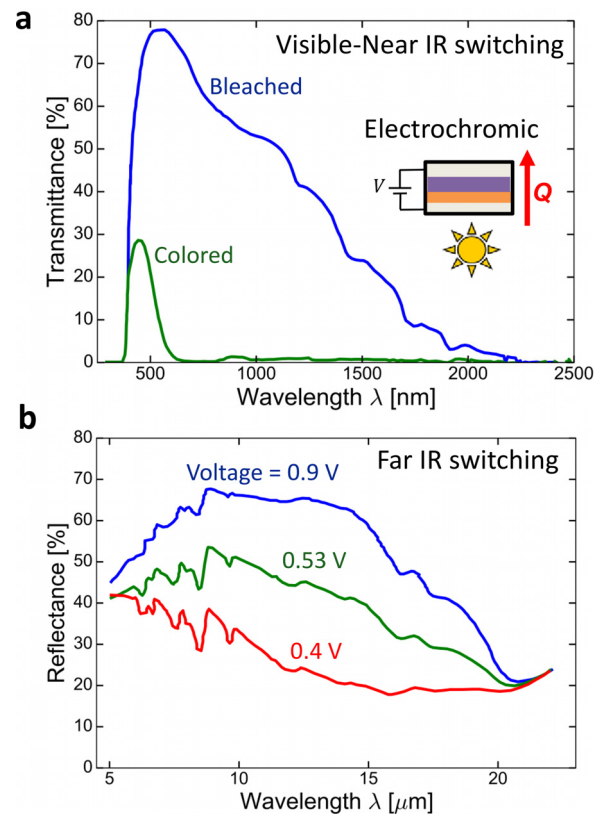


FIG. 12. Electrochromic control of transmissivity/reflectivity. (a) Metal oxide electrochromic materials show broadband transmittance switching between the bleached and colored states, achieving a switching ratio of $r = 9$ for the integrated transmittance from $\lambda = 300$ –2500 nm. Therefore, the total transmitted solar power Q can be efficiently switched by reversing the polarity of the applied DC voltage, which is on the order of 0.5–2 V. The electrochromic device combines WO_3 and Prussian Blue films for improved switching performance. Data from Ref. 259. (b) Conducting polymers can also show electrochromic performance in the far infrared wavelengths that are important for room temperature thermal emission, with measured total reflectivity switching ratios around $r = 2.5$ when integrated from $\lambda = 5$ –20 μm . Data from Ref. 262.

filters, the total transmissivity can be switched by orienting the liquid crystals;^{265,266} however, strong absorption losses in the infrared²⁶⁷ coupled with polarization filtering losses limits the achievable r . Polymer dispersed liquid crystals have been used as broadband unpolarized infrared switches,²⁶⁸ with $r = 5$ in the 2–5 μm range and $r = 2$ in the 8–14 μm range. The transient microstructure reorientation in ferroelectric liquid crystals²⁶⁹ has also been used to decrease the transmissivity by a factor of 2 in the 8–12 μm band, and even larger switching ratios²⁷⁰ on the order of $r = 10$ have been reported over 0.5–1.5 μm wavelengths.

Electrostatically tuned resonances: E fields can shift the resonant absorption peaks in metamaterials or thin films, though this has only a small effect on the heat transfer. Electrostatic gating reduced the reflectance of graphene on a thin silica film²⁷¹ by 3% for λ between 3 and 6 μm , and increased ϵ_λ of a patterned graphene resonator²⁷² by 1% in the mid-IR. Narrowband $\epsilon_\lambda(E)$ has also been observed in quantum well structures^{273,274} with photonic crystal patterning. A MEMS device²⁷⁵ displayed a 50% decrease in the normal reflectivity at 6 μm , but the integrated reflectivity between 5 and 10 μm only decreased by 5%. Likewise,

electrostatic control of the gap size in a MEMS plasmonic structure²⁷⁶ caused a factor of 2 increase in the reflectivity at 1.6 μm , but only a 10% decrease in the integrated reflectivity from 1 to 2 μm . Generally, it appears difficult to achieve large r by controlling resonance phenomena due to the broadband, hemispherical, and unpolarized nature of far-field thermal radiation. Although narrow bandpass filters placed in series could be used to emphasize the importance of thermal radiation within the small wavelength range which can be efficiently switched, this filter will dramatically reduce the total radiative heat transfer, and parasitic conduction or convection pathways will become more important.

4. View factor switching

The radiative heat transfer between surfaces depends on the view factor (F_{12}), defined as the fraction of the total energy leaving surface 1 which is intercepted by surface 2. By controlling the view factors using mechanical actuation, the heat transfer can be efficiently switched. A common implementation uses low- ϵ metallic mechanical louvers^{21,99} covering a high- ϵ emitter. When the louvers are closed, there is a higher resistance to radiation, and the emitter cannot efficiently dump the heat to the environment. Switching ratios of $r=6$ have been achieved in spacecraft applications.⁹⁹ Thermal regulators can also be constructed by actuating the louvers using a bimetallic switch, or using a shape-memory alloy actuator to unfold a stowed radiator with a high ϵ .^{277,278}

5. Near field radiation

Thermal radiation is typically a far-field phenomena, since the distance between radiating objects L is almost always large compared with the thermal photon wavelengths λ . However, recent experiments near room temperature reviewed by Song *et al.*²⁷⁹ have probed heat transfer in the near-field, where $L \ll \lambda$. In this regime, evanescent electromagnetic waves tunnel between materials, increasing the heat flux above the far-field blackbody limit. Since the tunneling currents depend critically on L , near-field heat transfer can lead to impressive switching. Recent room temperature measurements²⁸⁰ showed r as large as 100–1000 for SiO_2 - SiO_2 surfaces or Au-Au surfaces as the gap was reduced to $L < 100\text{ nm}$. For larger values of $L = 3\ \mu\text{m}$, Elzouka and Ndoa²⁸¹ reported thermal rectifications of 10% at $\Delta T = 150\text{ K}$ using the asymmetric thermal expansion of a MEMS structure to control L . Overall, for the purpose of thermal switching it is likely more practical (and effective²⁸²) to bring materials fully in and out of contact (see Sec. III A 4) than to rely on near field mechanisms, since it is difficult to maintain and control such small yet finite L over macroscopic distances.

Interestingly, theory predicts that near-field radiation between semiconductors can be tuned with electric²⁸³ or magnetic²⁸⁴ fields. Demonstrating this switching using external fields would highlight the unique capabilities of near-field radiation, since the heat conduction through interfaces in contact is insensitive to external fields. Theory also predicts that near-field thermal diodes could be constructed using materials which have temperature-dependent

electromagnetic resonances. Otey, Tung, and Fan²⁸⁵ first proposed this concept and analyzed the rectification between SiC polytypes, and Song *et al.*²⁷⁹ reviewed subsequent theoretical predictions of near-field thermal rectification. In a similar exploitation of temperature-dependent properties, Ito *et al.*²³⁸ recently demonstrated a near-field thermal regulator which used the metal-insulator transition (MIT) of VO_2 to reduce the heat transfer across a gap of $L = 370\text{ nm}$ by a factor of 1.6.

IV. POTENTIAL APPLICATIONS AND THERMAL CIRCUITS

Now that we have examined the mechanisms of switchable and nonlinear heat transfer in great detail, we consider several potential applications of thermal diodes, switches, and regulators in simple thermal circuits. First, we examine applications to solid-state refrigeration cycles. We then consider energy scavenging schemes. Finally, we present eight additional thermal circuits that can be implemented using nonlinear and switchable thermal devices. These thermal circuits are directly analogous to commonly utilized electrical circuits, and offer new thermal capabilities.

A. Solid state refrigeration using thermal diodes

Thermal diodes or thermal switches can be used to implement both the adiabatic and isothermal portions of solid state thermodynamic cycles at a single physical location. Here, we examine a solid state refrigeration cycle in detail to see why thermal diodes are useful in this application, and to quantify the rectification ratios γ required to obtain good cycle performance. Though we focus here on an electrocaloric refrigeration example,^{14–16,286} many of the same principles will also apply to adiabatic demagnetization refrigeration (magnetocaloric) cycles.^{4,13,287}

Electrocaloric: Figure 13 summarizes an electrocaloric (EC) Brayton refrigeration cycle described by the temperature-entropy diagram in Fig. 13(a). Adiabatically applying an electric field (E) during process 1 \rightarrow 2 increases the EC temperature by the amount θ (which can be as large as $\sim 10\text{ K}$ in ferroelectric polymers,²⁸⁸ but is more typically $< 1\text{ K}$). Heat then flows from the EC material to the hot reservoir at T_h (2 \rightarrow 3). After the E field is adiabatically removed (3 \rightarrow 4) the EC temperature T_{EC} decreases below the cold reservoir temperature T_c , and finally (4 \rightarrow 1) heat flows from the cold reservoir to the EC material to complete the cycle. Clearly, if at any point in the cycle, heat can flow back from the hot reservoir into the EC material, or from the EC material into the cold reservoir, the cycle performance is degraded. One way to block this undesirable heat flow, while still allowing for strong thermal coupling to pump heat out of the cold reservoir, is to use two thermal diodes. The thermal circuit describing the EC system is shown in Fig. 13(b), where the thermal capacitance of the EC material is C_r . Each diode is reverse-biased for 3 of the 4 stages of the cycle: the hot-side diode is only in the forward mode during (2 \rightarrow 3) when heat flows from T_{EC} to T_h , and the cold-side diode is only in the forward mode during (4 \rightarrow 1) when heat flows from T_c to

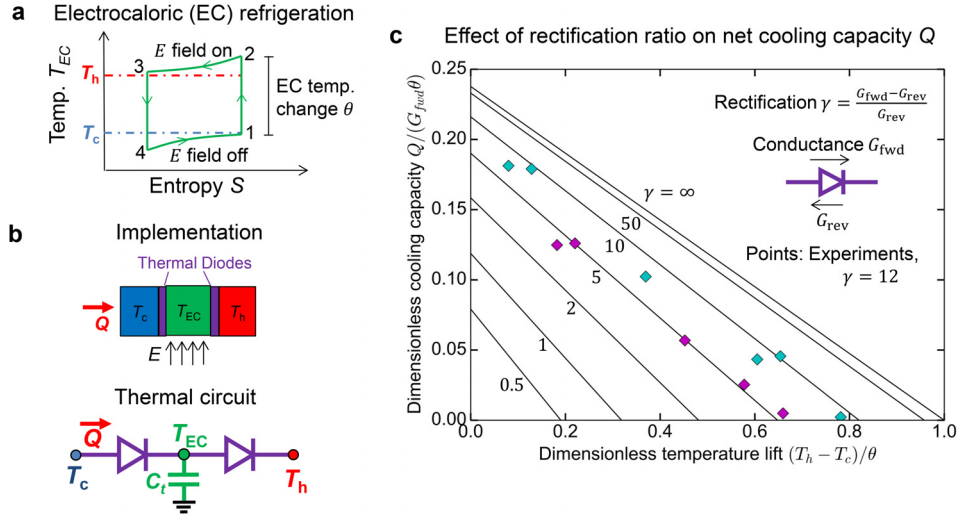


FIG. 13. Solid-state refrigeration using thermal diodes. (a) Temperature vs. entropy diagram for an electrocaloric (EC) Brayton refrigeration cycle. In process (1→2), adiabatically applying an electric field E increases the EC material temperature T_{EC} by an amount θ above the cold reservoir temperature T_c . During (2→3), heat flows from the EC material to the hot reservoir at T_h . Removing the E field in (3→4) cools the electrocaloric material below T_c , and in (4→1) heat is extracted from the cold reservoir, providing the desired refrigeration effect. (b) In a physical implementation (top) and a thermal circuit (bottom) of this EC cycle, thermal diodes allow for strong heat transfer when transferring heat from the cold reservoir into the EC thermal mass [process (4→1) of (a)], and similarly from the EC mass to the hot reservoir [process (2→3)], while blocking undesirable heat leakages back into the cold reservoir during the other phases of the cycle. (c) The thermal diode rectification ratio γ dictates the performance of this refrigeration cycle. Calculations (lines, following Smullin *et al.*²⁸⁶) show that large γ enhances both the net cooling capacity Q and temperature lift $(T_h - T_c)$, while small γ allows heat leakage that degrades performance. Experimental results¹⁵ are also shown for a BaTiO₃ EC thin film with an estimated $\theta = 0.25$ °C (blue points) and $\theta = 0.45$ °C (magenta points) in a thermal circuit using contact thermal switches with an effective $\gamma = 12$ and $G_{on} = 0.35$ W/K. The experimental data show the expected tradeoff between Q and $(T_h - T_c)$, and the magnitude of the dimensionless Q agrees fairly well with the modeling predictions using no free parameters.

T_{EC} . At all other times, the diodes block heat from flowing back into the refrigerator.

Thermal switches are also used to mimic thermal diode behavior during the different stages of the cycle; in fact, all experimental implementations of EC cycles that we are aware of have utilized contact thermal switches, since solid state thermal diodes are less common than contact switches. We present this new implementation because using passive thermal diodes rather than active switches could substantially reduce the system complexities associated with active thermal switching, and the performance of the diode circuit and switch circuit for refrigeration will be identical if the diode's forward/reverse conductances are equal to the switch's on/off conductances.

Following the analysis of Smullin, Wang and Schwartz,²⁸⁶ and making the experimentally reasonable assumptions that $\theta/T_c \ll 1$ and that the cycle time is on the order of the thermal RC time constant C_t/G_{fwd} , we have calculated the net cycle cooling capacity Q as a function of the temperature lift $(T_h - T_c)$ for different rectification ratios γ . Figure 13(c) shows these dimensionless Q vs. $(T_h - T_c)$ curves for several values of γ . If large temperature lifts are desired, high γ are needed to prevent the heat leakage from the hot to the cold reservoirs. This need for high γ was also observed in calculations of the cycle coefficient of performance (COP) for large $(T_h - T_c)$ by Epstein and Malloy.²⁸⁹ Fortunately, for smaller temperature lifts, the heat leakage from hot to cold reservoirs is not as severe, and good cooling performance can be obtained with only modest γ . For example, if $(T_h - T_c) = 0.4\theta$, diodes with $\gamma = 5$ would sustain a dimensionless Q that is half as large as the $\gamma \rightarrow \infty$ limit. The model is compared with experiments¹⁵ using

contact thermal switches with an effective $\gamma = 12$. These experiments were performed for two estimated values of θ , obtained by changing the E field. The agreement between theory and experiment in Fig. 13(c) is reasonably good with no free fitting parameters.

Recently, Ma *et al.*¹⁶ demonstrated a flexible electrocaloric cooling device which electrostatically shuttles an EC polymer between the hot and cold reservoirs using $E \sim 60$ MV/m (~ 900 V across a $15 \mu\text{m}$ dielectric). The added complexities of mechanical contact thermal switches are avoided because the EC polymer acts as both the electrostatic thermal switches and the EC material (typical $\theta = 3.6$ K for $E = 66$ MV/m). The reported switching times was 30 ms, and the device showed repeatable thermal performance over 30 000 cycles while reporting a relatively large Q and 6% COP relative to Carnot for $\Delta T = 1.4$ K. Ma *et al.*¹⁶ also showed that this device can quickly cool an overheated lithium ion battery. Future work to decrease the operating voltage while maintaining the performance and repeatable switching could be quite exciting for applications.

Thermoelectric: In a related application, a thermal diode has been used to implement a switched thermoelectric refrigeration cycle.²⁹⁰ This switched cycle has the potential to reduce power consumption and increase cooling COP compared with standard steady-state performance. During the portion of the cycle when the thermoelectric module is operating, the diode is in the forward mode to obtain high cooling capacity. When the module is turned off, the diode is in reverse mode to block the heat from leaking into the cold refrigerator. The ability to block parasitic leakage when the thermoelectric is not operating reduces the

required power consumption to maintain a given T_c without sacrificing the cooling performance when the thermoelectric is activated.

Finally, thermal switches have also been proposed²⁹¹ for use in supercooled pulsed thermoelectric cycles.²⁹² The thermal switch would make contact between the refrigerated space and the thermoelectric module when the electrical current is pulsed and the Peltier cooling is strong. The switch then breaks thermal contact before the detrimental Joule heat diffuses through the thermoelectric to reach the refrigerator.

B. Waste heat scavenging using switchable and nonlinear thermal devices

In this section, we highlight three different thermal circuits which have been developed to improve the performance of thermal energy scavenging systems. Though each circuit utilizes different components, a similar underlying concept drives all of the circuit designs: the Carnot efficiency $\eta_c = (T_h - T_c)/T_h = \Delta T/T_h$ increases linearly with ΔT for small temperature differences. This increased η_c at larger ΔT incentivizes the use of switchable or nonlinear thermal devices to store the heat in a thermal capacitor for some period of time, rather than letting the heat directly flow through the heat engine at all times. As compared with steady-state generation from the same thermal reservoirs and heat engine, such strategies can result in a transiently larger ΔT which yields a higher η_c when the heat is finally allowed to flow.

Though increasing ΔT is always thermodynamically advantageous, we focus here on thermoelectric²⁹³ or thermogalvanic²⁹⁴ waste heat scavenging engines, for which the hot-side heat flow Q_h is linearly proportional to ΔT and an effective thermal resistance $R_t = \Delta T/Q_h$ can be defined.^{295,296} Thus, in the small- ΔT regime relevant for waste heat scavenging, the Carnot output power $P_{out} = \eta_c Q_h$ of these devices scales as $(\Delta T)^2$. This strong scaling was recently used to

demonstrate that periodic heating improves the thermoelectric conversion efficiency when compared with steady-state heating with the same T_{avg} , due to the larger time-averaged $(\Delta T)^2$ in the AC heating scenario.²⁹⁷ We now present three experimentally demonstrated thermal circuits that use switchable or nonlinear components to transiently increase ΔT in waste heat scavenging systems.

Thermal switch scavenging circuit: Figure 14 shows an energy scavenging scheme using thermal switches. McKay and Wang⁸⁴ performed analysis and experiments on several different scavenging schemes using periodic heating and thermal switches; here, we consider only the simplest of their circuits, which is shown in Fig. 14(a). In the steady periodic (long time) limit, the constant heat input Q_h charges a thermal capacitor of capacitance C_t when the switch is thrown open at $t = 0$. When the switch is closed at time $t = t_o$ the capacitor discharges through the heat engine for a time t_c until the switch is opened again at $t = (t_o + t_c)$ to restart the cycle. The ideal heat engine considered here has a thermal resistance R_t and a Carnot efficiency η_c . The goal is to maximize the average output power P_{out} and therefore the average Carnot cycle efficiency $\langle \eta_c \rangle$ for a fixed Q_h and ground temperature T_g .

Figure 14(b) shows the switch state, the hot temperature T_h , and P_{out} as functions of time. The dotted lines represent the steady-state values with no switching. Adding the switch increases T_h above the steady-state value, and increases the cycle-average P_{out} due to the larger Carnot efficiency at higher T_h . Figure 14(c) illustrates the expected effect of thermal switching on the efficiency of a Carnot engine. McKay and Wang⁸⁴ measured the temperatures across a thermal resistor in series with a contact thermal switch. The cycle-averaged Carnot efficiency $\langle \eta_c \rangle$ was calculated based on the measured temperatures for different dimensionless switch closed times $t_c/R_t C_t$. In these experiments, the dimensionless heat flow $Q_h R_t / T_g = 0.01$ was fixed, and the switch duty

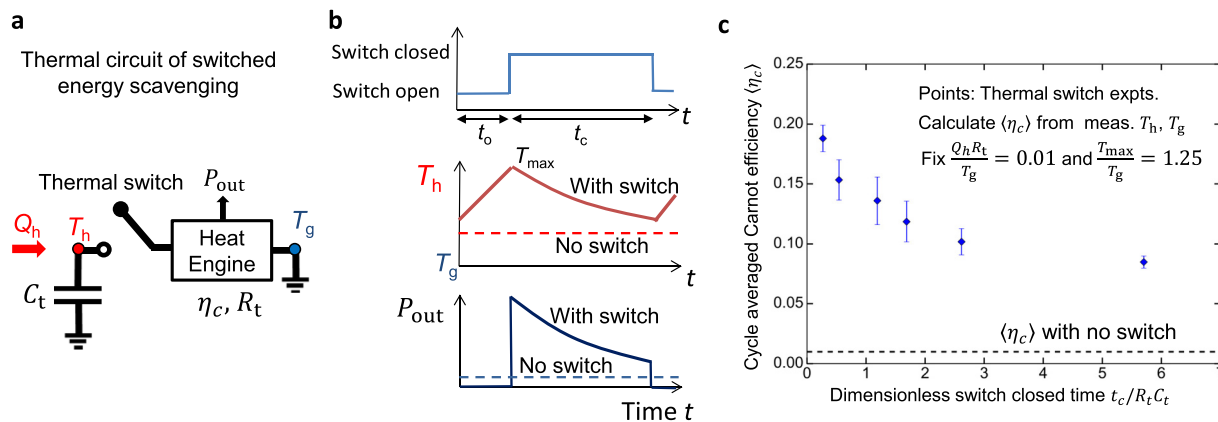


FIG. 14. Energy scavenging using a thermal switch. (a) Thermal circuit for a switched heat engine. For this ideal condition of a constant hot-side heat input Q_h and a Carnot heat engine of thermal resistance R_t , adding a thermal capacitor and periodically switching a thermal switch can increase the time-averaged T_h , enhancing the conversion efficiency above the “no switch” value. (b) Schematics of the steady-periodic response. While the switch is open (for a time t_o), T_h linearly ramps up as the capacitor charges, but there is no heat flow through the heat engine and therefore no power output P_{out} . While the switch is closed (t_c), the capacitor discharges through the heat engine, and the higher temperature differences lead to larger Carnot efficiencies and P_{out} . (c) McKay and Wang⁸⁴ measured the temperatures T_h and T_g in this thermal circuit using a contact thermal switch and passive R_t and calculated the expected cycle averaged Carnot efficiency $\langle \eta_c \rangle$ based on their experimental temperatures. Their results indicate that $\langle \eta_c \rangle$ can be dramatically boosted above the value with no thermal switch (dashed line), particularly for small dimensionless switch closed times $t_c/R_t C_t$. At steady state, similar enhancements in η_c would also be possible by using a larger R_t (not shown, see main text).

cycle $t_c/(t_o + t_c)$ was varied to maintain a fixed maximum temperature $T_{max} = 1.25 T_g$. The maximum calculated efficiency obtained was $\langle \eta_c \rangle \approx 1 - (T_g/T_{max}) = 0.2$, which is more than a factor of 20 improvement over the no-switch efficiency $\langle \eta_{NS} \rangle = 0.01$.

Although this startling improvement in the Carnot efficiency is exciting, it should also be noted that in real applications, the efficiency would be limited either by heat leakage from the thermal capacitor, or more fundamentally by the breakdown of the constant Q_h input assumption. Also, if a source of constant Q_h regardless of T_h were truly available, similarly large increases in η_c could also be obtained at steady-state by scaling the heat engine to have a larger R_t , since for $R_t \gg T_g/Q_h$ it is readily shown that $\eta_c \rightarrow 1$. The advantage of this switched circuit approach is that when the constant Q_h assumption is reasonable and a heat engine with a small R_t is desirable (or readily available), enhanced performance can be obtained by simply controlling the switch duty cycle.

Thermal regulator scavenging circuit: A conceptually similar scavenging scheme (not shown) can be implemented using a thermal regulator instead of a thermal switch in the circuit of Fig. 14(a). If the thermal regulator displays negative differential resistance (NDR; see also Sec. IVC 3), the hot-side temperature T_h will oscillate around the regulator's critical temperature T_c even with a DC hot-side heat input Q_h . The regulator needs to have a high thermal resistance (R_{off}) at low temperatures when the thermal capacitor (C_t) is charging. At temperatures above T_c , the regulator has a low resistance (R_{on}), and the higher-grade heat in the capacitor discharges through the heat engine (R_t) to the ground temperature T_g . Once the capacitor cools back below T_c , the cycle resets as the regulator switches to the high-resistance state and the thermal capacitor begins charging again. Thermal switches can also mimic this regulator behavior, since the switch circuit of Fig. 14(a) is functionally identical to the regulator circuit if the switch duty cycle is chosen to achieve $T_{max} = T_c$. Though we have described here the circuit behavior for NDR regulators (or switches mimicking regulators), we also note that regulators which do not display NDR also can be used to hold T_h near T_c .

Regulating the hot side temperature near T_c leads to an increase in efficiency only for small heat flows ($Q_h < (T_c - T_g)/R_t$); for larger Q_h , the steady-state temperature drop across the engine is large enough that the regulator is always in the low-resistance state, and there is no benefit to using this thermal regulator; instead, a regulator with higher T_c should be selected. As in the thermal switch case considered above, it will also be important to consider parasitic heat losses and the breakdown of the constant Q_h assumption in real applications. Experimentally, Gou *et al.*²⁹⁸ and McCarty *et al.*²⁹⁹ have shown modest (20%) increases in efficiency for thermoelectric generation systems using contact thermal switches to mimic this thermal regulator circuit (i.e., selecting the on/off switch timing based on the measured temperature, rather than switching based on a predetermined duty cycle).

Thermal diode scavenging circuit: Figure 15 shows an example of using thermal diodes in a "temperature doubler"

thermal circuit for energy scavenging. The temperature doubler is analogous to a voltage doubler circuit in the electrical domain. In the temperature doubler, the input is an AC temperature and the output is a (nearly) DC temperature difference with twice the magnitude of the AC input's amplitude. Although this example uses an input AC temperature, the circuit's functionality is similar for an AC heat flux boundary condition.

Figure 15(a) shows the thermal circuit for a temperature doubler proposed for solar-thermal energy harvesting. The input AC temperature T_{plate} is the temperature of an energy collector plate exposed to the sky; the plate is hot during the day and cold at night. The purpose of the diodes is to block heat from flowing between the plate and the thermal masses at T_1 and T_2 , except during the charging portion of the cycle when $T_{plate} > T_1$ and the reset portion of the cycle when $T_{plate} < T_2$. During the remainder of the cycle, both diodes are reverse-biased. Throughout all phases of the cycle, heat flows from the hot mass at T_1 to the cold mass at T_2 through the heat engine to produce power. Figure 15(b) shows a comparison energy scavenging cycle without thermal diodes or capacitors that directly drives the heat engine from the temperature difference between T_{plate} and the constant ground temperature T_g .

In a recent demonstration of the temperature doubler,⁸⁵ contact thermal switches and additional insulation were used to mimic thermal diodes, with estimated rectification ratios $\gamma \approx 2000$. Aluminum blocks were used as thermal capacitors, and a thermoelectric generator was used as the heat engine. Figure 15(c) shows the experimentally measured temperature profiles as a function of time for the temperature doubler. Throughout the entire oscillating T_{plate} cycle, the quasi-steady T_1 is nearly as large as the maximum value of T_{plate} , while simultaneously maintaining a quasi-steady T_2 nearly as small as the minimum value of T_{plate} . Analytical models³⁰⁰ of this temperature doubler were in good agreement with the experiments. Figure 15(d) shows the measured power output for the temperature doubler and the comparison case. Since the temperature doubler increases the average temperature difference across the thermoelectric by approximately a factor of 2, the average power output increases by approximately a factor of 4, in accordance with the expected $P_{out} \propto (\Delta T)^2$ scaling of thermoelectric engines mentioned above. This experiment was driven by a nearly perfect $T_{plate}(t)$ source with negligible output impedance. The performance in a real application such as solar-thermal scavenging would also be impacted by the finite output impedance of the source, which would limit the maximum Q that can be provided during the diode on-state unless $R_{SourceOutput} \ll G_{Diode,on}^{-1}$.

C. Analogous thermal and electrical circuits

Many useful electrical circuits can be immediately translated into the thermal domain if all of the necessary electrical components have thermal analogies. In this section, we survey a selection of circuits which have been developed for the electrical domain and consist exclusively of components with thermal analogs (diodes, regulators, switches, resistors,

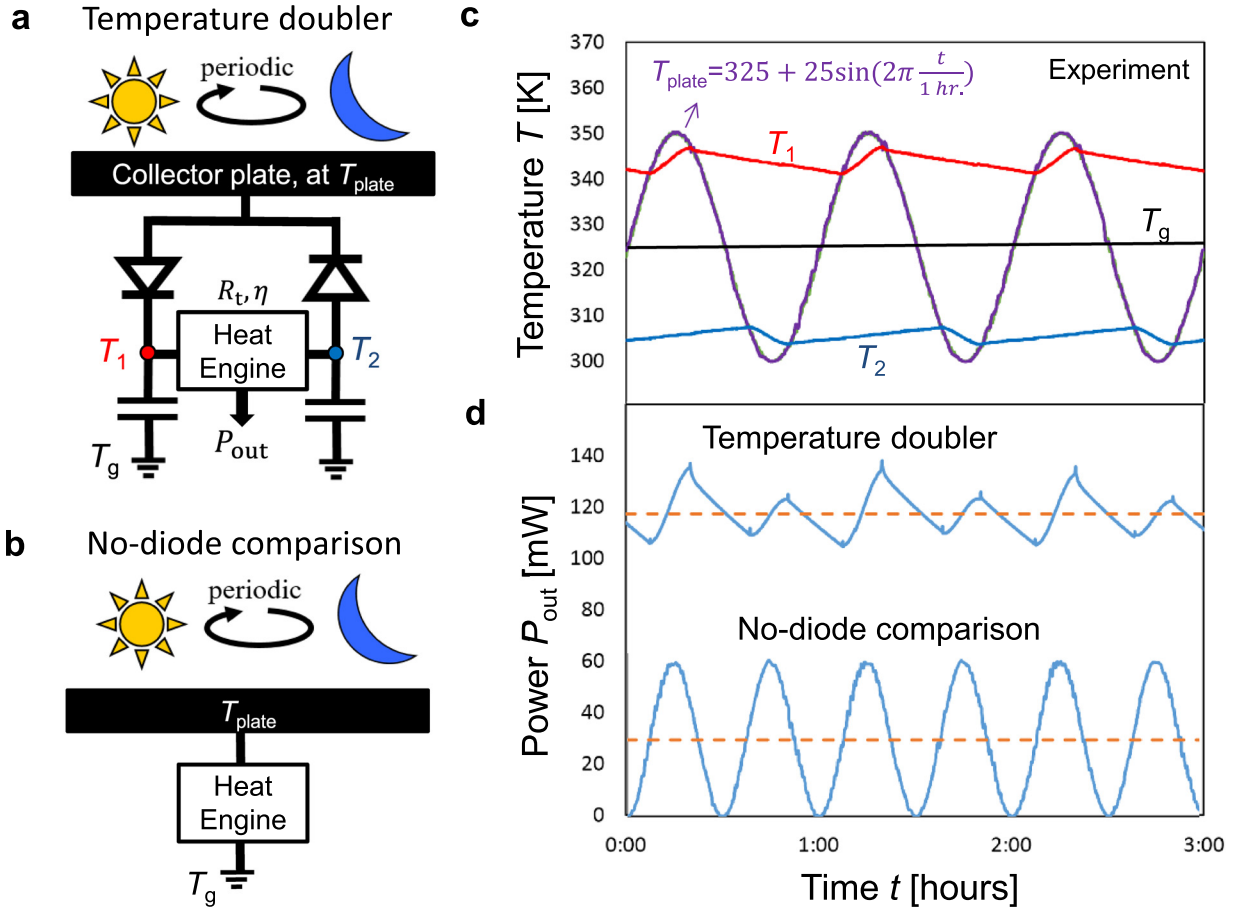


FIG. 15. Temperature doubler for energy harvesting of a periodic heat resource. (a) In a temperature doubler circuit, thermal diodes and capacitors rectify an AC temperature profile $T_{plate}(t)$ to a quasi-DC temperature difference $T_1 - T_2$, driving a heat engine of thermal resistance R_t and efficiency η . As a motivating example of such an AC temperature profile, an energy collecting plate exposed to the open sky has a T_{plate} that oscillates due to the diurnal temperature cycle. (b) The temperature doubler can be compared with a “no-diode” implementation where the heat engine is directly connected between the oscillating T_{plate} and the physical ground temperature T_g . (c) Measured temperature profiles for the temperature doubler scheme in a benchtop experiment using a sinusoidal T_{plate} . The thermal diodes are mimicked using contact thermal switches with estimated rectification ratios $\gamma \approx 2000$. In the long-time (steady periodic) response shown here, the temperature doubler maintains a nearly constant temperature difference $T_1 - T_2$ (red – blue), even as T_{plate} (purple) oscillates. (d) Measured electrical power output P_{out} from a thermoelectric generator heat engine as a function of time for the temperature doubler (top curves) and the no-diode comparison (bottom curves) configurations, both using the same $T_{plate}(t)$ and T_g . The average power output (dashed lines) is a factor of 4 larger for the temperature doubler than the no-diode comparison, reflecting the $P_{out} \propto (\Delta T)^2$ scaling of thermoelectric heat engines for small ΔT . Data from Ref. 85.

and grounded capacitors) and can therefore be implemented in the thermal domain. We discuss the circuit behavior and performance metrics for each circuit below, with references to the previous descriptions of their electrical counterparts. Our naming convention also adapts the established terminology from the electrical domain.

1. Thermal diode application circuits

Thermal peak detector: In Fig. 16(a), a simple peak detector circuit³⁰¹ maintains the temperature of a thermal mass (C_t) at the peak temperature T_{peak} reached by the fluctuating ambient temperature T_{amb} . When T_{amb} falls below T_{peak} , the diode is in reverse-mode, and the capacitor temperature ideally remains constant until T_{amb} increases above T_{peak} and the diode switches back into forward-mode. The upper limit of the detector bandwidth is inversely proportional to the forward-mode diode time constant $\tau_{fwd} = R_{fwd}C_t$, and the peak temperature hold time is set by the reverse-mode time constant $\tau_{rev} = R_{rev}C_t$. Thermal peak detectors could be

useful for *ex-situ* failure studies, since the maximum temperature is stored for later analysis. Peak detector circuits can also capture thermal energy to later use when demand is high. For example, a peak detector could store the heat from mid-day until the thermal energy discharges later at night, as in Fig. 15(a).

A similar circuit called an envelope detector³⁰² (not shown) can be constructed by adding a grounded resistor R_{env} in parallel with C_t in the peak detector circuit, allowing the heat to leak out of the capacitor over a timescale $R_{env}C_t$. In the electrical domain, envelope detectors are used to demodulate AM signals, recovering the slowly-varying envelope signal and discarding the high-frequency carrier signal. In the thermal domain, the envelope detector could be used to track the time-varying amplitude of periodic thermal waveforms.

Thermal load shifter: In Fig. 16(b), a steady-state load shifter³⁰³ controls the relative amount of heat flowing from two reservoirs at T_1 and T_2 . For example, the amount of heat flowing from reservoir 2 (Q_2) through a grounded load

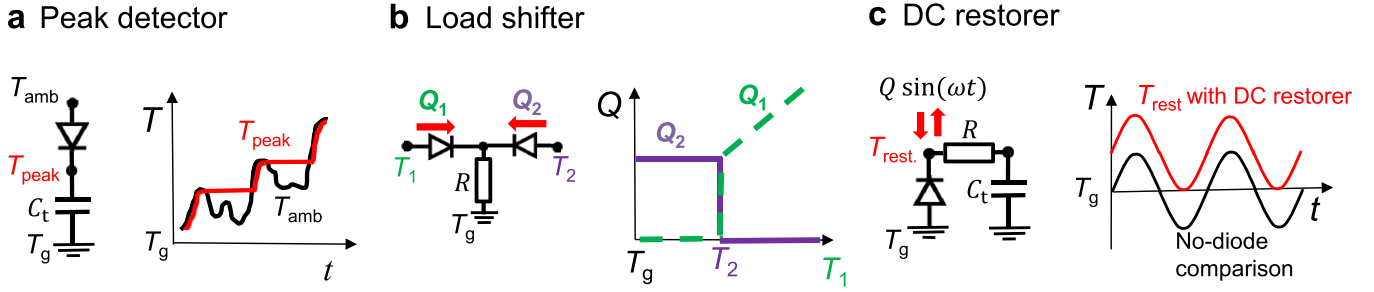


FIG. 16. Thermal diode application circuits. Electrical circuits which use diodes, resistors, and grounded capacitors can be directly translated and implemented in the thermal domain. (a) A thermal peak detector uses a thermal diode and capacitor to store the peak temperature T_{peak} reached by the fluctuating ambient temperature T_{amb} . (b) (Left) A load shifter uses a common junction between thermal diodes to shift the relative amount of heat Q flowing from reservoirs 1 and 2 as the temperatures T_1 and T_2 are varied. (right) For example, when T_2 is held constant, small changes in T_1 near $T_1 = T_2$ cause large changes in Q_1 and Q_2 . (c) A DC restorer ensures that a fluctuating heat source adding or removing heat never causes the restored temperature T_{rest} to be colder than the ground temperature T_g . This T_{rest} has the same amplitude and phase as a similar thermal circuit without a diode (“no diode comparison”).

resistor R can be controlled by tuning T_1 at fixed T_2 . When $T_g < T_1 \ll T_2$, diode 2 is in forward mode and Q_2 is independent of T_1 , since diode 1 is in reverse mode. However, as T_1 increases above T_2 , diode 2 switches to reverse mode, Q_2 abruptly decreases, and Q_1 increases as diode 1 switches to forward mode. Using better thermal diodes leads to a sharper transition near $T_1 = T_2$ and to improved load shifting capabilities, since it can be shown that the crossover breadth ΔT_b scales as $(T_2 - T_g) * (R_{fwd}/R)$, and the load shifting ratio $Q_{2,max}/Q_{2,min}$ scales as R_{rev}/R as long as R_{fwd}/R is small.

Thermal DC restorer: To understand the DC restorer³⁰² shown in Fig. 16(c), first consider the same series RC circuit without the thermal diode. If heat is periodically added and removed at the node labeled T_{rest} , that nodal temperature will oscillate symmetrically above and below the ground temperature T_g . The effect of adding the thermal diode as shown is to yield a new T_{rest} with the same phase and amplitude of the thermal waveform as in the “no-diode” comparison, but to keep T_{rest} from dropping below T_g . The thermal diode effectively adds a DC offset temperature to the waveform. To achieve restoration, the oscillation frequency ω must be substantially greater than $1/\tau_{rev} = 1/R_{rev}C_t$ to prevent leakage through the reverse-biased diode, and R_{rev}/R needs to be well above than 1 to avoid attenuating the temperature rise. Such a DC restorer circuit might be used to prevent the working fluids in spacecraft or vehicle thermal management systems from freezing when exposed to an oscillating hot and cold environment if a suitable T_g reservoir inside the spacecraft is available.

2. Thermal switch application circuits

Besides the most obvious application of thermal switches for active thermal management systems, Fig. 17 shows two examples of thermal circuits which use time-periodic thermal switching for tunable thermal control.

Switched-capacitor thermal resistor: The cycle shown in Fig. 17(a) is used to create a tunable effective thermal resistance R_{eff} which depends on the switching frequency.³⁰⁴ During the charging portion of the cycle, the cold thermal capacitor (initially at T_c) is connected to the hot reservoir (switch S_1 closed, S_2 open). Assuming the capacitor fully

thermalizes with the hot reservoir, then the energy transferred into the capacitor is $E = C_t(T_h - T_c)$. Similarly, during the discharging portion of the cycle (S_1 open, S_2 closed), that same amount of energy is dumped to the cold reservoir. The cycle then repeats with a frequency f . The effective heat transfer rate is thus simply $Q_{eff} = Ef = C_t f(T_h - T_c)$. Therefore, the effective thermal resistance $R_{eff} = (T_h - T_c)/Q_{eff} = 1/C_t f$ can be tuned by changing the switch frequency. The cycle frequency should be high enough that the heat cannot leak out of the capacitor ($f > 1/R_{off}C_t$), but small enough that the capacitor has time to charge and discharge ($f < 1/R_{on}C_t$).

Puga *et al.*²¹¹ recently demonstrated a switched-capacitor resistor in the thermal domain using a magnetic nanofluid thermal switch. Applying (removing) a magnetic field causes the nanofluid to make (break) contact with the heat sink, leading to thermal switching. They found that increasing the switching frequency from $f = 0.1$ to 30 Hz decreased R_{eff} by a factor of 2.5. However, more complicated thermal modeling beyond the lumped-capacitance analysis discussed here was required for that demonstration, since the cycle period $1/f$ was fast compared with the thermal diffusion time through the nanofluid, and convective heat transfer in the ferrofluid was also important.

Thermal switching mixer: Figure 17(b) shows a thermal mixer,³⁰⁵ which uses periodic thermal switching to effectively utilize thermal energy from a high-frequency thermal source. If the thermal switch S_1 is always closed, the thermal resistor R and capacitor C_t act as a standard low-pass filter to attenuate the oscillating input temperature T_i . For oscillation frequencies $f \gg 1/RC_t$, the output temperature T_o is damped by a factor of $(1/fRC_t)$ compared with T_i . This damping can sometimes be desirable to reduce thermal fluctuations at the output, but in other cases, we may want to harness the thermal energy from T_i to provide DC heating or cooling at some other T_o . This can be accomplished using a thermal switching mixer. If S_1 is switched between R_{on} and R_{off} at the same frequency as T_i (and with the same phase), then the thermal switch acts as a half-wave rectifier, and the temperature at the switch-resistor junction T_s has a DC offset which is proportional to the amplitude of T_i . This DC component of T_s easily passes through the thermal RC filter to appear at T_o . If S_1 is switched at the same frequency but with

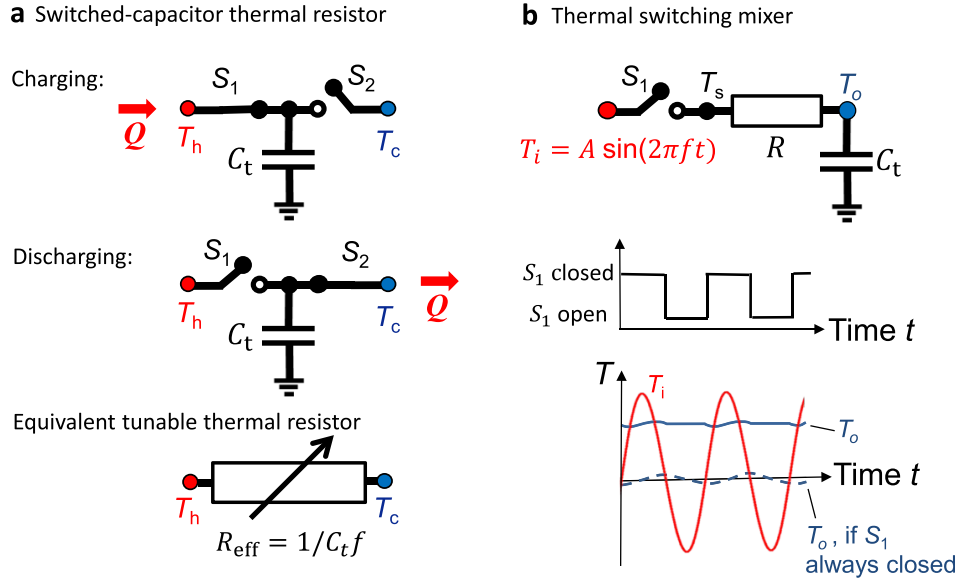


FIG. 17. Thermal switch application circuits. Thermal circuits using time-periodic switching can be constructed by analogy with known electrical circuits. (a) A switched-capacitor cycle is equivalent to a linear thermal resistance R_{eff} which depends on the switching frequency f . At the beginning of each cycle, the thermal capacitor C_t charges up from the hot reservoir at T_h (thermal switch S_1 closed, S_2 open). Then, C_t discharges to the cold reservoir at T_c (S_1 open, S_2 closed), thereby transferring $E = C_t(T_h - T_c)$ Joules from the hot to cold side. Since the corresponding average heat flow rate is simply Ef , this device is equivalent to a passive thermal resistor with a variable effective resistance $R_{\text{eff}} = 1/C_t f$. Puga *et al.*²¹¹ demonstrated a thermal switched-capacitor resistor using a magnetic nanofluid thermal switch (see main text). (b) A thermal switching mixer is used to transmit the thermal energy in high frequency input temperature oscillations at T_i through a low-pass thermal RC filter to the output terminal T_o . If the switch S_1 is always closed, this is a standard RC low-pass filter, and the output T_o (dashed line) is much smaller than T_i for high-frequency oscillations ($f > 1/RC_t$). However, if S_1 is square-wave switched at the same frequency f and phase as T_i , then a substantial DC temperature offset can also be passed through the RC filter to appear at T_o . Thermal mixers can also be used for thermal lock-in detection or thermal heterodyning (see main text).

a relative phase ϕ to the sinusoidal input temperature $T_i = A \sin(2\pi ft)$, the output DC temperature is $T_o = A(2/\pi) \cos(\phi)$ in the regime $f \gg 1/RC_t$. The thermal mixer therefore allows the energy in the high frequency thermal oscillations to be utilized at the output, rather than spending most of the energy to simply heat and cool the capacitor.

This mixer could also be used as a thermal lock-in detector to measure the amplitude A and phase ϕ of the unknown T_i from the measured DC output $T_o = A(2/\pi) \cos(\phi)$. For the mixer circuit shown in Fig. 17(b), ϕ and A can be determined by manually tuning the switching phase until T_o is maximized. If two thermal mixers with switching phases shifted by 90° are used, A and ϕ can be automatically calculated from the “in-phase” and “out-of-phase” signals

measured by the two mixers, thus playing the same role as the two phase sensitive detectors in a standard lock-in amplifier. It is also interesting to recognize that a thermal switching mixer with a switching frequency $f_s \neq f_o$ could heterodyne the input T_i , shifting the oscillation frequency f_o to a more convenient ($f_o \pm f_s$) beat frequency.

3. Thermal regulator and negative differential resistance circuits

Regulation: Figure 18(a) shows a regulator³⁰² designed to maintain a constant temperature T_{reg} , even in the presence of a fluctuating ambient temperature T_{amb} . At low temperatures, the regulator has a high resistance R_{off} , which

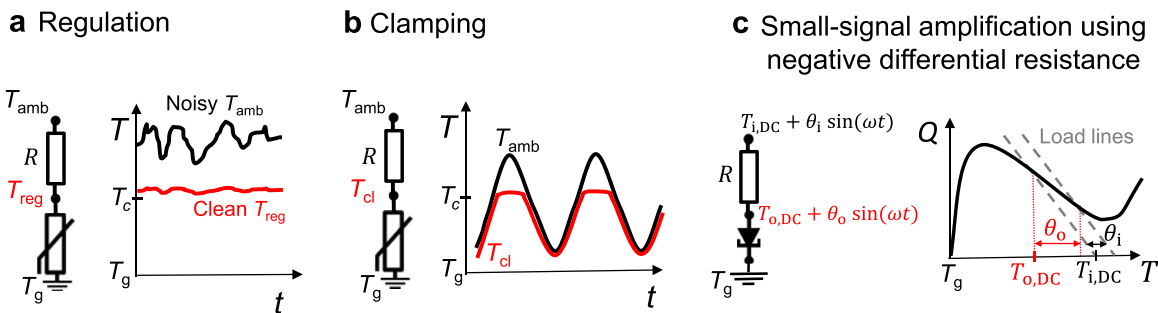


FIG. 18. Thermal regulator and negative differential resistance circuits. Electrical circuits for regulation, clamping, and small signal amplification can be adapted to the thermal domain. (a) A thermal regulator with a sharp change in thermal conductance near a critical temperature T_c can be used to maintain a regulated temperature T_{reg} in the presence of a noisy ambient temperature T_{amb} . (b) The same thermal regulator circuit can also be used to obtain a clamped temperature $T_{\text{cl}}(t)$ which closely tracks $T_{\text{amb}}(t)$ for low temperatures, but is clipped at the critical temperature T_c when $T_{\text{amb}} > T_c$. (c) Some regulator systems, [such as VO_2 radiative regulators (Sec. III C 2) or liquid-vapor boiling regulators (Sec. III B 2)] display negative differential resistance (NDR), a regime where Q decreases as the temperature difference increases. If the regulator is biased into this NDR regime, small temperature oscillations at the input are amplified at the output, $|\theta_o| > |\theta_i|$. The operating regime and amplification gain can be obtained graphically using a load line analysis (dashed lines).

transitions to a low R_{on} above the regulator's critical temperature T_c . Fluctuations in $(T_{amb} - T_c)$ appear at $(T_{reg} - T_c)$ damped (multiplied) by a factor (R_{on}/R) , which should be much less than one. For successful regulation, T_{amb} must always be greater than $T_{amb,min} = T_c + (R/R_{off})(T_c - T_g)$ to keep the regulator in the high temperature state. In scenarios where T_{amb} may temporarily dip below $T_{amb,min}$, a thermal capacitor could be placed in parallel with the regulator to buffer the temperature drop, or a thermal regulator with a large latent heat could be used to hold T_{reg} at T_c until T_{amb} again increases above $T_{amb,min}$. In the electrical domain, electrical regulators are commonly used to provide stable voltage sources. Analogous thermal implementations could be used to damp out unwanted temperature fluctuations for improved climate control, or in manufacturing applications and precision experiments when a stable and repeatable temperature is required.

Clamping: Figure 18(b) shows that the same regulator circuit in **a** can also be used as a clamp.³⁰² When $T_{amb} < T_c$, the ratio (R/R_{off}) should be small such that the clamped temperature T_{cl} is similar to T_{amb} . However, the regulator prevents T_{cl} from following T_{amb} above T_c , since the regulator switches into its low-resistance mode and holds T_{cl} near T_c . Clamping is useful for preventing sensitive components from overheating, while still allowing for strong thermal coupling and fast thermal response at lower temperatures.

Small-signal amplification: Figure 18(c) shows that a regulator with negative differential resistance (NDR) can amplify small temperature oscillations. NDR is observed in several types of regulators, such as the VO₂ radiative regulator discussed in Sec. III C 2 and the boiling heat transfer regulator discussed in Sec. III B 2. Since most regulators do not display NDR, here to help emphasize the unique NDR characteristics in Fig. 18(c) we use the symbol for an electrical tunnel diode, which displays similar NDR in the electrical domain. There has been a great deal of analytical and numerical research on thermal NDR, as reviewed by Li *et al.*¹ and by Ben-Abdallah and Biehs.² Here, we only discuss the most basic NDR circuit implemented in the electrical domain.³⁰⁶

To obtain small-signal AC amplification, the regulator must be DC biased into the regime of NDR by the series thermal resistor R . This DC bias input temperature $T_{i,DC}$ and the resulting DC output temperature $T_{o,DC}$ can be graphically determined using a load-line analysis, where the DC operating point is found as the intersection of the regulator's transfer function [solid line in Fig. 18(c)] with the load line (dashed line with slope $(-1/R)$ and abscissa intercept $T_{i,DC}$). Then, for an input temperature $T_i(t) = T_{i,DC} + \theta_i \sin(\omega t)$ representing oscillations of amplitude θ_i around $T_{i,DC}$, the output temperature response will be $T_o(t) = T_{o,DC} + \theta_o \sin(\omega t)$. To calculate the output oscillation amplitude θ_o the key property of the regulator is the differential resistance $R_{NDR} = \frac{d(T-T_g)}{dQ}$ near $T_{o,DC}$, where T_g is the ground temperature. In the most interesting regime, R_{NDR} is negative, as depicted in Fig. 18(c) by the negative slope of the regulator transfer function near $T_{o,DC}$. A simple voltage divider analysis equating the oscillating heat flow in the series and NDR resistors then shows that $\theta_o = \theta_i \left(\frac{R_{NDR}}{R + R_{NDR}} \right)$. DC biasing the regulator into the NDR

regime requires that $R_{NDR} < -R$, so $|\theta_o| > |\theta_i|$ and thus the input oscillations are amplified by the NDR regulator. The small-signal gain diverges as $R_{NDR} \rightarrow -R$; the physical gain is limited by the finite region of negative R_{NDR} . These amplification trends also have a convenient graphical explanation from the load line analysis, as illustrated in Fig. 18(c) by perturbing the load-line intercept at $T_{i,DC}$ by θ_i and graphically finding the resulting shift θ_o away from $T_{o,DC}$.

D. Summary and outlook

We have seen that there are a wide variety of physical mechanisms which lead to switchable and nonlinear heat transfer in the vicinity of room temperature. Very good performance can be achieved using mature mechanisms such as contact thermal switches, phase change thermal regulators, and heat pipes, or indeed with active convection control by valves and pumps. However, such traditional mechanisms are not suitable for all applications due to size constraints, the required orientation with respect to gravity, or maintenance requirements.

Looking ahead, there would be much excitement if solid-state thermal switches, regulators, and diodes could be developed with similarly high performance as those traditional mechanisms. This need motivates fundamental research into new solid-state mechanisms. Promising avenues of exploration for solid-state components include intercalation, gating the thermal conductivity of 2D materials, exploiting solid-solid phase transitions, and further optimization of shape memory alloy actuators, MEMS contact thermal switches, and thermal expansion regulators.

In the area of convective heat transfer, advances in surface science have led to gravity-independent thermal switches using superhydrophobic and superhydrophilic surfaces. Large switch ratios have also been obtained using electric fields to control boiling. Experimental demonstrations of new radiative thermal components are relatively sparse, in no small part due to the difficulty of achieving highly nonlinear and switchable radiative properties across a broad thermal spectrum. However, promising material systems include electrochromic materials, phase-change chalcogenides, and vanadium dioxide, and further demonstrations of near-field thermal switches or thermal diodes would be of great fundamental interest.

For all of these mechanisms, this review emphasized the on/off ratio r and rectification ratio γ as the primary figures of merit, since those characteristics are most fundamental to the definition of a switch, regulator, or diode. These figures of merit for thermal diodes and regulators will in general depend on both the temperature difference and the absolute magnitude of the temperature. Mechanisms involving phase change (e.g., the jumping drop diode in Fig. 8 and the VO₂ radiative diode in Fig. 11) have large jumps in γ or r near the critical temperature, but are relatively independent of ΔT as long as it is large enough to span the transition. Other mechanisms involving continuous processes (e.g., the continuous $k(T)$ junction diodes discussed in Sec. III A 2 and natural convection diodes in Sec. III B 1) have figures of merit which increase with ΔT . The temperature dependence of a given

mechanism should be carefully considered in the design of nonlinear thermal systems. For any particular application, many additional concerns such as cyclability, time response, the absolute magnitude of the on and off state conductances, cost, and integration within existing engineered systems will also play important roles. Therefore, researchers who are able to demonstrate improved performance of nonlinear or switchable components may also be well-served to quantify the cycling performance, hysteresis, and durability of the device, with an eye towards potential applications.

This review also discussed potential applications of thermal diodes, switches, and regulators. Thermal switches and thermal diodes have been used to implement all-solid state (electrocaloric or thermoelectric) refrigeration cycles. Thermal diodes can rectify an oscillating thermal source to provide a large DC temperature difference for waste heat scavenging. Thermal switches have also been used to increase the temperature difference across a thermoelectric module, which would lead to improved conversion efficiency. Other thermal circuits can be implemented by exploiting the analogies between thermal and electrical circuits; examples include a thermal load shifter using thermal diodes, a tunable switched-capacitance thermal resistor, and a thermal clamp to prevent overheating. Further experimental efforts are needed to provide insight on fundamental behavior of these circuits, and to determine which circuit and mechanisms are most appropriate for a given application.

There is still a great deal of work to be done in the field of nonlinear and switchable thermal components. As in the early days of electrical engineering, there are currently motivating applications driving the development of new devices, and many more unforeseen applications are sure to arise if a new generation of compact high performance thermal diodes, regulators, and switches can be developed. The pursuit of nonlinear and switchable thermal components should remain a motivating challenge to researchers for years to come.

ACKNOWLEDGMENTS

G.W. acknowledges the support by the NSF GRFP under Grant No. 1106400. J.W. acknowledges the support by NSF under Grant No. DMR-1608899. C.D. acknowledges the support from the Toyota Research Institute of North America.

- ¹N. Li, J. Ren, L. Wang, G. Zhang, P. Hänggi, and B. Li, *Rev. Mod. Phys.* **84**, 1045 (2012).
- ²P. Ben-Abdallah and S.-A. Biehs, *AIP Adv.* **5**, 053502 (2015).
- ³N. A. Roberts and D. G. Walker, *Int. J. Therm. Sci.* **50**, 648 (2011).
- ⁴M. J. Dipirro and P. J. Shirron, *Cryogenics* **62**, 172 (2014).
- ⁵A. Shahriari, P. Birbarah, J. Oh, N. Miljkovic, and V. Bahadur, *Nanoscale Microscale Thermophys. Eng.* **21**, 102 (2016).
- ⁶S. R. Sklan, *AIP Adv.* **5**, 053302 (2015).
- ⁷J. H. Lienhard V and J. H. Lienhard IV, *A Heat Transfer Textbook* (Dover, Mineola, 2011), p. 197.
- ⁸A. S. Grove, *Physics and Technology of Semiconductor Devices* (John Wiley and Sons, Inc., New York, 1967), pp. 180–191.
- ⁹L. Brillouin, *Phys. Rev.* **78**, 627 (1950).
- ¹⁰C. Dames, *J. Heat Transfer* **131**, 061301 (2009).
- ¹¹K. G. Sandeman, *Scr. Mater.* **67**, 566 (2012).
- ¹²J. F. Scott, *Annu. Rev. Mater. Res.* **41**, 229 (2011).

- ¹³T. Tsukamoto, M. Esashi, and S. Tanaka, *J. Micromech. Microeng.* **22**, 094008 (2012).
- ¹⁴Y. Jia and Y. Sungtaek Ju, *Appl. Phys. Lett.* **100**, 242901 (2012).
- ¹⁵Y. D. Wang, S. J. Smullin, M. J. Sheridan, Q. Wang, C. Eldershaw, and D. E. Schwartz, *Appl. Phys. Lett.* **107**, 134103 (2015).
- ¹⁶R. Ma, Z. Zhang, K. Tong, D. Huber, R. Kornbluh, Y. S. Ju, and Q. Pei, *Science* **357**, 1130 (2017).
- ¹⁷A. D. Laws, Y. J. Chang, V. M. Bright, and Y. C. Lee, *J. Electron. Packag.* **130**, 021011 (2008).
- ¹⁸S. D. Burch, M. A. Keyser, C. P. Colucci, T. F. Potter, D. K. Benson, and J. P. Biel, SAE Technical Paper No. 961134 (1996).
- ¹⁹D. K. Benson, T. F. Potter, and C. E. Tracy, SAE Technical Paper No. 940315 (1994).
- ²⁰J. Kimling, R. B. Wilson, K. Rott, J. Kimling, G. Reiss, and D. G. Cahill, *Phys. Rev. B* **91**, 144405 (2015).
- ²¹D. W. Hengeveld, M. M. Mathison, J. E. Braun, E. A. Groll, and A. D. Williams, *HVAC&R Res.* **16**, 189 (2010).
- ²²D.-W. Oh, C. Ko, S. Ramanathan, and D. G. Cahill, *Appl. Phys. Lett.* **96**, 151906 (2010).
- ²³H. Kizuka, T. Yagi, J. Jia, Y. Yamashita, S. Nakamura, N. Taketoshi, and Y. Shigesato, *Jpn. J. Appl. Phys., Part 1* **54**, 053201 (2015).
- ²⁴S. Lee, K. Hippalgaonkar, F. Yang, J. Hong, C. Ko, J. Suh, K. Liu, K. Wang, J. J. Urban, X. Zhang, C. Dames, S. A. Hartnoll, O. Delaire, and J. Wu, *Science* **355**, 371 (2017).
- ²⁵C. N. Berglund and H. J. Guggenheim, *Phys. Rev.* **185**, 1022 (1969).
- ²⁶V. N. Andreev, F. A. Chudnovskii, A. V. Petrov, and E. I. Terukov, *Phys. Status Solidi (a)* **48**, K153 (1978).
- ²⁷N. L. Wang, G. H. Cao, P. Zheng, G. Li, Z. Fang, T. Xiang, H. Kitazawa, and T. Matsumoto, *Phys. Rev. B* **69**, 153104 (2004).
- ²⁸K.-T. Ko, H.-H. Lee, D.-H. Kim, J.-J. Yang, S.-W. Cheong, M. J. Eom, J. S. Kim, R. Gammag, K.-S. Kim, H.-S. Kim, T.-H. Kim, H.-W. Yeom, T.-Y. Koo, H.-D. Kim, and J.-H. Park, *Nat. Commun.* **6**, 7342 (2015).
- ²⁹J. Hejtmánek, Z. Jiráček, M. Maryško, C. Martin, A. Maignan, M. Hervieu, and B. Raveau, *Phys. Rev. B* **60**, 14057 (1999).
- ³⁰M. Wuttig and N. Yamada, *Nat. Mater.* **6**, 824 (2007).
- ³¹E. Bozorg-Grayeli, J. P. Reifenberg, M. Asheghi, H.-S. P. Wong, and K. E. Goodson, in *Annual Review of Heat Transfer* (Begell House, Inc., 2013), pp. 397–420.
- ³²H.-K. Lyeo, D. G. Cahill, B.-S. Lee, J. R. Abelson, M.-H. Kwon, K.-B. Kim, S. G. Bishop, and B. Cheong, *Appl. Phys. Lett.* **89**, 151904 (2006).
- ³³J. P. Reifenberg, M. A. Panzer, S. Kim, A. M. Gibby, Y. Zhang, S. Wong, H. S. P. Wong, E. Pop, and K. E. Goodson, *Appl. Phys. Lett.* **91**, 111904 (2007).
- ³⁴J. Lee, E. Bozorg-grayeli, S. Kim, M. Asheghi, H. Philip, and K. E. Goodson, *Appl. Phys. Lett.* **102**, 191911 (2013).
- ³⁵A. B. Batdalov, A. M. Aliev, L. N. Khanov, V. D. Buchel'nikov, V. V. Sokolovskii, V. V. Koledov, V. G. Shavrov, A. V. Mashirov, and E. T. Dil'mieva, *J. Exp. Theor. Phys.* **122**, 874 (2016).
- ³⁶H. Liu, X. Shi, F. Xu, L. Zhang, W. Zhang, L. Chen, Q. Li, C. Uher, T. Day, and G. J. Snyder, *Nat. Mater.* **11**, 422 (2012).
- ³⁷K. Tyagi, B. Gahtori, S. Bathula, M. Jayasimhadri, N. K. Singh, S. Sharma, D. Haranath, A. K. Srivastava, and A. Dhar, *J. Phys. Chem. Solids* **81**, 100 (2015).
- ³⁸G. T. Hohensee, M. R. Fellingner, D. R. Trinkle, and D. G. Cahill, *Phys. Rev. B* **91**, 205104 (2015).
- ³⁹M. Núñez-Regueiro, J. Lopez-Castillo, and C. Ayache, *Phys. Rev. Lett.* **55**, 1931 (1985).
- ⁴⁰Y.-K. Kuo, C. S. Lue, F. H. Hsu, H. H. Li, and H. D. Yang, *Phys. Rev. B* **64**, 125124 (2001).
- ⁴¹T. Katsufuji, T. Okuda, R. Murata, T. Kanzaki, K. Takayama, and T. Kajita, *J. Phys. Soc. Jpn.* **85**, 013703 (2016).
- ⁴²S. D. Lubner, J. Choi, G. Wehmeyer, B. Waag, V. Mishra, H. Natesan, J. C. Bischof, and C. Dames, *Rev. Sci. Instrum.* **86**, 14905 (2015).
- ⁴³C. Velez, M. Khayet, J. M. Ortiz, and D. Zarate, *Appl. Energy* **143**, 383 (2015).
- ⁴⁴C. Y. Ho, R. W. Powell, and P. E. Liley, *J. Phys. Chem. Ref. Data* **1**, 279 (1972).
- ⁴⁵K. Kim and M. Kaviani, *Phys. Rev. B* **94**, 155203 (2016).
- ⁴⁶A. Bath, J. G. Gasser, and R. Kleim, *Phys. Lett. A* **91**, 355 (1982).
- ⁴⁷R. Zheng, J. Gao, J. Wang, and G. Chen, *Nat. Commun.* **2**, 289 (2011).
- ⁴⁸S. N. Schiffres, S. Harish, S. Maruyama, J. Shiomi, and J. A. Malen, *ACS Nano* **7**, 11183 (2013).
- ⁴⁹S. A. Angayarkanni and J. Philip, *J. Appl. Phys.* **118**, 094306 (2015).

- ⁵⁰S. Harish, D. Orejon, Y. Takata, and M. Kohno, *Thermochim. Acta* **600**, 1 (2015).
- ⁵¹S. A. Angayarkanni and J. Philip, *J. Phys. Chem. C* **118**, 13972 (2014).
- ⁵²R. J. Warzoha, R. M. Weigand, and A. S. Fleischer, *Appl. Energy* **137**, 716 (2015).
- ⁵³S. Harish, K. Ishikawa, S. Chiashi, J. Shiomi, and S. Maruyama, *J. Phys. Chem. C* **117**, 15409 (2013).
- ⁵⁴Y. Wu, X. Yan, P. Meng, P. Sun, G. Cheng, and R. Zheng, *Carbon N. Y.* **94**, 417 (2015).
- ⁵⁵A. A. Maznev, A. G. Every, and O. B. Wright, *Wave Motion* **50**, 776 (2013).
- ⁵⁶Z. Chen, C. Wong, S. Lubner, S. Yee, J. Miller, W. Jang, C. Hardin, A. Fong, J. E. Garay, and C. Dames, *Nat. Commun.* **5**, 5446 (2014).
- ⁵⁷Y. Kage, H. Hagino, R. Yanagisawa, J. Maire, K. Miyazaki, and M. Nomura, *Jpn. J. Appl. Phys., Part 1* **55**, 085201 (2016).
- ⁵⁸M. Schmotz, J. Maier, E. Scheer, and P. Leiderer, *New J. Phys.* **13**, 113027 (2011).
- ⁵⁹C.-L. Chiu, C.-H. Wu, B.-W. Huang, C.-Y. Chien, and C.-W. Chang, *AIP Adv.* **6**, 121901 (2016).
- ⁶⁰C. W. Chang, D. Okawa, A. Majumdar, and A. Zettl, *Science* **314**, 1121 (2006).
- ⁶¹A. Jezowski and J. Rafalowicz, *Phys. Status Solidi A* **47**, 229 (1978).
- ⁶²W. Kobayashi, Y. Teraoka, and I. Terasaki, *Appl. Phys. Lett.* **95**, 171905 (2009).
- ⁶³T. Takeuchi, H. Goto, R. S. Nakayama, Y. I. Terazawa, K. Ogawa, A. Yamamoto, T. Itoh, and M. Mikami, *J. Appl. Phys.* **111**, 093517 (2012).
- ⁶⁴R. S. Nakayama and T. Takeuchi, *J. Electron. Mater.* **44**, 356 (2015).
- ⁶⁵H. Wang, S. Hu, K. Takahashi, X. Zhang, H. Takamatsu, and J. Chen, *Nat. Commun.* **8**, 15843 (2017).
- ⁶⁶H. Tian, D. Xie, Y. Yang, T.-L. Ren, G. Zhang, Y.-F. Wang, C.-J. Zhou, P.-G. Peng, L.-G. Wang, and L.-T. Liu, *Sci. Rep.* **2**, 523 (2012).
- ⁶⁷Y. Wang, A. Vallabhaneni, J. Hu, B. Qiu, Y. P. Chen, and X. Ruan, *Nano Lett.* **14**, 592 (2014).
- ⁶⁸D. B. Go and M. Sen, *J. Heat Transfer* **132**, 124502 (2010).
- ⁶⁹F. A. Herrera, T. Luo, and D. B. Go, *J. Heat Transfer* **139**, 091301 (2017).
- ⁷⁰T. Zhang and T. Luo, *Small* **11**, 4657 (2015).
- ⁷¹A. L. Cottrill and M. S. Strano, *Adv. Energy Mater.* **5**, 1500921 (2015).
- ⁷²K. I. Garcia-Garcia and J. Alvarez-Quintana, *Int. J. Therm. Sci.* **81**, 76 (2014).
- ⁷³J. J. Martínez-Flores, L. Licea-Jimenez, S. A. Perez Garcia, and J. Alvarez-Quintana, *J. Appl. Phys.* **114**, 104904 (2013).
- ⁷⁴E. Pallecchi, Z. Chen, G. E. Fernandes, Y. Wan, J. H. Kim, and J. Xu, *Mater. Horiz.* **2**, 125 (2015).
- ⁷⁵W. Kobayashi, D. Sawaki, T. Omura, T. Katsufuji, Y. Moritomo, and I. Terasaki, *Appl. Phys. Express* **5**, 027302 (2012).
- ⁷⁶S. Wang, A. L. Cottrill, Y. Kunai, A. R. Toland, P. Liu, W.-J. Wang, and M. S. Strano, *Phys. Chem. Chem. Phys.* **19**, 13172 (2017).
- ⁷⁷J. Zhu, K. Hippalgaonkar, S. Shen, K. Wang, Y. Abate, S. Lee, J. Wu, X. Yin, A. Majumdar, and X. Zhang, *Nano Lett.* **14**, 4867 (2014).
- ⁷⁸J. Issi, J. Heremans, and M. S. Dresselhaus, *Phys. Rev. B* **27**, 1333 (1983).
- ⁷⁹G. Zhu, J. Liu, Q. Zheng, R. Zhang, D. Li, D. Banerjee, and D. G. Cahill, *Nat. Commun.* **7**, 13211 (2016).
- ⁸⁰J. Cho, M. D. Losego, H. G. Zhang, H. Kim, J. Zuo, I. Petrov, D. G. Cahill, and P. V. Braun, *Nat. Commun.* **5**, 4035 (2014).
- ⁸¹J. S. Kang, M. Ke, and Y. Hu, *Nano Lett.* **17**, 1431 (2017).
- ⁸²R. Prasher, *Proc. IEEE* **94**, 1571 (2006).
- ⁸³C. V. Madhusudana, *Thermal Contact Conductance*, 2nd ed. (Springer International Publishing, Switzerland, 2014).
- ⁸⁴I. S. McKay and E. N. Wang, *Energy* **57**, 632 (2013).
- ⁸⁵M. Westwood, M.S. thesis, University of California, Berkeley, 2015.
- ⁸⁶J. Cho, C. Richards, D. Bahr, J. Jiao, and R. Richards, *J. Micromech. Microeng.* **18**, 105012 (2008).
- ⁸⁷J. H. Cho, L. W. Weiss, C. D. Richards, D. F. Bahr, and R. F. Richards, *J. Micromech. Microeng.* **17**, S217 (2007).
- ⁸⁸G. Cha and Y. S. Ju, *Appl. Phys. Lett.* **94**, 211904 (2009).
- ⁸⁹Y. Jai and Y. S. Ju, *J. Heat Transfer* **136**, 074503 (2014).
- ⁹⁰S. H. Jeong, S. K. Nam, W. Nakayama, and S. K. Lee, *Appl. Therm. Eng.* **59**, 283 (2013).
- ⁹¹J. Currano, S. Moghaddam, J. Lawler, and J. Kim, *J. Thermophys. Heat Transfer* **22**, 360 (2008).
- ⁹²A. Ueno and Y. Suzuki, *Appl. Phys. Lett.* **104**, 093511 (2014).
- ⁹³T. Slater, P. Van Gerwen, E. Masure, F. Preud'homme, and K. Baert, *Sens. Actuators A* **53**, 423 (1996).
- ⁹⁴R. N. Supino and J. J. Talghader, *Appl. Phys. Lett.* **78**, 1778 (2001).
- ⁹⁵H. Kim, H. Liao, H. O. Song, and T. W. Kenny, in *IEEE 21st International Conference on Micro Electro Mechanical Systems* (Tuscon, AZ, 2008), pp. 852–855.
- ⁹⁶J. Yang, Y. Yang, S. W. Waltermire, X. Wu, H. Zhang, T. Gutu, Y. Jiang, Y. Chen, A. A. Zinn, R. Prasher, T. T. Xu, and D. Li, *Nat. Nanotechnol.* **7**, 91 (2012).
- ⁹⁷C. W. Chang, D. Okawa, H. Garcia, T. D. Yuzvinsky, A. Majumdar, and A. Zettl, *Appl. Phys. Lett.* **90**, 193114 (2007).
- ⁹⁸E. Sunada, K. Lankford, M. Pauken, K. S. Novak, and G. Birur, in *Space Technology and Applications International Forum*, edited by M. S. El-Genk and M. J. Bragg (AIP Publishing, Albuquerque, New Mexico, 2002), pp. 211–213.
- ⁹⁹D. G. Gilmore, *Spacecraft Thermal Control Handbook*, 2nd ed. (American Institute of Aeronautics and Astronautics/Aerospace Press, USA, 2002), Vol. 1, pp. 331–352.
- ¹⁰⁰D. Copic and A. J. Hart, *ACS Appl. Mater. Interfaces* **7**, 8218 (2015).
- ¹⁰¹X. Geng, P. Patel, A. Narain, and D. D. Meng, *J. Micromech. Microeng.* **21**, 085018 (2011).
- ¹⁰²M. dos S. Bernardes, *Int. J. Heat Mass Transfer* **73**, 354 (2014).
- ¹⁰³P. R. Gaddam, S. T. Huxtable, and W. A. Ducker, *Int. J. Heat Mass Transfer* **106**, 741 (2017).
- ¹⁰⁴L. Guo, X. Zhang, Y. Huang, R. Hu, and C. Liu, *Appl. Therm. Eng.* **113**, 1242 (2017).
- ¹⁰⁵B. Marland, D. Bugby, and C. Stouffer, *Cryogenics* **44**, 413 (2004).
- ¹⁰⁶H. S. Choe, J. Suh, C. Ko, K. Dong, S. Lee, Y. Lee, K. Wang, and J. Wu, *Sci. Rep.* **7**, 7131 (2017).
- ¹⁰⁷K. E. Bulgrin, Y. S. Ju, G. P. Carman, and A. S. Lavine, *J. Heat Transfer* **133**, 101401 (2011).
- ¹⁰⁸O. Benafan, W. U. Notardonato, B. J. Meneghelli, and R. Vaidyanathan, *Smart Mater. Struct.* **22**, 105017 (2013).
- ¹⁰⁹W. Guo, Y. Li, Y.-Z. Li, M.-L. Zhong, S.-N. Wang, J.-X. Wang, and J.-X. Zhang, *Appl. Therm. Eng.* **114**, 744 (2017).
- ¹¹⁰Y. Li, X. Shen, Z. Wu, J. Huang, Y. Chen, Y. Ni, and J. Huang, *Phys. Rev. Lett.* **115**, 195503 (2015).
- ¹¹¹C. Y. Tso and C. Y. H. Chao, *Int. J. Heat Mass Transfer* **93**, 605 (2016).
- ¹¹²C. Uher, *Thermal Conductivity: Theory, Properties and Applications* (Springer US, New York, 2004), pp. 21–91.
- ¹¹³D. G. Cahill, S. Watson, and R. Pohl, *Phys. Rev. B* **46**, 6131 (1992).
- ¹¹⁴N. W. Ashcroft and N. D. Mermin, *Solid State Physics* (Holt, Rinehart and Winston, 1976), pp. 340–342.
- ¹¹⁵G. J. Snyder and E. S. Toberer, *Nat. Mater.* **7**, 105 (2008).
- ¹¹⁶L. J. Li, E. C. T. O'Farrell, K. P. Loh, G. Eda, B. Özyilmaz, and A. H. Castro Neto, *Nature* **529**, 185 (2015).
- ¹¹⁷X. Xi, H. Berger, L. Forro, J. Shan, and K. F. Mak, *Phys. Rev. Lett.* **117**, 106801 (2016).
- ¹¹⁸C. Xu, L. Wang, Z. Liu, L. Chen, J. Guo, N. Kang, X.-L. Ma, H.-M. Cheng, and W. Ren, *Nat. Mater.* **14**, 1135 (2015).
- ¹¹⁹S. Thiel, G. Hammerl, A. Schmehl, C. W. Schneider, and J. Mannhart, *Science* **313**, 1942 (2006).
- ¹²⁰L. P. Kadanoff and P. C. Martin, *Ann. Phys. (N. Y.)* **24**, 419 (1963).
- ¹²¹M. Muller, L. Fritz, and S. Sachdev, *Phys. Rev. B* **78**, 115406 (2008).
- ¹²²M. A. Tanatar, J. Paglione, C. Petrovic, and L. Taillefer, *Science* **316**, 1320 (2007).
- ¹²³R. W. Hill, C. Proust, L. Taillefer, P. Fournier, and R. L. Greene, *Nature* **414**, 711 (2001).
- ¹²⁴N. Wakeham, A. F. Bangura, X. Xu, J.-F. Mercure, M. Greenblatt, and N. E. Hussey, *Nat. Commun.* **2**, 396 (2011).
- ¹²⁵J. L. Cohn, B. D. White, C. A. M. dos Santos, and J. J. Neumeier, *Phys. Rev. Lett.* **108**, 056604 (2012).
- ¹²⁶J. Crossno, J. K. Shi, K. Wang, X. Liu, A. Harzheim, A. Lucas, S. Sachdev, P. Kim, T. Taniguchi, K. Watanabe, T. A. Ohki, and K. C. Fong, *Science* **351**, 1058 (2016).
- ¹²⁷J. Crossno, X. Liu, T. A. Ohki, P. Kim, and K. C. Fong, *Appl. Phys. Lett.* **106**, 023121 (2015).
- ¹²⁸S. Yigen and A. R. Champagne, *Nano Lett.* **14**, 289 (2014).
- ¹²⁹P. E. Hopkins, C. Adamo, L. Ye, B. D. Huey, S. R. Lee, D. G. Schlom, and J. F. Ihlefeld, *Appl. Phys. Lett.* **102**, 121903 (2013).
- ¹³⁰J. F. Ihlefeld, B. M. Foley, D. A. Scrymgeour, J. R. Michael, B. B. McKenzie, D. L. Medlin, M. Wallace, S. Trolrier-McKinstry, and P. E. Hopkins, *Nano Lett.* **15**, 1791 (2015).
- ¹³¹I. Hatta and A. Ikushima, *J. Phys. Soc. Jpn.* **41**, 558 (1976).
- ¹³²K. Kalaidjiev, M. Mikhailov, G. I. Bozhanov, and S. R. Stoyanov, *Phys. Status Solidi A* **69**, 163 (1982).

- ¹³³A. G. Chynoweth, *J. Appl. Phys.* **27**, 78 (1956).
- ¹³⁴Z. Q. Liu, L. Li, Z. Gai, J. D. Clarkson, S. L. Hsu, A. T. Wong, L. S. Fan, M. W. Lin, C. M. Rouleau, T. Z. Ward, H. N. Lee, A. S. Sefat, H. M. Christen, and R. Ramesh, *Phys. Rev. Lett.* **116**, 097203 (2016).
- ¹³⁵J. M. Ziman, *Electrons and Phonons* (Oxford University Press, Great Britain, 1960), pp. 483–523.
- ¹³⁶J. Kimling, J. Gooth, and K. Nielsch, *Phys. Rev. B* **87**, 094409 (2013).
- ¹³⁷G. W. C. Kaye and W. F. Higgins, *London, Edinburgh, Dublin Philos. Mag. J. Sci.* **8**, 1056 (1929).
- ¹³⁸W. M. Yim and A. Amith, *Solid State Electron.* **15**, 1141 (1972).
- ¹³⁹F. Y. Yang, K. Liu, K. Hong, D. H. Reich, P. C. Searson, and C. L. Chien, *Science* **284**, 1335 (1999).
- ¹⁴⁰C. Shekhar, A. K. Nayak, Y. Sun, M. Schmidt, M. Nicklas, I. Leermakers, U. Zeitler, Y. Skourski, J. Wosnitza, Z. Liu, Y. Chen, W. Schnelle, H. Borrmann, Y. Grin, C. Felser, and B. Yan, *Nat. Phys.* **11**, 645 (2015).
- ¹⁴¹M. N. Baibich, J. M. Broto, A. Fert, F. N. Van Dau, F. Petroff, P. Eitenne, G. Creuzet, A. Friederich, and J. Chazelas, *Phys. Rev. Lett.* **61**, 2472 (1988).
- ¹⁴²J. Shi, K. Pettit, E. Kita, S. Parkin, R. Nakatani, and M. Salamon, *Phys. Rev. B* **54**, 15273 (1996).
- ¹⁴³H. Sato, H. Henmi, Y. Kobayashi, Y. Aoki, H. Yamamoto, T. Shinjo, and V. Sechovsky, *J. Appl. Phys.* **76**, 6919 (1994).
- ¹⁴⁴L. Piraux, M. Cassart, J. S. Jiang, J. Q. Xiao, and C. L. Chien, *Phys. Rev. B* **48**, 638 (1993).
- ¹⁴⁵F. Tsui, B. Chen, J. Wellman, C. Uher, and R. Clarke, *J. Appl. Phys.* **81**, 4586 (1997).
- ¹⁴⁶Y. Yang, J. G. Zhu, R. M. White, and M. Asheghi, *J. Appl. Phys.* **99**, 063703 (2006).
- ¹⁴⁷J. Kimling, K. Nielsch, K. Rott, and G. Reiss, *Phys. Rev. B* **87**, 134406 (2013).
- ¹⁴⁸S. Yuasa, T. Nagahama, A. Fukushima, Y. Suzuki, and K. Ando, *Nat. Mater.* **3**, 868 (2004).
- ¹⁴⁹R. B. Wilson and D. G. Cahill, *Phys. Rev. Lett.* **108**, 255901 (2012).
- ¹⁵⁰C. Monachon, L. Weber, and C. Dames, *Annu. Rev. Mater. Res.* **46**, 433 (2016).
- ¹⁵¹A. Ramirez, *J. Phys. Condens. Matter* **9**, 8171 (1997).
- ¹⁵²E. Dagatto, *Nanoscale Phase Separation and Colossal Magnetoresistance: The Physics of Manganites and Related Compounds* (Springer-Verlag, Berlin, Heidelberg, New York, 2013).
- ¹⁵³R. M. Kusters, J. Singleton, D. A. Keen, R. McGreevy, and W. Hayes, *Physica B* **155**, 362 (1989).
- ¹⁵⁴S. Jin, M. McCormack, T. H. Tiefel, and R. Ramesh, *J. Appl. Phys.* **76**, 6929 (1994).
- ¹⁵⁵D. Visser, A. Ramirez, and M. Subramanian, *Phys. Rev. Lett.* **78**, 3947 (1997).
- ¹⁵⁶C. Euler, P. Holuj, A. Talkenberger, and G. Jakob, *J. Magn. Magn. Mater.* **381**, 188 (2015).
- ¹⁵⁷O. D. Lavrentovich, *Oxford Handbook Soft Condensed Matter* (Oxford University Press, New York, 2015), pp. 96–146.
- ¹⁵⁸V. S. V. Rajan and J. J. C. Picot, *Mol. Cryst. Liq. Cryst.* **20**, 55 (1973).
- ¹⁵⁹J. Shin, M. Kang, T. Tsai, C. Leal, P. V. Braun, and D. G. Cahill, *ACS Macro Lett.* **5**, 955 (2016).
- ¹⁶⁰A. Hadj Sahraoui, S. Delenclos, S. Longuemart, and D. Dadarlat, *J. Appl. Phys.* **110**, 033510 (2011).
- ¹⁶¹S. Fumeron, E. Pereira, and F. Moraes, *Phys. Rev. E* **89**, 020501 (2014).
- ¹⁶²D. Melo, I. Fernandes, F. Moraes, S. Fumeron, and E. Pereira, *Phys. Lett. A* **380**, 3121 (2016).
- ¹⁶³I. Dierking, G. Scalia, P. Morales, and D. LeClere, *Adv. Mater.* **16**, 865 (2004).
- ¹⁶⁴T.-Z. Shen, S.-H. Hong, and J.-K. Song, *Nat. Mater.* **13**, 394 (2014).
- ¹⁶⁵F. Lin, Z. Zhu, X. Zhou, W. Qiu, C. Niu, J. Hu, K. Dahal, Y. Wang, Z. Zhao, Z. Ren, D. Litvinov, Z. Liu, Z. M. Wang, and J. Bao, *Adv. Mater.* **29**, 1604453 (2017).
- ¹⁶⁶P. C. Sun, Y. Huang, R. T. Zheng, G. A. Cheng, Q. M. Wan, and Y. L. Ding, *Mater. Lett.* **149**, 92 (2015).
- ¹⁶⁷Z. Chen, P.-C. Hsu, J. Lopez, Y. Li, J. W. F. To, N. Liu, C. Wang, S. C. Andrews, J. Liu, Y. Cui, and Z. Bao, *Nat. Energy* **1**, 15009 (2016).
- ¹⁶⁸S.-F. Lee, J. M. Gildemeister, W. Holmes, A. T. Lee, and P. L. Richards, *Appl. Opt.* **37**, 3391 (1998).
- ¹⁶⁹R. Xie, C. T. Bui, B. Varghese, Q. Zhang, C. H. Sow, B. Li, and J. T. L. Thong, *Adv. Funct. Mater.* **21**, 1602 (2011).
- ¹⁷⁰E. N. Lorenz, *J. Atmos. Sci.* **20**, 130 (1963).
- ¹⁷¹F. P. Incropera, D. P. DeWitt, T. L. Bergman, and A. S. Lavine, *Fundamentals of Heat and Mass Transfer*, 6th ed. (John Wiley & Sons, 2007), p. 588.
- ¹⁷²F. C. Prenger, W. F. Stewart, and J. E. Runyan, *Adv. Cryog. Eng.* **39**, 1707 (1994).
- ¹⁷³S. Varga, A. C. Oliveira, and C. F. Afonso, *Energy Build.* **34**, 227 (2002).
- ¹⁷⁴C. I. Ezekwe, *Energy Convers. Manag.* **30**, 403 (1990).
- ¹⁷⁵D. Reay, R. McGlen, and P. Kew, *Heat Pipes: Theory, Design and Applications* (Butterworth-Heinemann, 2013).
- ¹⁷⁶S. Sorensen, J. Smith, and J. P. Zarling, in *11th International Conference on Cold Regions Engineering* (American Society of Civil Engineers, Anchorage, Alaska, USA, 2002), pp. 1–12.
- ¹⁷⁷G. Cheng, Q. Wu, and W. Ma, *Sci. China, Ser. E Technol. Sci.* **52**, 530 (2009).
- ¹⁷⁸D. G. Gilmore and M. Donabedian, *Spacecraft Thermal Control Handbook: Cryogenics* (American Institute of Aeronautics & Astronautics, 2003), Vol. 2.
- ¹⁷⁹M. Groll, W. D. Munzel, W. Supper, and C. J. Savage, *J. Spacecr.* **16**, 195 (1979).
- ¹⁸⁰J. B. Boreyko, Y. Zhao, and C. H. Chen, *Appl. Phys. Lett.* **99**, 234105 (2011).
- ¹⁸¹J. B. Boreyko and C. H. Chen, *Int. J. Heat Mass Transfer* **61**, 409 (2013).
- ¹⁸²J. B. Boreyko and C. H. Chen, *Phys. Rev. Lett.* **103**, 184501 (2009).
- ¹⁸³F. Zhou, Y. Liu, S. N. Joshi, E. M. Dede, X. Chen, and J. A. Weibel, in *16th IEEE Intersociety Conference on Thermal and Thermomechanical Phenomena in Electronic Systems* (IEEE Inc., Orlando, FL, 2017), pp. 521–529.
- ¹⁸⁴T. Tsukamoto, T. Hirayanagi, and S. Tanaka, *J. Micromech. Microeng.* **27**, 045001 (2017).
- ¹⁸⁵V. P. Carey, *Liquid Vapor Phase Change Phenomena*, 2nd ed. (Taylor & Francis, 2007).
- ¹⁸⁶H. J. Cho, D. J. Preston, Y. Zhu, and E. N. Wang, *Nat. Rev. Mater.* **2**, 16092 (2016).
- ¹⁸⁷See National Technical Information Service Document No. N7223952, *Theory and Design of Variable Conductance Heat Pipes* (B. D. Marcus, NASA Report No. 19720016303, 1972).
- ¹⁸⁸W. G. Anderson and C. Tarau, *AIP Conf. Proc.* **969**, 679–688 (2008).
- ¹⁸⁹M. Leriche, S. Harmand, M. Lippert, and B. Desmet, *Appl. Therm. Eng.* **38**, 48 (2012).
- ¹⁹⁰R. P. Bywaters and R. A. Griffin, *Cryogenics* **13**, 344 (1973).
- ¹⁹¹M. Chau, B. A. F. Kopera, V. R. Machado, S. M. Tehrani, M. A. Winnik, E. Kumacheva, and M. Retsch, *Mater. Horiz.* **4**, 236 (2017).
- ¹⁹²H.-M. Chang and H.-J. Kim, *Cryogenics* **40**, 769 (2000).
- ¹⁹³F. Mugele and J.-C. Baret, *J. Phys. Condens. Matter* **17**, R705 (2005).
- ¹⁹⁴G. Cha, C. J. Kim, and Y. S. Ju, *Appl. Therm. Eng.* **98**, 189 (2016).
- ¹⁹⁵A. R. McLanahan, C. D. Richards, and R. F. Richards, *J. Micromech. Microeng.* **21**, 104009 (2011).
- ¹⁹⁶H. J. Cho, J. P. Mizerak, and E. N. Wang, *Nat. Commun.* **6**, 8599 (2015).
- ¹⁹⁷F. Celestini and G. Kirstetter, *Soft Matter* **8**, 5992 (2012).
- ¹⁹⁸A. Shahriari, J. Wurz, and V. Bahadur, *Langmuir* **30**, 12074 (2014).
- ¹⁹⁹A. Shahriari, M. Hermes, and V. Bahadur, *Appl. Phys. Lett.* **108**, 091607 (2016).
- ²⁰⁰N. Miljkovic, D. J. Preston, R. Enright, and E. N. Wang, *Nat. Commun.* **4**, 2517 (2013).
- ²⁰¹N. Miljkovic, D. J. Preston, R. Enright, and E. N. Wang, *ACS Nano* **7**, 11043 (2013).
- ²⁰²J. Oh, P. Birbarah, T. Foulkes, S. L. Yin, M. Rentauskas, J. Neely, R. C. N. Pilawa-Podgurski, and N. Miljkovic, *Appl. Phys. Lett.* **110**, 123107 (2017).
- ²⁰³I. Nkurikiyimfura, Y. Wang, and Z. Pan, *Renew. Sustain. Energy Rev.* **21**, 548 (2013).
- ²⁰⁴B. A. Finlayson, *J. Fluid Mech.* **40**, 753 (1970).
- ²⁰⁵A. Mukhopadhyay, R. Ganguly, S. Sen, and I. K. Puri, *Int. J. Heat Mass Transfer* **48**, 3485 (2005).
- ²⁰⁶R. Azizian, E. Doroodchi, T. Mckrell, J. Buongiorno, L. W. Hu, and B. Moghtaderi, *Int. J. Heat Mass Transfer* **68**, 94 (2014).
- ²⁰⁷J. Philip, P. D. Shima, and B. Raj, *Nanotechnology* **19**, 305706 (2008).
- ²⁰⁸A. Katiyar, P. Dhar, T. Nandi, and S. K. Das, *Exp. Therm. Fluid Sci.* **78**, 345 (2016).
- ²⁰⁹P. D. Shima and J. Philip, *J. Phys. Chem. C* **115**, 20097 (2011).
- ²¹⁰I. Seshadri, A. Gardner, R. J. Mehta, R. Swartwout, P. Keblinski, T. Borca-Tasciuc, and G. Ramanath, *Appl. Phys. Lett.* **102**, 203111 (2013).

- ²¹¹J. B. Puga, B. D. Bordalo, D. J. Silva, M. M. Dias, J. H. Belo, J. P. Araújo, J. C. R. E. Oliveira, A. M. Pereira, and J. Ventura, *Nano Energy* **31**, 278 (2017).
- ²¹²G. Cha, Y. S. Ju, L. A. Ahure', and N. M. Wereley, *J. Appl. Phys.* **107**, 09B505 (2010).
- ²¹³B. N. Reinecke, J. W. Shan, K. K. Suabedissen, and A. S. Cherkasova, *J. Appl. Phys.* **104**, 023507 (2008).
- ²¹⁴N. O. Weiss and M. R. E. Proctor, *Magnetoconvection* (Cambridge University Press, 2014).
- ²¹⁵M. F. Romig, *Adv. Heat Transfer* **1**, 267 (1964).
- ²¹⁶S. Cioni, S. Chaumat, and J. Sommeria, *Phys. Rev. E* **62**, R4520(R) (2000).
- ²¹⁷K. Okada and H. Ozoe, *J. Heat Transfer* **114**, 107 (1992).
- ²¹⁸J. M. Aurnou and P. L. Olson, *J. Fluid Mech.* **430**, 283 (2001).
- ²¹⁹R. Gardner and P. Lykoudis, *J. Fluid Mech.* **48**, 129 (1971).
- ²²⁰E. L. Resler and W. R. Sears, *Journal of Aerospace Sciences* **25**, 235 (1958).
- ²²¹T. B. Jones, *Adv. Heat Transfer* **14**, 107 (1979).
- ²²²D. B. Go, R. A. Maturana, T. S. Fisher, and S. V. Garimella, *Int. J. Heat Mass Transfer* **51**, 6047 (2008).
- ²²³P. H. G. Allen and T. G. Karayiannist, *Heat Recover. Syst. CHP* **15**, 389 (1995).
- ²²⁴D. Braithwaite, E. Beaunon, and R. Tournier, *Nature* **354**, 134 (1991).
- ²²⁵L. Thomas, W. Pesch, and G. Ahlers, *Phys. Rev. E* **58**, 5885 (1998).
- ²²⁶S. Weiss and G. Ahlers, *J. Fluid Mech.* **716**, R7 (2013).
- ²²⁷M. Modest, *Radiative Heat Transfer*, 1st ed. (McGraw-Hill, USA, 1993), pp. 96–98.
- ²²⁸F. P. Incropera, D. P. DeWitt, T. L. Bergman, and A. S. Lavine, *Fundamentals of Heat and Mass Transfer*, 6th ed. (John Wiley & Sons, 2007), p. 747.
- ²²⁹A. S. Barker, H. W. Verleur, and H. J. Guggenheim, *Phys. Rev. Lett.* **26**, 1286 (1966).
- ²³⁰E. E. Chain, *Appl. Opt.* **30**, 2782 (1991).
- ²³¹M. A. Kats, R. Blanchard, S. Zhang, P. Genevet, C. Ko, S. Ramanathan, and F. Capasso, *Phys. Rev. X* **3**, 041004 (2013).
- ²³²A. Hendaoui, N. Émond, S. Dorval, M. Chaker, and E. Haddad, *Sol. Energy Mater. Sol. Cells* **117**, 494 (2013).
- ²³³A. Hendaoui, N. Émond, M. Chaker, and É. Haddad, *Appl. Phys. Lett.* **102**, 061107 (2013).
- ²³⁴L. Liu, L. Kang, T. S. Mayer, and D. H. Werner, *Nat. Commun.* **7**, 13236 (2016).
- ²³⁵R. Naorem, G. Dayal, S. A. Ramakrishna, B. Rajeswaran, and A. M. Umarji, *Opt. Commun.* **346**, 154 (2015).
- ²³⁶H. Kocer, S. Butun, E. Palacios, Z. Liu, S. Tongay, D. Fu, K. Wang, J. Wu, and K. Aydin, *Sci. Rep.* **5**, 13384 (2015).
- ²³⁷S. Wang, M. Liu, L. Kong, Y. Long, X. Jiang, and A. Yu, *Prog. Mater. Sci.* **81**, 1 (2016).
- ²³⁸K. Ito, K. Nishikawa, A. Miura, H. Toshiyoshi, and H. Iizuka, *Nano Lett.* **17**, 4347 (2017).
- ²³⁹K. Shimazaki, S. Tachikawa, A. Ohnishi, and Y. Nagasaka, *High Temp. - High Pressures* **33**, 525 (2001).
- ²⁴⁰S. Tachikawa, A. Ohnishi, Y. Shimakawa, A. Ochi, A. Okamoto, and Y. Nakamura, *J. Thermophys. Heat Transfer* **17**, 264 (2003).
- ²⁴¹L. Xiao, H. Ma, J. Liu, W. Zhao, Y. Jia, Q. Zhao, K. Liu, Y. Wu, Y. Wei, S. Fan, and K. Jiang, *Nano Lett.* **15**, 8365 (2015).
- ²⁴²K. Shportko, S. Kremers, M. Woda, D. Lencer, J. Robertson, and M. Wuttig, *Nat. Mater.* **7**, 653 (2008).
- ²⁴³K. Du, Q. Li, Y. Lyu, J. Ding, Y. Lu, and Z. Cheng, in *Conference on Lasers Electro-Optics* (OSA Publishing, San Jose, California, 2017), p. STh4I.3.
- ²⁴⁴M. Jafari and M. Rais-Zadeh, *Opt. Lett.* **41**, 1177 (2016).
- ²⁴⁵A. Seeboth and D. Lotzsch, *Encyclopedia of Polymer Science and Technology* (John Wiley and Sons, 2002), pp. 143–165.
- ²⁴⁶I. Sage, *Liq. Cryst.* **38**, 1551 (2011).
- ²⁴⁷G. Qian and Z. Y. Wang, *Adv. Mater.* **24**, 1582 (2012).
- ²⁴⁸K. Fan and W. J. Padilla, *Mater. Today* **18**, 39 (2015).
- ²⁴⁹X. Liu and W. J. Padilla, *Adv. Mater.* **28**, 871 (2016).
- ²⁵⁰D. Jalas, A. Petrov, M. Eich, W. Freude, S. Fan, Z. Yu, R. Baets, M. Popović, A. Melloni, J. D. Joannopoulos, M. Vanwolleghem, C. R. Doerr, and H. Renner, *Nat. Photonics* **7**, 579 (2013).
- ²⁵¹L. Rayleigh, *Nature* **64**, 577 (1901).
- ²⁵²B. V. Budaev, *Nat. Commun.* **8**, 16135 (2017).
- ²⁵³Z. Chen, C. Wong, S. Lubner, S. Yee, J. Miller, W. Jang, C. Hardin, A. Fong, J. E. Garay, and C. Dames, *Nat. Commun.* **8**, 16136 (2017).
- ²⁵⁴C. Dames and Z. Chen, e-print [arXiv:1705.10902](https://arxiv.org/abs/1705.10902).
- ²⁵⁵J. R. Howell, R. Siegel, and M. P. Menguc, *Thermal Radiation*, 5th ed. (CRC Press, 2011), p. 271.
- ²⁵⁶K. Ito, K. Nishikawa, H. Iizuka, and H. Toshiyoshi, *Appl. Phys. Lett.* **105**, 253503 (2014).
- ²⁵⁷Y. Wang, E. L. Runnerstrom, and D. J. Milliron, *Annu. Rev. Chem. Biomol. Eng.* **7**, 283 (2016).
- ²⁵⁸R. J. Mortimer, *Annu. Rev. Mater. Res.* **41**, 241 (2011).
- ²⁵⁹A. Kraft and M. Rottmann, *Sol. Energy Mater. Sol. Cells* **93**, 2088 (2009).
- ²⁶⁰A. L. Dyer, C. R. G. Grenier, and J. R. Reynolds, *Adv. Funct. Mater.* **17**, 1480 (2007).
- ²⁶¹H. Demiryont and D. Moorehead, *Sol. Energy Mater. Sol. Cells* **93**, 2075 (2009).
- ²⁶²P. Topart and P. Hourquebie, *Thin Solid Films* **352**, 243 (1999).
- ²⁶³E. B. Franke, C. L. Trimble, M. Schubert, J. A. Woollam, and J. S. Hale, *Appl. Phys. Lett.* **77**, 930 (2000).
- ²⁶⁴S.-T. Wu, *Opt. Eng.* **26**, 262120 (1987).
- ²⁶⁵O. Buchnev, J. Y. Ou, M. Kaczmarek, N. I. Zheludev, and V. A. Fedotov, *Opt. Express* **21**, 1633 (2013).
- ²⁶⁶S. Brugioni and R. Meucci, *J. Opt. A: Pure Appl. Opt.* **6**, 6 (2003).
- ²⁶⁷S. T. Wu, U. Efron, and L. D. Hess, *Appl. Phys. Lett.* **44**, 1033 (1984).
- ²⁶⁸J. W. McCargar, R. Ondris-Crawford, and J. L. West, *J. Electron. Imaging* **1**, 22 (1992).
- ²⁶⁹K. L. Marshall, S. D. Jacobs, and J. E. Miller, *Appl. Opt.* **34**, 6704 (1995).
- ²⁷⁰K. Yoshino, M. Ozaki, and S. Kishio, *Jpn. J. Appl. Phys., Part 1* **24**, 45 (1985).
- ²⁷¹V. Thareja, J. H. Kang, H. Yuan, K. M. Milaninia, H. Y. Hwang, Y. Cui, P. G. Kik, and M. L. Brongersma, *Nano Lett.* **15**, 1570 (2015).
- ²⁷²V. W. Brar, M. C. Sherrott, M. S. Jang, S. Kim, L. Kim, M. Choi, L. A. Sweatlock, and H. A. Atwater, *Nat. Commun.* **6**, 7032 (2015).
- ²⁷³T. Inoue, M. De Zoysa, T. Asano, and S. Noda, *Nat. Mater.* **13**, 928 (2014).
- ²⁷⁴A. Benz, I. Montaña, J. F. Klem, and I. Brener, *Appl. Phys. Lett.* **103**, 263116 (2013).
- ²⁷⁵X. Liu and W. J. Padilla, *Adv. Opt. Mater.* **1**, 559 (2013).
- ²⁷⁶J.-Y. Ou, E. Plum, J. Zhang, and N. I. Zheludev, *Nat. Nanotechnol.* **8**, 252 (2013).
- ²⁷⁷H. Nagano, A. Ohnishi, and K. Higuchi, *J. Spacecr. Rockets* **46**, 185 (2009).
- ²⁷⁸H. Nagano, Y. Nagasaka, and A. Ohnishi, *J. Thermophys. Heat Transfer* **20**, 856 (2006).
- ²⁷⁹B. Song, A. Fiorino, E. Meyhofer, and P. Reddy, *AIP Adv.* **5**, 053503 (2015).
- ²⁸⁰B. Song, D. Thompson, A. Fiorino, Y. Ganjeh, P. Reddy, and E. Meyhofer, *Nat. Nanotechnol.* **11**, 509 (2016).
- ²⁸¹M. Elzouka and S. Ndao, *Sci. Rep.* **7**, 44901 (2017).
- ²⁸²V. Chiloyan, J. Garg, K. Esfarjani, and G. Chen, *Nat. Commun.* **6**, 6755 (2015).
- ²⁸³K. Chen, P. Santhanam, S. Sandhu, L. Zhu, and S. Fan, *Phys. Rev. B* **91**, 134301 (2015).
- ²⁸⁴E. Moncada-Villa, V. Fernandez-Hurtado, F. J. Garcia-Vidal, A. Garcia-Martin, and J. C. Cuevas, *Phys. Rev. B* **92**, 125418 (2015).
- ²⁸⁵C. R. Otey, W. T. Lau, and S. Fan, *Phys. Rev. Lett.* **104**, 154301 (2010).
- ²⁸⁶S. J. Smullin, Y. Wang, and D. E. Schwartz, *Appl. Phys. Lett.* **107**, 093903 (2015).
- ²⁸⁷P. Kittel, *AIP Conf. Proc.* **613**, 1167–1174 (2002).
- ²⁸⁸B. Neese, B. Chu, S.-G. Lu, Y. Wang, E. Furman, and Q. M. Zhang, *Science* **321**, 821 (2008).
- ²⁸⁹R. I. Epstein and K. J. Malloy, *J. Appl. Phys.* **106**, 064509 (2009).
- ²⁹⁰U. Ghoshal and A. Guha, *J. Electron. Mater.* **38**, 1148 (2009).
- ²⁹¹A. Miner, A. Majumdar, and U. Ghoshal, *Appl. Phys. Lett.* **75**, 1176 (1999).
- ²⁹²G. J. Snyder, J. Fleurial, T. Caillat, R. Yang, and G. Chen, *J. Appl. Phys.* **92**, 1564 (2002).
- ²⁹³M. Rowe, *CRC Handbook of Thermoelectrics* (CRC Press, 1995).
- ²⁹⁴A. Gunawan, C. Lin, D. A. Buttry, V. Mujica, R. A. Taylor, R. S. Prasher, and P. E. Phelan, *Nanoscale Microscale Thermophys. Eng.* **17**, 304 (2013).
- ²⁹⁵L. L. Baranowski, G. Jeffrey Snyder, and E. S. Toberer, *J. Appl. Phys.* **113**, 204904 (2013).
- ²⁹⁶S. K. Yee, S. LeBlanc, K. E. Goodson, and C. Dames, *Energy Environ. Sci.* **7**, 3441 (2014).
- ²⁹⁷Y. Yan and J. A. Malen, *Energy Environ. Sci.* **6**, 1267 (2013).
- ²⁹⁸X. Gou, H. Ping, Q. Ou, H. Xiao, and S. Qing, *Appl. Energy* **160**, 843 (2015).

- ²⁹⁹R. McCarty, D. Monaghan, K. Hallinan, and B. Sanders, *J. Thermophys. Heat Transfer* **21**, 505 (2007).
- ³⁰⁰X. Zhao, M.S. thesis, University of California, Berkeley, 2015.
- ³⁰¹P. Horowitz and W. Hill, *The Art of Electronics*, 3rd ed. (Cambridge University Press, USA, 2015), p. 254.
- ³⁰²P. Scherz and S. Monk, *Practical Electronics for Inventors*, 3rd ed. (McGraw-Hill, 2013), pp. 412–424.
- ³⁰³A. R. Hambley, *Electrical Engineering: Principles and Applications*, 5th ed. (Prentice Hall, 2011), p. 487.
- ³⁰⁴R. Gregorian, K. W. Martin, and G. C. Temes, *Proc. IEEE* **71**, 941 (1983).
- ³⁰⁵P. Horowitz and W. Hill, *The Art of Electronics*, 2nd ed. (Cambridge University Press, 1989), p. 889.
- ³⁰⁶P. Horowitz and W. Hill, *The Art of Electronics*, 2nd ed. (Cambridge University Press, 1989), p. 14.
- ³⁰⁷W. R. Thurber, R. L. Mattis, Y. M. Liu, and J. J. Filliben, *J. Electrochem. Soc.* **127**, 2291 (1980).
- ³⁰⁸R. D. Redin, T. Ashworth, and C. Y. Hsiung, *Thermal Conductivity 15* (Springer, 1978), pp. 57–62.
- ³⁰⁹H. Kim, C. M. G. Piqué, J. S. Horwitz, H. Mattoussi, H. Murata, Z. H. Kafafi, and D. B. Chrisey, *J. Appl. Phys.* **86**, 6451 (1999).
- ³¹⁰P. Zhu, Y. Imai, Y. Isoda, Y. Shinohara, X. Jia, and G. Zou, *Mater. Trans.* **46**, 2690 (2005).
- ³¹¹S. H. Chang, C. Chiang, F. Kao, C.-L. Tien, and C.-G. Wu, *IEEE Photonics J.* **6**, 8400307 (2014).
- ³¹²M. S. Dresselhaus and G. Dresselhaus, *Adv. Phys.* **30**, 139 (1981).
- ³¹³P. Y. Yu and M. Cardona, *Fundamentals of Semiconductors: Physics and Materials Properties*, 1st ed. (Springer, Germany, 1996), pp. 211–212.
- ³¹⁴V. V. Karataev, M. G. Mil'vidsky, N. S. Rytova, and V. I. Fistui, *Sov. Phys.-Semicond.* **11**, 1009 (1977).
- ³¹⁵E. Litwin-Staszewska, W. Szymanska, and R. Piotrkowski, *Phys. Status Solidi* **106**, 551 (1981).
- ³¹⁶Y. C. Kao and O. Eknoyan, *J. Appl. Phys.* **54**, 2468 (1983).
- ³¹⁷S. F. Nelson, K. Ismail, J. O. Chu, and B. S. Meyerson, *Appl. Phys. Lett.* **63**, 367 (1993).
- ³¹⁸A. S. Mayorov, R. V. Gorbachev, S. V. Morozov, L. Britnell, R. Jalil, L. A. Ponomarenko, P. Blake, K. S. Novoselov, K. Watanabe, T. Taniguchi, and A. K. Geim, *Nano Lett.* **11**, 2396 (2011).
- ³¹⁹C. R. Dean, A. F. Young, I. Meric, C. Lee, L. Wang, S. Sorgenfrei, K. Watanabe, T. Taniguchi, P. Kim, K. L. Shepard, and J. Hone, *Nat. Nanotechnol.* **5**, 722 (2010).
- ³²⁰L. Li, Y. Yu, G. J. Ye, Q. Ge, X. Ou, H. Wu, D. Feng, X. H. Chen, and Y. Zhang, *Nat. Nanotechnol.* **9**, 372 (2014).
- ³²¹B. Radisavljevic, A. Radenovic, J. Brivio, V. Giacometti, and A. Kis, *Nat. Nanotechnol.* **6**, 147 (2011).
- ³²²L. Tao, E. Cinquanta, D. Chiappe, C. Grazianetti, M. Fanciulli, M. Dubey, A. Molle, and D. Akinwande, *Nat. Nanotechnol.* **10**, 227 (2015).
- ³²³H. C. P. Movva, A. Rai, S. Kang, K. Kim, B. Fallahzad, T. Taniguchi, K. Watanabe, E. Tutuc, and S. K. Banerjee, *ACS Nano* **9**, 10402 (2015).
- ³²⁴D. A. Bandurin, A. V. Tyurina, G. L. Yu, A. Mishchenko, V. Zólyomi, S. V. Morozov, R. K. Kumar, R. V. Gorbachev, Z. R. Kudrynskiy, S. Pezzini, Z. D. Kovalyuk, U. Zeitler, K. S. Novoselov, A. Patane, L. Eaves, I. V. Grigorieva, V. I. Fal'ko, A. K. Geim, and Y. Cao, *Nat. Nanotechnol.* **12**, 223 (2016).
- ³²⁵W. Walukiewicz, H. E. Ruda, J. Lagowski, and H. C. Gatos, *Phys. Rev. B* **30**, 4571 (1984).